9 Magnetic Prussian Blue Analogs

M. Verdaguer and G. Girolami

9.1 Introduction

Magnetic solids have numerous and important technological applications: they find wide use in information storage devices, microwave communications systems, electric power transformers and dynamos, and high-fidelity speakers [1–3]. By far the largest application of magnetic materials is in information storage media, and the annual sales of computer diskettes, compact disks, optical disks, recording tape, and related items exceed those of the celebrated semiconductor industry [3–5]. The demand for higher bit-density information storage media and the emergence of new technologies such as magneto-optic devices makes it crucial to expand the search for entirely new classes of magnetic materials [2, 3].

In response to the increasing demands being placed on the performance of magnetic solids, over the last decade or so there has been a surge of interest in molecule-based magnets [6–20]. In such solids, discrete molecular building blocks are assembled, with their structures intact, into 0-, 1-, 2-, or 3-dimensional arrays. One of the attractive features of molecular magnets is that, by choosing appropriate building blocks, the chemist can exert considerable control over the connectivity and architecture as well as the resulting magnetic properties of the array. The local exchange interactions, which can be specifically tailored through judicious choice of appropriate molecular building blocks, dictate the bulk magnetic behavior of the solid. By choosing molecular building blocks whose singly occupied molecular orbitals (magnetic orbitals) are of specific symmetries, and by linking the building blocks into arrays with favorable geometric relationships between the building blocks, the synthetic chemist can exert powerful control over the properties of new molecule-based magnetic materials.

Although the high molecular weights and low bulk densities observed for essentially all molecule-based magnets preclude their use as permanent magnets, they are potentially useful as magnetic recording media [21] or quantum computing devices [22]. More significantly, however, some molecule-based magnets exhibit bulk properties quite unlike those of conventional magnetic solids. For example, some are optically transparent, and others are non-magnetic in the dark but magnetic in

Magnetism : Molecules to Materials V. Edited by J. S. Miller and M. Drillon
Copyright © 2004 WILEY-VCH Verlag GmbH & Co. KGaA, Weinheim
ISBN : 3-527-30665-X

the light. Until quite recently, the magnetic ordering temperatures of these unusual solids were too low (< 100 K) to make them of practical use. If room-temperature molecule-based magnets could be discovered, however, they could serve as the basis of entirely new magneto-optical technologies and be the keys to the development of so-called "photonic" computers that use photons instead of electrons as the information carriers [22–25]. The first room-temperature molecule-based magnet was $V(TCNE)_2 \cdot xCH_2Cl_2$ an amorphous air-sensitive substance that decomposes thermally at about 80 ºC [26]. The discovery of other room temperature molecule-based magnets with improved properties could lead to significant applications of these unusual materials.

In this context, Prussian Blues (PBs) and their analogs (which we will refer to as PBAs) are an especially amazing and evergreen family of compounds. Recent investigations of the chemistry and physical properties of PBs have stimulated an astonishing rebirth of interest in the magnetism of complex solids, and a revival of the chemistry of inorganic cyanide chemistry. Prussian Blues and their analogs can easily be synthesized by the simple reaction of hexacyanometalates $[B(CN)_6]^{p-}$ with transition metal Lewis acids A^{q+} in water to give neutral three-dimensional networks $A_p[B(CN)_6]_q \cdot nH_2O$. We shall see, however, that this apparent simplicity can be misleading.

After this introduction, we present in section 2 a brief historical survey and the general structure of PBs. In Section 3, we describe their magnetic properties including theoretical models that allow one to predict and to understand the exchange interactions between adjacent spin centers in PB frameworks. In Section 4, we summarize some of our efforts and successes in synthesizing magnetic Prussian Blue (MPB) analogs with magnetic ordering temperatures (T_C) around or above room temperature [27–39] and even above the boiling point of water [40, 41]. The last part of this section describes possible applications of high T_C PBs. Section 5 is devoted to new trends such as photomagnetic properties, tuning of the magnetisation, nanomagnetism and prospects in the context of a blossoming of cyanide chemistry and molecular magnetism.

9.2 Prussian Blue Analogs (PBA), Brief History, Synthesis and Structure

In 1704 by a Berlin draper named Diesbach discovered by chance a recipe to make a new blue pigment useful for paints and fabrics. This discovery was reported anonymously in 1710 [42] and the recipe itself was described in 1724 by Woodward and Brown [43, 44]. This pigment, now called Prussian Blue (or Berlin Blue), was the first synthetic coordination compound. The history of its discovery, and the various theories about its nature and the origin of its bright colour, were reviewed

recently in the context of the development of chemical ideas in the 18th and 19th centuries [45, 46]. A more complete history of this remarkable bright blue pigment is in preparation [47]. Information about its history is available in the very useful book by Sharpe [48].

9.2.1 Formulation and Structure

The parent species Prussian Blue has the idealized formula $Fe^{II}_4[Fe^{III}(CN)_6]_3 \bullet 14H_2O$ and a conventional unit cell shown in Figure 9.1a. Its stoichiometry is sometimes written as $Fe^{II}[Fe^{III}(CN)_6]_{3/4} \bullet 7/2H_2O$. In fact, the formulas of Prussian Blue and its analogs are often written in two different ways: as $M_xA[B(CN)_6]_z \bullet nH_2O$ or as $M_{4x}A_4[B(CN)_6]_{4z}\square_{4(1-z)} \bullet nH_2O$, where M is an alkali metal cation [45, 46, 49, 50]. In the latter formulation (which is based on the conventional cell), the presence of the intrinsic vacancies □ and their amount per cell is easily seen; hereafter, we will use both formulations, the choice depending on what feature we wish to emphasize.

For $z = 1$, the Prussian Blue solids adopt face-centered cubic (fcc) structures (Figures 9.1b and c), as first proposed by Keggin and Miles [49], with unit cells that comprise eight octants (the interiors of the octants are referred to as interstitial or tetrahedral or cuboctahedral sites). There are two types of octahedral metal sites in the fcc structure: strong ligand-field sites (C_6 coordination environments) and weak ligand-field sites (N_6 coordination environments).

For $z < 1$, and therefore for Prussian Blue itself, Keggin and Miles proposed that the interstitial sites contained the "excess" A ions [49], but this suggestion was later disproven by Ludi and coworkers [50–56], who proposed from powder diffraction data and density measurements that the B sites are fractionally occupied, and that the A centers surrounding the vacant sites have one (or more) water molecules in their coordination spheres (Figure 9.1a). Zeolitic water molecules and/or charge

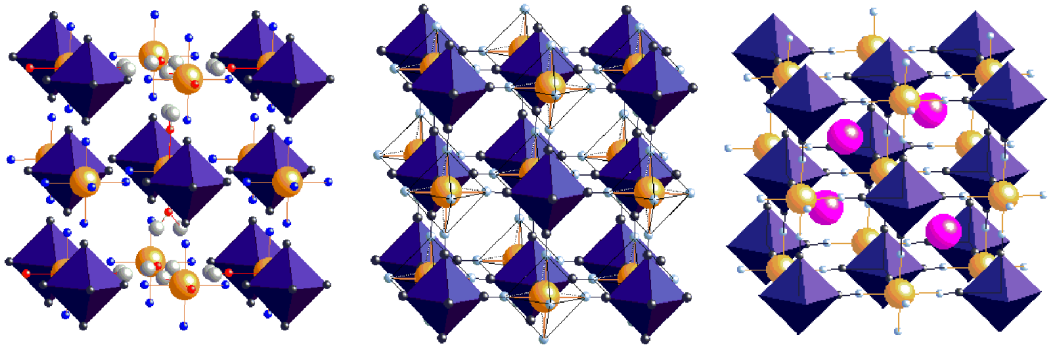

(a) (b) (c)

Fig. 9.1. Three structures of cubic Prussian blue analogues: (a) $A^{II}_1[B^{III}(CN)_6]_{2/3} \cdot nH_2O$, $A_1B_{2/3}$; (b) $A^{III}[B^{III}(CN)_6]$, A_1B_1; (c) $CsA^{II}[B^{III}(CN)_6]$, $Cs_1A_1B_1$.

balancing cations generally occupy the interstitial sites; the hydrogen bond network may help to stabilize the structure as suggested by Beall et al. [57].

The crystal structure of Prussian Blue $Fe^{III}_4[Fe^{II}(CN)_6]_3 \bullet 14H_2O$ was determined by Buser, Ludi, and Güdel in 1972 from a single crystal obtained by slowly mixing very dilute solutions of $FeCl_2$ and $K_4[Fe(CN)_6]$ in concentrated hydrochloric acid [55]. The most intense reflections suggest that the space group is *Fm*3*m*, but the actual space group (taking into account the weak reflections) is *Pm*3*m*. Interestingly, depending on the crystallization conditions, the $[Fe(CN)_6]$ vacancies are either (i) disordered in the crystal, giving an apparent high-symmetry structure with a fractional occupancy (3/4) of the $[Fe(CN)_6]$ sites or (ii) ordered, thereby lowering the symmetry. An important structural point to keep in mind is that the presence of vacancies is *intrinsic* to PBs whenever $z < 1$. It is *not* a "defect" structure as too often claimed in the literature. Some important properties are determined by these vacancies (see below).

Ludi and Güdel summarized their findings in their beautiful review [50]. The Prussian Blue structural framework is closely related to that of perovskites ABO_3, such as $CaTiO_3$, except that: (i) the octahedral metal centers are connected by cyanide bridges instead of oxide ions to form the cubic framework, and (ii) the $[B(CN)_6]^{p-}$ units found in the solid are unchanged from the hexacyanometalate reactant used in the synthesis. In other words, unlike the $[Ti^{IV}O_6]^{4-}$ units in perovskite, which are not stable in water, the $[B(CN)_6]^{p-}$ units have an independent existence in solution. Prussian Blue and its analogs can therefore be considered as molecule-based materials, because they can be synthesized directly from prebuilt molecular precursors.

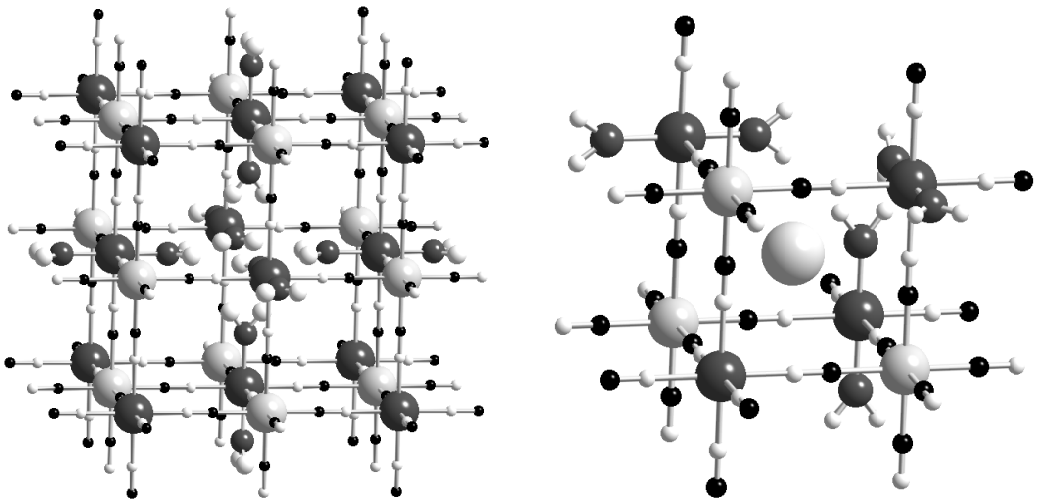

(a) (b)

Fig. 9.2. Scheme of a $[B(CN)_6]$ vacancy in Prussian blue analogue: (a) vacancy; (b) detail of an octant with a vacancy and an alkali cation.

In a "perfect" model of Prussian Blue, the A–N≡C–B unit is linear, and the metal atoms in the A and B sites have perfect octahedral geometries. In fact, detailed X-ray diffraction Rietveld analyses show that the $[B(CN)_6]$ units are often tilted, as is often found for the $[BO_6]$ octahedra in the ABO_3 perovskites. The tilting results in A–N≡C angles that are less than 180°. Such distortions have important consequences on the overlap of local wave functions and on the magnetic properties.

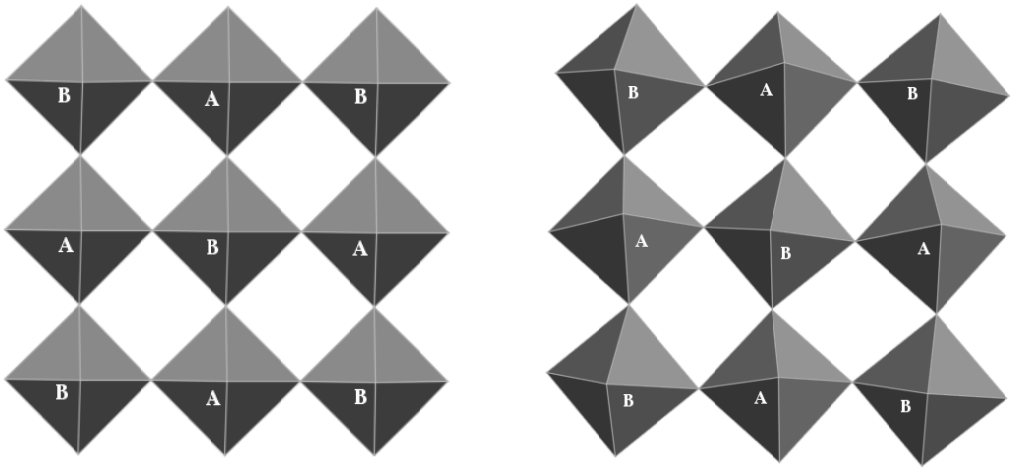

(a) (b)

Fig. 9.3. Schematic tilting of the octahedra in perovskites and Prussian Blue analogs.

Prussian Blue is obtained by the addition of iron(III) salts to potassium hexacyanoferrate(II); among the puzzling aspects of Prussian Blue was its relationship to a similar substance known as Turnbull's blue, which was obtained by addition of iron(II) salts to potassium hexacyanoferrate(III). The problem was solved by Mössbauer spectroscopy which revealed that the two compounds are actually identical: very rapid electron-transfer between the iron(II) and the hexacyanoferrate(III) ions gives rise to the same mixed-valence compound as before. The so-called "soluble forms" of PB are actually colloïdal suspensions of $K_xFe^{III}[Fe^{II}(CN)_6]_z \bullet nH_2O$.

Robin was the first to point out that the bright blue color of Prussian Blue is due to an intervalence transition between the iron(II) and iron(III) centers [58]. Indeed, PB is a typical example of Robin and Day's second class of mixed-valence complexes: the valence is delocalized at high temperatures and localized at low temperatures [59].

9.2.2 Synthesis

The syntheses of compounds in the Prussian Blue family are simple, at first glance. In one common recipe, an aqueous solution containing a $[A(H_2O)]^{q+}$ cation is added dropwise to an aqueous solution containing a $[B(CN)_6]^{p-}$ anion. The stoichiometry of the product will depend on the oxidation states of A and B and also on the amount of charge-balancing alkali metal cations C^+ that are incorporated into the interstitial sites. If no alkali metal ions are incorporated, a neutral precipitate is formed with stoichiometry $A[B(CN)_6]_{q/p}\bullet nH_2O$. For example, if an A^{2+} cation is added to a potassium salt of a $[B^{III}(CN)_6]^{3-}$ anion, one usually obtains a solid of stoichiometry $A[B(CN)_6]_{2/3}\bullet 4H_2O$, which is often referred to as the 3:2 compound $A_3[B(CN)_6]_2\bullet xH_2O$ where $x \sim 12$. In contrast, if an A^{2+} cation is added to a cesium salt of the $[B^{III}(CN)_6]^{3-}$ anion, one usually obtains the 1:1 compound $CsA[B(CN)_6]\bullet xH_2O$, where $x \sim 1$. The different stoichiometries reflect the better fit of the larger Cs^+ cations in the interstitial sites of the fcc structure.

Hexacyanometalate anions are known for many of the transition elements, and thus Prussian Blue analogs can be prepared with a variety of metals in the B sites. The paramagnetic derivatives of the first-row transition elements (i.e., excluding the well-known derivatives of Fe^{II} and Co^{III}) are as follows:

- $[B(CN)_6]^{4-}$ is known for B = V^{II} and Mn^{II}
- $[B(CN)_6]^{3-}$ is known for B = Ti^{III}, Cr^{III}, Mn^{III}, and Fe^{III}
- $[B(CN)_6]^{2-}$ is known only for B = Mn^{IV}

The syntheses of some of these precursors have long been known, and others were designed or improved for the purpose of obtaining magnetic Prussian Blues; among the latter are $[Ti^{III}(CN)_6]$ [33], $[Mn^{IV}(CN)_6]$ [34], $[Cr^{III}(CN)_6]$ [35] and $[Mo^{III}(CN)_6]$ [199]. All of these species are low-spin owing to the large ligand field splitting induced by the cyanide ligands, and the spins of these anions vary from $S = 1/2$ for the Ti^{III}, Mn^{II}, and Fe^{III} derivatives, to $S = 1$ for the Mn^{III} derivative, to $S = 3/2$ for the V^{II}, Cr^{III}, and Mn^{IV} derivatives. It is advantageous when these anions are kinetically inert (and indeed most of them are), so that the cyanide ligands do not dissociate during the synthesis of the Prussian Blue phase. The $[B(CN)_6]^{n-}$ anions are Lewis bases. They may be treated with a large variety of Lewis acids, particularly transition metal cations, to generate compounds in the Prussian Blue family. Among the paramagnetic metallic ions that can be placed in the A sites are V^{II}, Cr^{II}, Mn^{II}, Fe^{II}, Co^{II}, Ni^{II}, Cu^{II}, and Fe^{III}. Generally, these ions are added as aquated salts of weakly coordinating anions. When located in the A sites, the paramagnetic ions generally remain high-spin because the N-coordinated cyanide and water molecules are weak field ligands. Thus, the spins of the A ions in Prussian Blue analogs range from $S = 1/2$ for Cu^{II} to $S = 5/2$ for Mn^{II} and Fe^{III}. Interestingly, in the case of Cr^{II} and Co^{II}, low spin states can be adopted when they are ligated by four or more N-bound cyanides [36]. In contrast to the $[B(CN)_6]$ precursors, it is better for these A ions to be kinetically labile so that the complexation with the

nitrogen atoms of the $[B(CN)_6]$ anions is facilitated. Inert ions such as Cr^{III} are more difficult to incorporate into the A sites. Despite the apparent simplicity of the syntheses, many complications can arise. For example, some of the hexacyanometalate precursors are difficult to purify, and even when pure salts are obtained, the $[B(CN)_6]$ anions may hydrolyze, oxidize, or disproportionate in solution before reacting with the A cation. Protecting the solutions from air and keeping the solutions at 0 °C sometimes helps to minimize these problems.

The solid Prussian Blue analogs can also suffer from one or more of the following problems:

1. The product may contain a variety of species in the interstitial sites. The Prussian Blue analogs behave like sponges and tend to fill the interstitial sites with solvent molecules or with the counterions used in the synthesis. Even the solvents used to wash the solid product can enter these sites. If these species are incorporated randomly into the interstitial sites, the resulting disruption of the regularity of the structure can lower the magnetic ordering temperature. It is sometimes helpful either to add an excess of an alkali metal cation so as to fill as many of the interstitial sites as possible with well-defined counterions, or to use starting materials with large counterions such as tetraalkylammonium cations and *p*-toluenesulfonate anions, so that water molecules are the only available species that are small enough to fit into the interstitial sites [40, 41].
2. The solid may be amorphous, poorly crystalline, or contain several phases. These problems relate to the kinetics and thermodynamics of the crystallization process. For example, in the series $M_xCo[Fe(CN)_6]_z$, where M is an alkali cation, the product consists of a single phase when M = Cs but two phases when M = Rb, K, or Na. The two phases in the latter salts differ in the chemical environments about the A sites, which lead to the cobalt atoms being high spin Co^{II} in one phase, and low-spin Co^{III} in the other. The homogeneity of Prussian Blue analogs powders must be carefully checked. The crystallinity and purity of the product can sometimes be improved by adding the reagents as slowly as possible, by changing the identity of the alkali metal cation, by diluting, by changing the reaction temperature, or by adjusting the pH. In some cases, carrying out the synthesis by slow diffusion in H tubes or in gels may be effective in improving the crystallinity of the solids, although hydrolysis of the $[B(CN)_6]$ anions may be a problem with slow-growth techniques. We have found that poorly crystalline materials are usually obtained from organic solvents, probably because the growth of the solid from solution is irreversible.
3. The water content may vary from sample to sample. The water content, especially for compounds with a stoichiometry different from 1/1, is very dependent on the work-up and storage conditions. The amount of water can sometimes affect the magnetic properties.
4. The bridging cyanide ligands may undergo linkage isomerism [27, 36, 38]. This troublesome problem involves the two possible ways that cyanide can be linked

in a bimetallic or mixed valence compound: B–C≡N–A or B–N≡C–A. The extent of linkage isomerism depends strongly on the electronic structure of A and B, and is related to the change in ligand field stabilization energies that results. For example, linkage isomerism does not occur at all in $CsMn^{II}[Cr^{III}(CN)_6]$ but is easy in $CsNi^{II}[Cr^{III}(CN)_6]\bullet 2H_2O$. The latter compound is pale gray when first prepared but turns yellow within days at room temperature due to the formation of square planar diamagnetic $[Ni^{II}(CN)_4]^{2-}$ entities in the structure. Although in this case the linkage isomerism causes the nickel atoms to change from high-spin to low-spin, breaks up the 3D structure, and deeply changes the magnetic properties of the solid, in other cases linkage isomerism has only a small effect.

5. Intermetallic charge transfer and redox processes may occur. Prussian Blue itself is a good example of this phenomenon because it can be obtained either by treatment of $[Fe^{II}(CN)_6]^{4-}$ with Fe^{3+} or by treatment of $[Fe^{III}(CN)_6]^{3-}$ with Fe^{2+}; the latter reaction leads, after a very quick electron transfer, to the same compound, $Fe^{III}_4[Fe^{II}(CN)_6]_3\bullet 14H_2O$. Ludi and Gudel observed that PB is also obtained in air from $[Fe^{II}(CN)_6]^{4-}$ and Fe^{2+} [55]. We observed that $[Fe^{III}(CN)_6]^{3-}$ is easily reduced and leads to solid state compounds containing $[Fe^{II}(CN)_6]^{4-}$ units. The photoinduced magnetism of some Prussian Blues also depends on an electron transfer process (see Section 9.4).

We hope it is clear from the preceding discussion that Prussian Blue analogs must be prepared very carefully to obtain pure samples with reproducible magnetic properties.

9.3 Magnetic Prussian Blues (MPB)

Solids with the Prussian Blue structure are especially attractive as candidates for new molecule-based magnets for several reasons: they can be prepared at room temperature from well-characterized and chemically stable building blocks, the metal centers are linked covalently into a 3D network, and a wide range of metals with different spin states and oxidation states can be substituted into the structure. Furthermore, the bridging cyanide ligands can promote strong magnetic exchange couplings between paramagnetic centers. These features allow considerable control over the nature and magnitude of the local magnetic exchange interactions. These features were recognized progressively in the past and we begin with a brief historical survey.

9.3.1 Brief Historical Survey of Magnetic Prussian Blues

The magnetic properties of Prussian Blue analogs were summarized in 1997 by Dunbar *et al.* in a review on modern perspectives of the chemistry of metal cyanide compounds [60]. We focus here on some complementary and critical aspects.

In 1928, Davidson and Welo published the first magnetic investigation of the parent species Prussian Blue; they measured the magnetic susceptibility at three temperatures in the range 200–300 K [61]. This early work was followed by more extensive studies of Prussian Blue and some analogs in 1940 [62], but it was not until much later, in 1968, that Prussian Blue was shown to be a ferromagnet with T_C = 5.6 K [63]. The parallel alignment of the magnetic moments in Prussian Blue was confirmed later by neutron diffraction [64] and polarized neutron diffraction studies [65]; there is weak but significant delocalization of spin onto the "diamagnetic" Fe^{II} centers. The low magnetic ordering temperature is a consequence of the diamagnetism of half of the metal centers (the low-spin d^6 Fe^{II} centers, which occupy the strong ligand-field sites) so that the through-bond distance between high-spin d^5 Fe^{III} is 10.28 Å and the exchange coupling very weak. Mayoh and Day showed quantitatively that the ferromagnetism between the high-spin Fe^{III} ions is due to the admixture of the low-lying intervalence Fe^{II}-Fe^{III} excited state with the ground state [66].

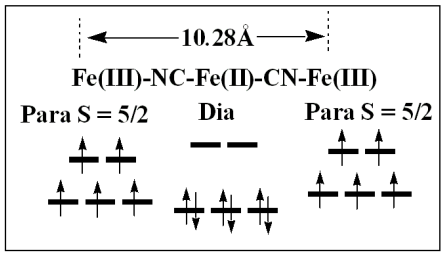

Fig. 9.4. Fe^{III}–NC–Fe^{II}–CN–Fe^{III} entities in Prussian Blue. The exchange interaction is very weak between the two paramagnetic Fe^{III} ions, which are separated by more than 10 Å.

By preparing other metal-substituted analogs of Prussian Blue in which every metal center is paramagnetic, however, the through-bond distance between nearest spin centers is reduced from 10 Å to about 5 Å, and the exchange coupling should be much stronger than it is in Prussian Blue itself. Such metal-substituted analogs of Prussian Blue should have ordering temperatures much higher than 5.6 K, and determining how high has been one of our goals.

The first low temperature investigations of the magnetic properties of metal-substituted analogs of Prussian Blue appeared in the 1950s. Bozorth et al. studied a series of solids prepared by adding Mn^{2+}, Fe^{2+}, Fe^{3+}, Co^{2+}, Ni^{2+}, and Mn^{2+} to $[Fe^{III}(CN)_6]^{3-}$; selected reactions with $[Mn^{III}(CN)_6]^{3-}$ and $[Cr^{III}(CN)_6]^{3-}$ were also performed [67]. Unfortunately, the solids prepared from the latter two anions were not analyzed chemically, and the solids prepared from $[Fe^{III}(CN)_6]^{3-}$ were shown to contain between 25 and 45 % by weight of inert material (oxide, sulfate, and potassium). Nevertheless, this paper is notable for the finding that some of

these solids had magnetic ordering temperatures between 3 and 50 K, the latter being observed for a material prepared from Mn^{2+} and $[Mn^{III}(CN)_6]^{3-}$. At about the same time, Anderson et al. reported some similar (though less well documented) findings [68], concluding that "certain of the complex cyanides of elements of the 3d transition group appear to be ferromagnetic at very low temperature".

In 1980, Trageser and Eysel oxidized $Na_3[Mn^{III}(CN)_6]$ with perchloric acid and obtained a brown-purple material formulated as $Mn^{II}[Mn^{IV}(CN)_6]\bullet 1.14H_2O$ [69]. Magnetic studies carried out by Klenze and Kanellakopulos showed that the compound is a ferrimagnet with an ordering temperature of 49 K. These workers proposed a superexchange mechanism in which adjacent metal orbitals of π symmetry communicated by means of both the filled π-orbitals and the empty π^* orbitals of the cyanide ligand. In the early 1980s, Babel investigated the magnetic properties of a series of Prussian Blues analogs [70–74]. He obtained mainly *paramagnetic* phases because either A or B in the $CsA[B(CN)_6]\bullet nH_2O$ structure was diamagnetic. In one case, however, Babel got a striking result: $CsMn^{II}[Cr^{III}(CN)_6]$ was a ferrimagnet with a magnetic ordering temperature of 90 K (Figure 9.5).

In a review paper [74], he reported on cyanocomplexes with different dimensionalities and proposed that the exchange mechanism involved interactions through the π and π^* orbitals of the cyanide ligand. By the late 1980s, no molecule-based

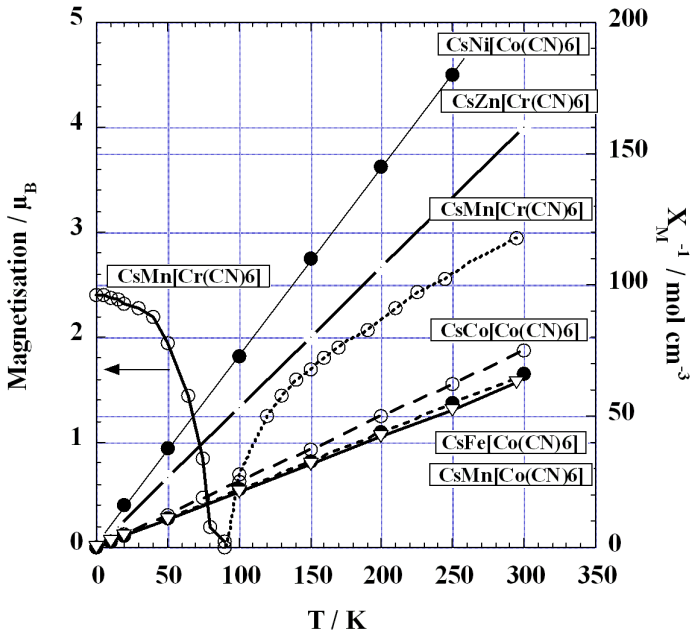

Fig. 9.5. Inverse of the molar susceptibility (right scale) vs temperature in magnetic Prussian Blues analogs $CsA^{II}[B^{III}(CN)_6]$, with A:B, 1:1 stoichiometry. A Curie law is observed when only one of A and B is paramagnetic. Long range magnetic order is observed at 90 K for $CsMn^{II}[Cr^{III}(CN)_6]$ whose magnetisation at low T is reported (left scale) (adapted from Ref. [66]).

magnet of any kind had been reported with an ordering temperature higher than 90 K. At that time, our groups concluded that Prussian Blue magnets with significantly higher ordering temperatures should be obtainable if a proper strategy could be followed. We achieved the goal of obtaining Prussian Blues with high ordering temperatures both by synthesizing many new members of this family and investigating their low-temperature magnetic properties, and by better understanding the factors that lead to larger magnetic couplings between adjacent spin centers. The following sections summarize some of the exchange models used and the results over the last fifteen years. Our steps were very much inspired by the theoretical model and the experimental results of the late Olivier Kahn.

9.3.2 Interplay between Models and Experiments

For any two interacting centers carrying spins S_1 and S_2, the magnetic interaction is described by the Hamiltonian $H = -J\ S_1 \bullet S_2$, where J is the strength of the interaction. The spin of the ground state of the resulting coupled system will depend on the magnitudes of S_1 and S_2, and also on the sign of J. The possible spin arrangements are shown in Figure 6.

To obtain magnetic materials, we need to have a non-zero resultant spin. We must avoid situation (a), in which two identical spins couple antiferromagnetically ($J < 0$), giving a zero resulting spin. In case (b), a diamagnetic neighbor is present; longer-ranged coupling between spin centers can occur (as in Prussian Blue itself), but J and the ordering temperature will be small. In case (c), a ferromagnetic interaction between nearest neighbors ($J > 0$) aligns the magnetic moments and provides a long range magnetic order. We shall see that ferromagnetic interactions are rare in Prussian Blue analogs. Finally, case (d) represents a very appealing situation, in which the usual antiferromagnetic interaction gives rise to a non-zero resultant spin, if the two spins S_1 and S_2 are different in absolute value. Unfortunately, the spin Hamiltonian does not provide insights into how to control the sign or magnitude of J. For this, we needed to find the proper orbital strategy.

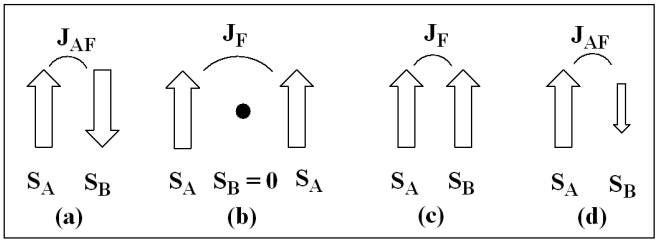

Fig. 9.6. Spin arrangements in Prussian blues: (a) antiferromagnetic interaction between identical neighboring spins; (b) ferromagnetic interaction through a diamagnetic neighbor (double exchange in Prussian blue); (c) ferromagnetic interaction between identical neighboring spins; (d) antiferromagnetic interaction between different neighboring spins: ferrimagnetism.

9.3.2.1 Mean Field, Ligand Field and Exchange Models

The most successful model to understand the magnetic properties of insulating magnetic solids is the "mean field model," which was originally suggested by Weiss and refined by Néel [75]. Here, we briefly give the basic elements of this model.

Consider an insulating two-component magnetic solid AB in which A and B are interpenetrating subnetworks, each of which consists of a set of identical spin centers. The mean field model assumes that all the spins within each subnetwork are oriented in the same direction. It further postulates that the interaction between the two subnetworks A and B can be described by the molecular field coefficient W, and that the interaction within each subnetwork can be described by the coefficients W_A and W_B. The parameter W can be positive (for ferromagnetic interactions) or negative (for antiferromagnetic interactions); the parameters W_A, and W_B are always positive.

The effective local magnetic fields H_A and H_B acting on the magnetic moments of the sub-networks A and B are:

$$H_A = H_0 + W M_B + W_A M_A$$
$$H_B = H_0 + W M_A + W_B M_B \qquad (9.1)$$

where H_0 is the applied field, and M_A and M_B are the mean magnetisations of sub-networks A and B. At high temperatures, the magnetisations of subnetworks A and B are proportional to the effective local field, so that:

$$M_A = [H_0 + W M_B + \alpha W M_A] \bullet C_A / T$$
$$M_B = [H_0 + W M_A + \beta W M_B] \bullet C_B / T \qquad (9.2)$$

where C_A and C_B are the Curie constants of the spins constituting sub-networks A and B, respectively, and where $\alpha = W_A/W$ and $\beta = W_B/W$. Solving these equations for M_A and M_B, and then calculating the magnetic susceptibility χ from the definition $\chi = (M_A + M_B)/H_0$ gives the following expression:

$$1/\chi = \frac{(T - \theta)}{C} - \frac{\gamma}{(T - \theta_a)} \qquad (9.3)$$

where the parameters C, θ, θ_a, and γ are functions of C_A, C_B, W, α, and β (see Ref. 75 for the exact form of these functions).

The mean field model has not been extensively used for ferromagnets, where fluctuations in the mean field restrict the analysis to the high temperature range and impede analysis of the data close to the magnetic ordering temperature, but the model is well adapted for ferrimagnets (antiferromagnetic interactions between the A and B subnetworks). For such solids, the mean field model predicts that the plot of $1/\chi$ vs. T at high temperatures should be hyperbolic, and this curve is often referred to as a Néel hyperbola.

For a magnetic solid consisting of an array of identical $S = 1/2$ centers, the magnetisation at low temperature is given by:

$$M = N\,\mu\,\tanh[\mu H/kT] \tag{9.4}$$

where N is Avogadro's constant, μ is the magnetic moment, H is the local magnetic field, and k is Boltzmann's constant. More generally, for the case in which the solid consists of two subnetworks A and B whose constituent spin centers have spins S_A and S_B and g values g_A and g_B, respectively, the magnetisation within the A subnetwork is (β, Bohr magneton):

$$M_A = g_A S_A B_S [\, g_A S_A \beta\,(H + h_A)] / kT \tag{9.5}$$

where $h_A = W(\varepsilon M_B + \alpha M_A)$, B_S is the Brillouin function (with its argument in square brackets), and ε equals 1 if W is positive and –1 if W is negative. To obtain this expression, we have assumed that the applied field is negligible compared to the mean field (so that the mean field dominates). We can obtain a similar expression for M_B; the total magnetisation M is equal to $(M_A + \varepsilon M_B)$.

Solving the system of two equations for M_A and M_B (which is usually done numerically rather than analytically) and finding the total magnetisation as a function of temperature gives magnetisation curves that depend on the details of the exact system studied: the results depend on the nature of A and B, on the fraction of occupied sites, on the parameters α and β, and, for ferrimagnetic systems, on the parameters $x = \mu_A / \mu_B$ and $y = n_A / n_B$, where μ_A and μ_B are the magnetic moments on A and B, and n_A and n_B are the number of atoms A and B in the unit considered. Depending on the values of x and y, Néel predicted very different shapes for magnetisation curves $M(T)$ including some that change sign at a certain temperature (called the "compensation temperature") at which the magnetisations of the sub-networks A and B are exactly equal and opposite in direction [75]. The model was used in a predictive and clever way by Okhoshi et al. in their studies of the compensation points in the magnetisation curves of polymetallic magnetic Prussian Blues (see Section 9.5.2).

The ideas developed by Néel in his 1948 paper [75] (see also Herpin [76] and Goodenough [77]) within the frame of molecular field theory to interpret the magnetism of perovskite ferrimagnets ABO_3 are fully valid for MPBs. In particular, the expression for the susceptibility close to the ordering temperature T_C can be used to extract the following very useful relation:

$$k\,T_C = Z\,|J|\,\sqrt{C_A\,C_B}\,/\,N_A g^2 \beta^2 \tag{9.6}$$

where Z is the number of magnetic neighbors, $|J|$ is the absolute value of the exchange interaction between A and B, C_A and C_B are the Curie constants of A and B, weighted by the stoichiometry, N_A is Avogadro's constant, g is a mean Lande factor for A and B, and β is the Bohr magneton. *Equation (9.6) clearly shows that T_C can be maximized by increasing the number of magnetic neighbors, by increasing the magnitude of J, and by increasing C_A and C_B.* For the Prussian

Blues of stoichiometry $M_xA[B(CN)_6]_z \bullet nH_2O$, we can follow several strategies to maximize T_C:

- Maximize Z by controlling the Prussian Blue stoichiometry. The number of nearest neighbors Z is dictated by the value of z in the Prussian Blue formula. In Prussian Blues with a 1:1 A:B stoichiometry (i.e., lacking vacancies in the $[B(CN)_6]$ sites), the number of nearest neighbors Z adopts its maximum possible value of 6. In the frequently encountered 3:2 A:B systems (in which $z = 2/3$ and one-third of the B sites are vacant), the number of nearest neighbors Z is only 4. *As the number of vacancies in the PBM structure decreases, T_C becomes larger.* We shall use these conclusions later.
- Maximize $|J|$ by changing the identities of the spin centers A and B in the two subnetworks. We develop this point in the following paragraph.
- Maximize the Curie constants C_A and C_B by proper choice of the metals A and B. This approach to maximize T_C proves to be less useful than the other two, as we shall see.

Ligand field model

In Prussian Blue magnets, the exchange mechanisms that dictate the magnitude of J involve the delocalization of spin from the metal centers onto the cyanide bridges. The extent of spin delocalization is readily explicable in terms of ligand field theory.

In the idealized Prussian Blue structure of stoichiometry $M_xA[B(CN)_6]_z \bullet nH_2O$, each B atom is surrounded by the carbon atoms of six cyanide ligands and will always experience a large ligand field (with very large $\Delta_{octahedral}$ splitting). As a result, the B atoms will be low spin with unpaired electrons (if any) only in the t_{2g} orbitals (Figure 9.7a). It may be noted that the $\Delta_{octahedral}$ is sufficiently large (and the antibonding orbitals e_g^* so high in energy) that no $[B(CN)_6]$ complex exists with more than six d-electrons: such complexes are not stable. In contrast, the A atom is surrounded by the nitrogen atoms of six cyanide ligands (when the stoichiometry is $z = 1$), or by four cyanides and two water molecules (when the stoichiometry is $z = 2/3$). The A atoms thus experience weak ligand fields, and are usually high-spin (Figure 9.7b and c), although in a few cases [Cr^{II}, Mn^{III}, Co^{II}, see below] the A atoms can be low-spin.

Because cyanide is a moderate σ-donor, a weak π-donor, and a moderate π-acceptor, spin delocalization can occur by means of both σ and π mechanisms. The nitrogen p_z orbital mixes with the d_{z^2} orbital of the A ion to which it is directly attached (σ symmetry), and the nitrogen p_x and p_y orbitals mix with the d_{xz} and d_{yz} orbitals of the A ion (π symmetry). The singly occupied orbitals (or magnetic orbitals) on both metals are sketched in Figure 9.7: $\phi(t_{2g})$ magnetic orbitals on the B site, and either $\phi(t_{2g})$ or $\phi^*(e_g)$ magnetic orbitals (or both) on the A site. The dotted lines represent the nodal surface of the orbitals on the internuclear axis.

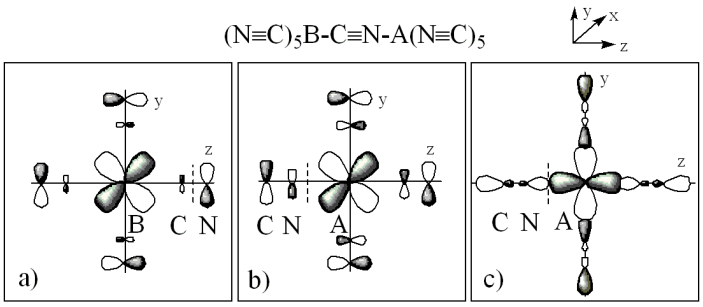

Fig. 9.7. Local magnetic orbitals in an isolated $(NC)_5B–CN–A(NC)_5$ binuclear unit: (a) $\phi(t_{2g})$ magnetic orbitals in $B(CN)_6$; (b) $\phi(t_{2g})$ magnetic orbitals in $A(NC)_6$; (c) $\phi^*(e_g)$ magnetic orbitals in $A(NC)_6$.

Previous experimental studies of paramagnetic molecules containing C-bonded cyanide ligands show that there is a small spin density on the carbon atom but a larger spin density on the nitrogen atom. Figure 7a closely follows the spin density maps obtained from polarized spin neutron diffraction [78] and solid state paramagnetic NMR studies [79] of $[B^{III}(CN)_6]$ salts (B= Fe, Cr). From this simple ligand field analysis, it is possible to draw an important conclusion about the exchange: the empty π^* orbitals of the cyanide ligands play an important role in the antiferromagnetic exchange interactions in Prussian Blue analogs. Consequently, we predicted that substituting into the structure metals that have single electrons in high-energy (and more radially expanded) t_{2g} orbitals should afford Prussian Blues with higher magnetic ordering temperatures. Higher-energy d-orbitals are characteristic of the early transition metals in lower oxidation states, owing to the lower effective nuclear charges of these elements. Accordingly, building blocks such as aquated salts of V^{II} and Cr^{II}, and hexacyanometalate derivatives of V^{II}, Cr^{II}, and Cr^{III}, should afford Prussian Blue compounds with much higher magnetic ordering temperatures.

Orbital symmetry and the nature of the magnetic exchange coupling

The relationship between the symmetry of the singly-occupied orbitals on two adjacent spin carriers and the nature of the resulting magnetic exchange interaction is one of the most useful concepts available to the synthetic chemist interested in designing molecule-based magnetic systems with specifically tailored magnetic properties [6–8, 19, 80].

To predict the value of $|J|$, two different approaches have been used: Kahn's model, in which the magnetic orbitals are non-orthogonalized, and Hoffmann's approach, in which the magnetic orbitals are orthogonalized. Both models predict that orthogonal orbitals give rise to ferromagnetism and that non-orthogonal orbitals give rise to antiferromagnetism.

Consider the case of two electrons residing in two identical orbitals a and b on two adjacent sites. In Kahn's model [7, 81–83], the singlet-triplet energy gap, J

(= $E_{singlet} - E_{triplet}$), is given by:

$$J = 2\,k + 4\,\beta\,S \tag{9.7a}$$

where k is the two-electron exchange integral (positive) between the two non-orthogonalized magnetic orbitals a and b; β is the corresponding monoelectronic resonance or transfer integral (negative), and S is the monoelectronic overlap integral (positive) between a and b. In Hoffmann's model [84], J is given by:

$$J = 2\,K_{ab} - (E_1 - E_2)^2 / (J_{aa} - J_{ab}) \tag{9.7b}$$

where K_{ab} is the two-electron exchange integral (positive) between two identical orthogonalized magnetic orbitals a′ and b′; $(E_1 - E_2)$ is the energy gap between the molecular orbitals Ψ_1 and Ψ_2 built from a′ and b′, J_{aa} is the bielectronic interelectronic repulsion on one centre, and J_{ab} the equivalent on two centres. In both Eqs. (9.7a) and (9.7b), the first term is positive and the second term is negative; thus J can be represented as the sum of two components, a positive term J_F that favors a parallel alignment of the spins and ferromagnetism, and a negative term J_{AF} that favors an antiparallel alignment of the spins and short-range antiferromagnetism.

$$J = J_F + J_{AF} \tag{9.7c}$$

When the two a and b orbitals are different, no rigorous analytical treatment is available, but a semi-empirical relation was proposed by Kahn [85]:

$$J = 2\,k + 2\,S\,(\Delta^2 - \delta^2)^{1/2} \tag{9.8}$$

where δ is the energy gap between the (unmixed) a and b orbitals, and Δ is the energy gap between the molecular orbitals built from them.

When several electrons are present on each centre, n_A on one side, n_B on the other, J can be described as the sum of the different "orbital pathways" $J_{\mu\nu}$, weighted by the number of electrons [85]:

$$J = \left(\sum_{\mu\nu} J_{\mu\nu}\right) / n_A\,n_B \tag{9.9}$$

where μ varies from 1 to n_A and ν varies from 1 to n_B.

When only one electron is present per site, the situation is simple: a short-range ferromagnetic interaction leads to a triplet ground state [86]; a short-range antiferromagnetic interaction leads to a singlet ground state. When each site bears a different number of electrons, the short-range ferromagnetic coupling leads to a total spin ground state which is the sum of the spins: $S_T = S_A + S_B$; the short-range antiferromagnetic coupling leads to a total spin ground state which is the difference of the spins: $S_T = |\,S_A - S_B\,|$. Figure 9.6 illustrates these situations. A key point is that antiferromagnetism between two neighbors bearing different spins leads to a non-zero spin in the ground state. For a bulk solid [75], this situation is known as ferrimagnetism.

9.3.2.2 Application to Magnetic Prussian Blue Analogs

The Prussian Blues are excellent "textbook" examples of the use of symmetry to analyze the exchange interactions in magnetic solids, because their cubic structures greatly simplify the analysis. Furthermore, magnetic exchange is a short-range phenomenon, and thus we can neglect interactions with second nearest neighbors (which are more than 10Å away) and with more distant magnetic centers, and consider only the interactions between adjacent metal atoms. The analysis thus reduces to a consideration of the exchange interactions present between two metal centers connected by a cyanide linkage: i.e., in a $(CN)_5A–N{\equiv}C–B(CN)_5$ subunit (Scheme 9.1).

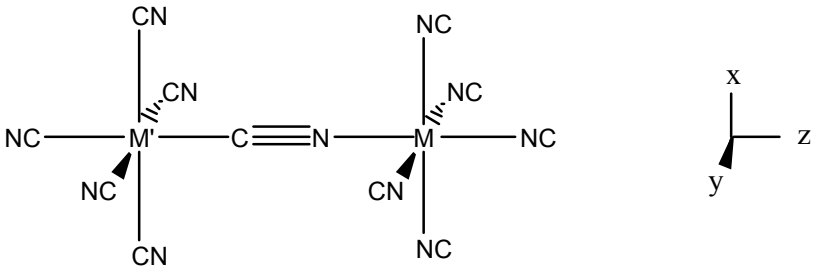

Scheme 9.1

Suppose that the two adjacent metal centers each carries a single unpaired electron in a d-orbital (we will refer to such orbitals as "magnetic orbitals" after Kahn). If the two magnetic orbitals are orthogonal, then the ground state of the system has parallel electron spins. In contrast, if the two magnetic orbitals are not orthogonal, then the ground state of the system generally has antiparallel electron spins. In other words, orthogonal orbitals lead to local ferromagnetic interactions whereas non-orthogonal orbitals favor local antiferromagnetic interactions. The behavior is simply a two-site analog of Hund's rule, and has the same quantum mechanical origin.

For systems in which the interacting magnetic centers each contain several magnetic orbitals, or that consist of arrays of many spin centers, the symmetry relationship between each magnetic orbital on one spin carrier must be considered with respect to the various magnetic orbitals on the adjacent spin carriers. Mutually orthogonal magnetic orbitals will contribute to the ferromagnetic exchange term, whereas non-orthogonal magnetic orbitals will contribute to the antiferromagnetic term. The net interaction is simply the sum of all the ferromagnetic and antiferromagnetic contributions.

In a Prussian Blue compound, the A and B centers are octahedral and connected together by nearly linear A–N≡C–B cyanide bridges. (Even when this linkage is somewhat non-linear, the basic conclusions remain unchanged.) The B atom, which is surrounded by the carbon atoms of six cyanide ligands, is in a large ligand field. As a result, all known $[B(CN)_6]$ units are invariably low spin and have electrons

only in the t_{2g} orbitals. In contrast, the A atom, which is surrounded by nitrogen atoms of cyanide ligands or oxygen from water molecules, is in a weak ligand field and is almost always high-spin. For the A atoms, it is possible for unpaired electrons to be present only in the t_{2g} orbitals (for d^2 or d^3 ions), only in the e_g orbitals (for d^8 and d^9 ions), or in both the t_{2g} and e_g orbitals (for d^4 through d^7 ions).

For the Prussian Blues, therefore, three situations arise:

1. When only e_g magnetic orbitals are present on A, all the exchange interactions with the t_{2g} magnetic orbitals present on $[B(CN)_6]$ will be ferromagnetic. Thus, if a Prussian Blue is prepared by adding a d^8 or d^9 A cation such as Ni^{II} or Cu^{II} to a paramagnetic $[B(CN)_6]$ anion, a ferromagnet should result. The accuracy of this analysis was illustrated by the preparation in 1991 of $Ni^{II}_2[Fe^{III}(CN)_6]_3 \bullet xH_2O$ and $Cu^{II}_2[Fe^{III}(CN)_6]_3 \bullet xH_2O$, both of which are ferromagnetic as predicted [87].
2. When only t_{2g} magnetic orbitals are present on A, all the exchange interactions with the t_{2g} magnetic orbitals present on $[B(CN)_6]$ will be antiferromagnetic. In this case, if the Prussian Blue is prepared by adding a d^2 or d^3 cation to a paramagnetic $[B(CN)_6]$ anion, a ferrimagnet should result. The first such compounds were described in 1995 [29] and will be discussed below.
3. When both t_{2g} and e_g magnetic orbitals are simultaneously present on A, ferromagnetic and antiferromagnetic interactions with the t_{2g} magnetic orbitals on $[B(CN)_6]$ coexist and compete. Here, the overall nature of the interaction is not so simple to predict. Usually, the antiferromagnetic interactions dominate and the solid orders ferrimagnetically. For example, Babel's compound $CsMn^{II}[Cr^{III}(CN)_6] \bullet xH_2O$ falls into this class and is ferrimagnetic. But this may not always be the case. $Fe^{II}_3[Cr^{III}(CN)_6]_2 \bullet xH_2O$ and $Co^{II}_3[Cr^{III}(CN)_6]_2 \bullet xH_2O$ are ferromagnetic with low T_Cs and weak exchange interaction.

9.3.2.3 Molecular Orbital Analysis

Semi-empirical extended Hückel calculations have afforded detailed information about the high energy molecular orbitals directly related to exchange in the $(CN)_5A–N{\equiv}C–B(CN)_5$ units. Typical molecular orbitals constructed from linear combinations of the magnetic $\phi(t_{2g})$ orbitals appear in Figure 9.8 (for clarity, our graphical representation exaggerates the amount of A-B mixing):

$$\text{bonding:} \quad \varphi_1 = \lambda_+ \phi(t_{2g})(B) + \mu_+ \phi(t_{2g})(A) \quad (\lambda_+ << \mu_+) \quad (9.10a)$$

$$\text{antibonding:} \quad \varphi_2 = \lambda_- \phi(t_{2g})(B) - \mu_- \phi(t_{2g})(A) \quad (\lambda_- >> \mu_-) \quad (9.10b)$$

The precise contribution of each atomic orbital to these MOs depends on their energies and radial extensions. Nevertheless, the importance of the participation of the cyanide bridge in the exchange phenomenon is clearly apparent.

Before mixing, the energy difference between the magnetic orbitals $\phi(t_{2g})(A)$ and $\phi(t_{2g})(B)$ is δ; after mixing the energy gap between φ_2 and φ_1 is Δ. The dotted lines display the nodal surfaces in the orbitals along the internuclear axis: there is one nodal surface in the bonding orbital, and two in the antibonding orbital.

The situation in the case of orthogonal $\phi(t_{2g})(B)$ orbitals and $\phi(e_g)(A)$ orbitals is shown in Figure 9a. In the insert (Figure 9.9b), we emphasize the spin density borne by the nitrogen in the two orthogonal p_y and p_z orbitals. The overlap density ρ, which is given by the expression:

$$\rho = \phi(t_{2g})(B) \cdot \phi(e_g)(A) \tag{9.11}$$

is strong on the nitrogen and from this situation, we expect a strong ferromagnetic interaction because the exchange integral k is proportional to ρ^2 [86]. In all the cases, Figures 9.8 and 9.9 display the triplet electronic configuration.

The conclusions from Figures 9.8 and 9.9 are straightforward: the $t_{2g}(B)$–$e_g(A)$ pathways lead to ferromagnetic (F) interactions, the magnitude of which is expected to be significant, owing to the electronic structure of the cyanide bridge and the

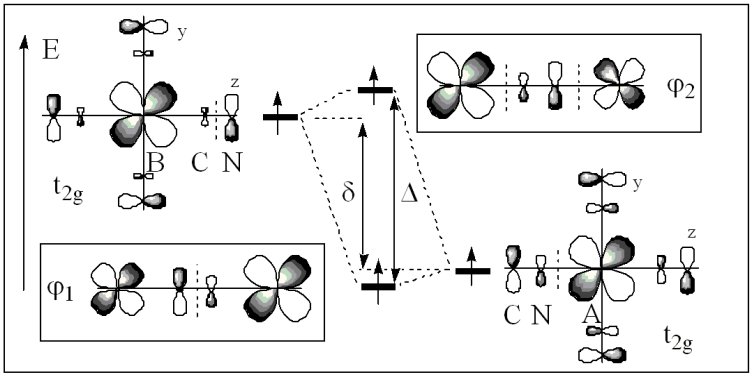

Fig. 9.8. Molecular orbitals φ_1 and φ_2 built from $\phi(t_{2g})$ magnetic orbitals in the $(NC)_5B$–CN–$A(NC)_5$ binuclear unit.

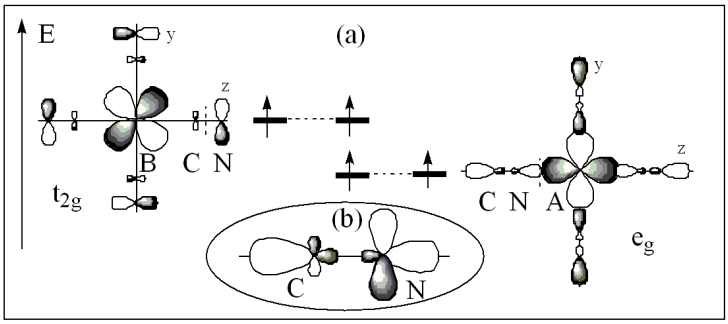

Fig. 9.9. Orthogonal magnetic orbitals in the $(NC)_5B$–CN–$A(NC)_5$ binuclear unit: (a) Orthogonal $\phi(t_{2g})(B)$ and $\phi(e_g)(A)$ orbitals left unchanged in the binuclear unit; (b) Insert: spin density in two orthogonal p orbitals of nitrogen (p_y and p_z).

special role of nitrogen; the $t_{2g}(B)$-$t_{2g}(A)$ pathways lead to antiferromagnetic (AF) interactions; as the $(\Delta - \delta)$ gap becomes larger, so does $|J|$.

9.3.2.4 Experimental Answers

We can use this orbital analysis to predict the nature of the interaction between various paramagnetic cations with a representative hexacyanometalate ion, $[Cr^{III}(CN)_6]$, in which the octahedral Cr^{III} center is spin 3/2 with a $(t_{2g})^3$ electronic configuration. The number and the nature of the exchange pathways are represented in Figure 9.10 and summarized in Table 9.1 for known divalent cations A^{II} of the first period of the transition elements, from V^{II} to Cu^{II}.

Table 9.1. Curie temperatures as a function of A in $A^{II}[Cr^{III}(CN)_6]_{2/3}\bullet xH_2O$

A^{II} ion	V	Cr	Mn	Fe	Co	Ni	Cu
Configuration d^n	d^3	d^4	d^5	d^6	d^7	d^8	d^9
Nature of the transition[a]	AF	AF	AF	F	F	F	F
T_C / K	330	240	66	16	23	60	66

[a] AF = ferrimagnetic, F = ferromagnetic

A simple overlap model predicts that A ions with d^3 through d^7 configurations should couple antiferromagnetically, and those with d^8 and d^9 configurations should couple ferromagnetically. As Table 9.1 shows, this prediction holds true except for the A = Fe and Co; the reasons for these exceptions will be discussed below.

If we now look at the results given in Figure 9.11 and Table 9.2 (including Ref [88–94]), we can check other aspects of the theoretical predictions given above.

To begin, comparisons between two particular compounds are especially interesting: Babel's $CsMn^{II}[Cr^{III}(CN)_6]\bullet H_2O$ is a ferrimagnet with T_C = 90 K, and Gadet's compound $CsNi^{II}[Cr^{III}(CN)_6]\bullet H_2O$ is a ferromagnet with the same ordering temperature. The T_C values are relatively high for molecule-based magnets, and this fact supports the conclusions of Figure 9.9 about the strength of ferromagnetic pathways. If the J values for the Ni and Mn derivatives are evaluated from formulae (9.1) and (9.4), we find that, if everything is equal, $J_{CrNi} \approx 2\ |J_{CrMn}|$ and that j_F, the mean coupling of a single ferromagnetic orbital pathway, and j_{AF}, the corresponding antiferromagnetic coupling, are roughly equal in absolute value. Similar conclusions about the importance of ferromagnetic pathways can be drawn from the study of discrete molecular analogs of Prussian Blues, for which J values can be computed using analytical expressions [95].

It is also interesting to compare the T_C values of Babel's and Gadet's compounds (which have six magnetic neighbors) with the ordering temperatures of related

Table 9.2. Curie temperatures T_C of Prussian Blue analogs.

Compound $C_xA_1[B(CN)_6]_z \bullet nH_2O$ [(a)]	Ordering Nature	T_C/K	Ref.
$K_1V^{II}{}_1[Cr^{III}(CN)_6]_1$	Ferri	376	41
$V^{II}{}_1[Cr^{III}(CN)_6]_{0.86} \bullet 2.8H_2O$	Ferri	372	89
$K_{0.5}V_1[Cr(CN)_6]_{0.95} \bullet 1.7H_2O$	Ferri	350	89
$Cs_{0.8}V_1[Cr(CN)_6]_{0.94} \bullet 1.7H_2O$	Ferri	337	41
$V^{II}{}_1[Cr^{III}(CN)_6]_{2/3} \bullet 3.5H_2O$	Ferri	330	41
$V_1[Cr^{III}(CN)_6]_{0.86} \bullet 2.8H_2O$	Ferri	315	30
$Cr^{II}{}_1[Cr^{III}(CN)_6]_{2/3} \bullet 10/3H_2O$	Ferri	240	32
$(Et_4N)_{0.4}Mn^{II}{}_1[V^{II}(CN)_5]_{4/5} \bullet 6.4H_2O$	Ferri	230	32
$Cs_{2/3}Cr^{II}{}_1[Cr(CN)_6]_{8/9} \bullet 40/9H_2O$	Ferri	190	29
$Cs_2Mn^{II}{}_1[V^{II}(CN)_6]_1$	Ferri	125	32
$(V^{IV}O)_1[Cr^{III}(CN)_6]_{2/3} \bullet 4.5H_2O$	Ferri	115	90
$Cs_1Mn^{II}{}_1[Cr^{III}(CN)_6]_1$	Ferri	90	71
$Cs_1Ni^{II}{}_1[Cr^{III}(CN)_6]_1 \bullet 2\text{-}4H_2O$	Ferro	90	28
$Mn^{II}{}_1[Cr^{III}(CN)_6]_{2/3} \bullet 5\text{–}6H_2O$	Ferri	66	37
$Cu^{II}{}_1[Cr^{III}(CN)_6]_{2/3} \bullet 5\text{–}6H_2O$	Ferro	66	37
$Ni^{II}{}_1[Cr^{III}(CN)_6]_{2/3} \bullet 4H_2O$	Ferro	53	28
$(NMe_4)Mn^{II}[Cr^{III}(CN)_6]$	Ferri	59	75
$Mn^{II}{}_1[Mn^{IV}(CN)_6]_1$	Ferri	49	66
$CsNi^{II}{}_1[Mn^{III}(CN)_6]_1 \cdot H_2O$	Ferro	42	33
$K_2Mn^{II}{}_1[Mn^{II}(CN)_6]_1 \bullet 0.5H_2O$	Ferri	41	31
$Co^{II}{}_3[Co^{II}(CN)_5]_2 \cdot 8H_2O$	Ferri	38	91
$Mn^{II}{}_1[Mn^{III}(CN)_6]_{2/3} \cdot 4H_2O$	Ferri	37	31
$Cs_1Mn^{II}{}_1[Mn^{III}(CN)_6]_1 \bullet 0.5H_2O$	Ferri	31/27	31
$Mn^{III}{}_1[Mn^{III}(CN)_6]_1$	Ferri	31	92
$Ni^{II}{}_1[Mn^{III}(CN)_6]_{2/3} \cdot 12H_2O$	Ferro	30	33
$Mn^{III}{}_1[Mn^{II}(CN)_6]_{2/3} \cdot$solvent	Ferri	29	92
$(Me_4N)Mn^{II}[Mn^{III}(CN)_6]$	Ferri	28.5	71
$V^{III}{}_1[Mn^{III}(CN)_6]_1$	Ferri	28	92
$Co^{II}{}_1[Cr^{III}(CN)_6]_{2/3} \bullet 4H_2O$	Ferro	23	37
$Ni^{II}{}_1[Fe^{III}(CN)_6]_{2/3} \bullet nH_2O$	Ferro	23	93
$Cr^{III}{}_1[Mn^{III}(CN)_6]_1$	Ferri	22	92
$Cu^{II}{}_1[Fe^{III}(CN)_6]_{2/3} \bullet nH_2O$	Ferro	20	88
$Co^{II}{}_1[Cr^{III}(CN)_6]_{2/3} \bullet nH_2O$	Ferro	19	37
$Fe^{II}{}_1[Cr^{III}(CN)_6]_{2/3} \bullet 4H_2O$	Ferro	16	37
$Co^{II}{}_1[Fe^{III}(CN)_6]_{2/3} \bullet nH_2O$	Ferri	14	88
$Cr^{II}{}_1[Ni^{II}{}_2(CN)_4]_{2/3} \bullet nH_2O$	Ferri	12	94
$Mn^{II}{}_1[Fe^{III}(CN)_6]_{2/3} \bullet nH_2O$	Ferri	9	88
$Fe^{III}{}_1[Fe^{II}(CN)_6]_{3/4} \bullet 3.7H_2O$	Ferro	5.6	95

[a] The formulae given in the Table were adapted from the literature by rescaling them to one A cation – $A_1[B(CN)_6]_z \bullet nH_2O$. We did not include explicitly the vacancies $A_1[B^{III}(CN)_6]_z\square_{1-z} \bullet nH_2O$. In the references the same compound is sometimes written with different formulas. For example, one can find nickel(II) hexacyanoferrate(III) written as $Ni^{II}{}_3[Fe^{III}(CN)_6]_2\square_1 \bullet nH_2O$, the simplest formula that indicates the neutral character of the precipitate but is not related to any special structural entity; as $Ni^{II}{}_4[Fe^{III}(CN)_6]_{8/3}\square_{4/3} \bullet 4n/3H_2O$, which is related to the conventional cell with four nickel(II) centres, in line with the Ludi's structural model; as $Ni^{II}{}_1[Fe^{III}(CN)_6]_{2/3}\square_{1/3} \bullet n/3H_2O$, based on one metal in the A sites, which is the one we adopted for simplicity; and as $Ni^{II}{}_{3/2}[Fe^{III}(CN)_6]_1 \bullet 3n/8\ H_2O$, based on one metal in the B sites, which is misleading because it suggests that there are no $[Fe^{III}(CN)_6]$ vacancies and that some of the nickel(II) ions are in the centre of the octant (Keggin model).

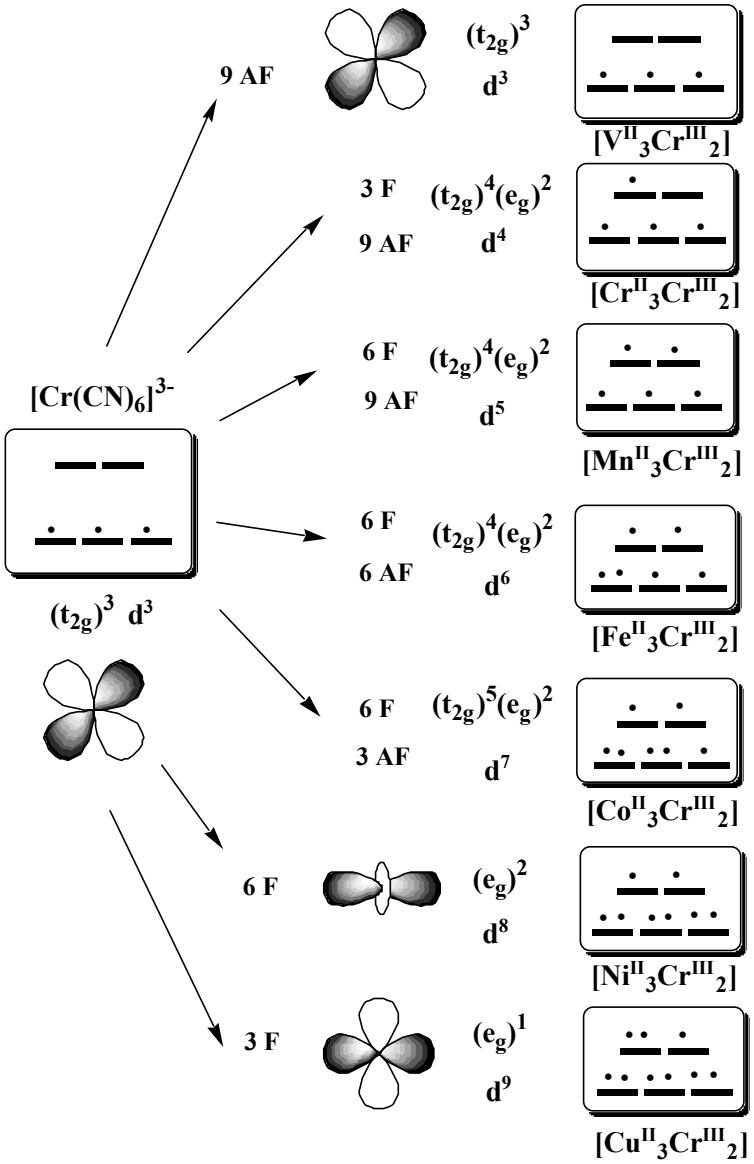

Fig. 9.10. Nature and number of exchange pathways between chromium(III) and the divalent transition metal ions of the first row of the periodic table.

$A_1B_{2/3}$ systems with the same A and B pairs but with four magnetic neighbors. The mean field theory predicts that the latter compounds should have ordering temperatures 4/6 times 90 K, or 60 K. In fact, the prediction is quite accurate: $Ni^{II}_2[Cr^{III}(CN)_6]_3 \bullet xH_2O$ has T_C = 53 K and $Mn^{II}_2[Cr^{III}(CN)_6]_3 \bullet xH_2O$ has T_C = 60 K.

A more subtle prediction of the ligand field and exchange models is that early transition metals should give higher exchange interactions thanks to a better interaction of their d orbitals with the π^* orbitals of the bridging cyanide. The example

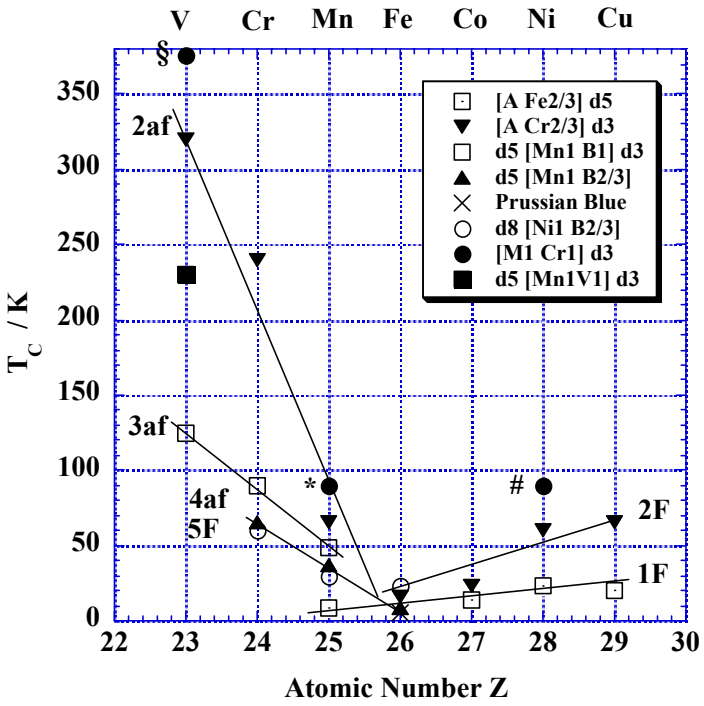

Fig. 9.11. Variation of the experimental Curie temperatures of series of MPBs $A_1[B(CN)_6]_z$ as a function of the atomic number *Z*, for different stoichiometries and electronic structures of the A and B transition metal elements: (a) Series 1F: $A_1Fe(CN)_6]_{2/3}$; (b) Series 2F and 2af: $A_1Cr(CN)_6]_{2/3;}$ (c) Series 3af: $Mn_1[B(CN)_6]_1$; (d) Series 4af: $Mn_1[B(CN)_6]_{2/3;}$ (e) Series 5F: $Ni_1[B(CN)_6]_{2/3}$; (f) Selected compounds: × Prussian blue; §, $KV[Cr(CN)_6]$; *, $CsMn[Cr(CN)_6]$; #, $CsNi[Cr(CN)_6]$; elements A or B are shown by their atomic number *Z* (bottom) and their symbol (top) (See table 2 for numerical values).

of $Cs_2Mn^{II}[V^{II}(CN)_6]\bullet H_2O$ synthesized and published by Girolami in 1995 is especially revealing [31]. This material is a ferrimagnet with a Néel temperature of 125 K. It can be compared with the two other *isoelectronic* Prussian Blue analogs, $CsMn^{II}[Cr^{III}(CN)_6]\bullet H_2O$ and $Mn^{II}[Mn^{IV}(CN)_6]\bullet xH_2O$. All three compounds have high-spin d^5 Mn^{II} centers in the weak ligand-field sites (N_6 coordination environments) and furthermore d^3 metal centers in the strong ligand-field sites (C_6 coordination environments). The main differences are the oxidation states of B, which increase as the metal changes from V^{II} to Cr^{III} to Mn^{IV}, and the energies and the expansion of the B t_{2g} orbitals, which decrease in the same order. The relative magnetic ordering temperatures of 125, 90, and 49 K for these three materials clearly show that incorporation of transition metals with higher-energy and more diffuse t_{2g} orbitals into the strong ligand field sites leads to higher magnetic ordering temperatures. As the backbonding with the cyanide π^* orbitals becomes more effective, the coupling between the adjacent spin centers increases, and so does T_C.

9.3.3 Quantum calculations

The above qualitative theoretical approach was based on simple symmetry or energy considerations and did not rely on precise quantum calculations. The apparent simplicity of the structure of Prussian Blues (especially the linearity of the A–N≡C–B linkages and the octahedral environments of A and B), and the availability of a large set of experimental data constitute a favorable situation for theoreticians to compute, reproduce, and predict the magnetic properties of Prussian Blue analogs, including their magnetic ordering temperatures T_C. It is therefore not surprising that several theoretical methods at various level of sophistication have been applied to magnetic Prussian Blues.

In volume II of this series, in a chapter entitled "Electronic Structure and Magnetic Behavior in Polynuclear Transition-metal Compounds," Ruiz, Alvarez and coworkers present different theoretical models of exchange interactions [96]. They point out that the study of the electronic structure of coupled systems is more challenging than that of closed-shell molecules, in large part because the J values are several orders of magnitude smaller than the total energy of the system. They point out that "no single qualitative model [is] able to explain satisfactorily all features of exchanged coupled systems and there are still a number of controversies about the advantages and limits of the various approaches that have been devised." Other sources of valuable information about theoretical treatments of molecule-based magnets are the books by Kahn [7] and Boca [97].

In the following sections, we focus on some computational studies of Prussian Blues. We start with semi-empirical calculations (extended Hückel), which allow the considerations in the preceding section to be evaluated semi-quantitatively. Then we present some results obtained from density functional calculations based on the broken symmetry approach [96]. Finally, a perturbative approach by Weihe and Güdel is briefly presented.

9.3.3.1 Extended Hückel calculations

The antiferromagnetic contribution J_{AF}

We performed extended Hückel calculations on a series of bimetallic dinuclear units $[(CN)_5A^{II}–N≡C–B^{III}(CN)_5]$, where A = Ti, V, Cr, Mn, Fe, or Co and B = Ti, V, Cr, Mn, or Fe [36, 98–100]. All of the B ions have $(t_{2g})^n$ electron configurations; the A ions possess no more than seven d-electrons, so that in the high-spin state they also have partly filled t_{2g} orbitals. As a result, there is always at least some antiferromagnetic contribution to the exchange between A and B. All bond distances were kept fixed for all the combinations.

As shown previously in Figure 8, key features of Prussian Blue analogs are interactions (via the cyanide ligands) of a t_{2g} orbital on one metal center with a t_{2g} orbital on an adjacent metal center. Although in a binuclear model system some

of the pairwise t_{2g}-t_{2g} interactions are zero by symmetry, in a three-dimensional Prussian Blue network every t_{2g} orbital can find a related orbital on a neighboring metal center with which it can interact strongly. Owing to the symmetry of the Prussian Blue structure, it is sufficient to analyse the interaction for a single pair of orbitals and to sum all the combinations presented by a three-dimensional network. Two of the possible interactions between t_{2g} and e_g orbitals are also shown in Figure 9.9. In this case the overlap is zero and the exchange interaction is strictly ferromagnetic. Although a direct estimation of the strength of this ferromagnetic contribution is not possible in the frame of semi-empirical methods, we will describe below how qualitative estimates can be obtained. From Eq. (9.11), the antiferromagnetic contribution to the coupling J is given approximately by the expression $2\ S\ (\Delta^2 - \delta^2)^{1/2}$, where δ is the energy gap between the (unmixed) a and b orbitals, Δ is the energy gap between the molecular orbitals built from them, and S is the monoelectronic overlap integral between a and b. For each pair of metals in the list above, the values of Δ and δ (Figure 8) have been calculated. Some features may be highlighted by decomposing the antiferromagnetic term as $(\Delta^2 - \delta^2) = (\Delta - \delta)\ (\Delta + \delta)$. Indeed, two effects contribute to the tendency of the electrons to pair: (i) a strong interaction between the two magnetic orbitals, which stabilises the bonding molecular orbital (the strength of the interaction is gauged by the term $\Delta - \delta$), and (ii) the stabilization of charge transfer states in which an electron is tranferred from one magnetic orbital to the other (the importance of this phenomenon is gauged by the term $\Delta + \delta$). Therefore, to have a strong antiferromagnetic interaction, it is best if both $(\Delta - \delta)$ and $(\Delta + \delta)$ are large. It should be noted that there is a non-trivial dependence of Δ on δ. The energy gap after mixing, Δ is equal to the energy gap before mixing, δ plus the energy change upon mixing, but the energy change is enhanced when δ is small. Thus, $(\Delta - \delta)$ becomes larger as δ becomes smaller, whereas $(\Delta + \delta)$ becomes larger as δ becomes larger.

Our calculations show that both Δ and δ have similar trends: their values are maximized when metal atoms A and B possess d orbitals of very different energy, and minimized when they are very similar. Such behaviour can be understood with the help of Figure 7a and b (and Figure 5 in Ref. [99], not reproduced here). The energies of the t_{2g} orbitals on the A and B metals are affected by interactions with both the low-energy filled CN π orbitals (a destabilizing interaction) and the high-energy empty CN π^* orbitals (a stabilizing interaction involving back-donation). As a general rule, the metal-carbon interaction is stronger than the metal-nitrogen interaction, and both interactions are stronger for the early transition metals, which possess higher energy and more diffuse d orbitals (low values of the ζ coefficient). The final energy of the t_{2g} orbitals also depends on the relative energies of the (unmixed) d orbitals on the metallic ions with respect to the energy of the (unmixed) cyanide π and π^* orbitals. Our calculations show that the stabilizing interaction with the cyanide π^* orbitals dominates (thus lowering the t_{2g} orbital energies) when the A sites are occupied by Ti^{II}, V^{II}, or Cr^{II}, but that the interactions with the

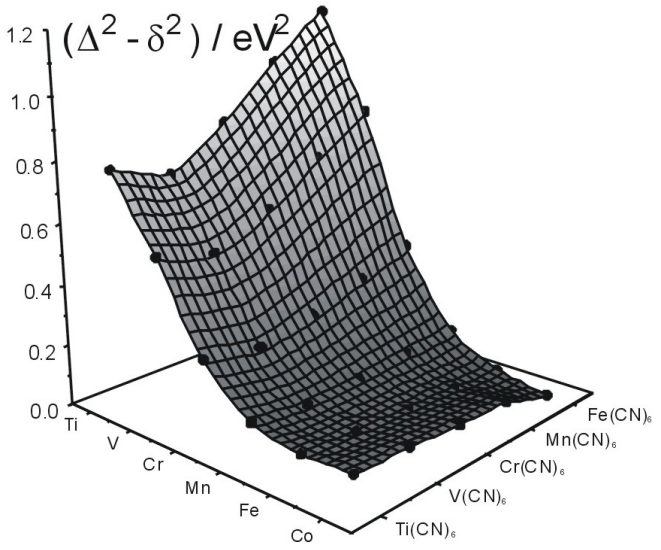

Fig. 9.12. Plot of the quantity $(\Delta^2 - \delta^2)$ obtained from Extended Hückel calculations for a series of binuclear complexes $[(CN)_5A^{II}(\mu\text{–}NC)B^{III}(CN)_5]$ with A = Ti to Co and B = Ti to Fe (see text).

cyanide π and π^* orbitals cancel each other out (thus leaving the energies of the t_{2g} orbitals unchanged) when the A sites are occupied by Mn^{II}, Fe^{II}, or Co^{II}. This delicate balance affects the composition of the magnetic orbitals and the overlap between them. In Figure 9.12 the corresponding $(\Delta^2 - \delta^2)$ values are shown. The higher $(\Delta^2 - \delta^2)$ values are seen for the $[(CN)_5Ti^{II}\text{–}N{\equiv}C\text{–}B^{III}(CN)_5]$ dinuclear units, and the highest value of all is found for the $Ti^{II}Fe^{III}$ couple. This result, which at first seems counter-intuitive, is understandable once one recalls the effect of the cyanide π and π^* orbitals on the energies the d orbitals. Indeed, for such a $Ti^{II}Fe^{III}$ system, the values of $(\Delta + \delta)$ and $(\Delta - \delta)$ are both maximized: $(\Delta + \delta)$ is large because the t_{2g} orbitals on Ti and Fe are so different in energy, and $(\Delta - \delta)$ is large because the diffuseness of the d orbital on Ti promotes efficient overlap between the magnetic orbitals. The calculated surface suggests that Prussian Blue compounds containing an early transition metal A cation should always possess strong antiferromagnetic interactions, irrespective of the identity of the B metal ion (this is one of the important qualitative arguments presented in a preceding section).

As predicted by the Néel expression (Eq. (9.9), the T_C values of MPB analogs depend not only on the strength of J_{AF} but also on the number of unpaired spins n_A and n_B on both sites and the number of possible interactions $N = n_A n_B$ between them. Taking this effect into account, we multiply $(\Delta^2 - \delta^2)$ by the factor $n_A n_B \sqrt{(n_A + 2)(n_B + 2) / n_A n_B}$ to obtain the new surface shown in Figure 9.13.

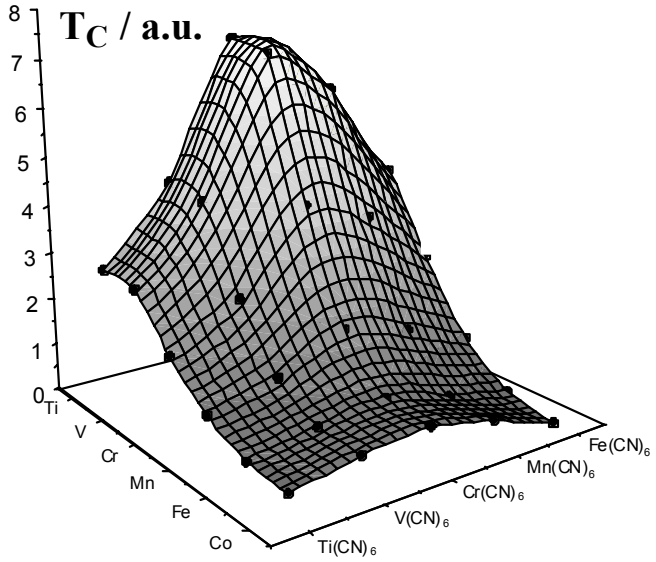

Fig. 9.13. Plot of the quantity $(\Delta^2 - \delta^2)\ N\ \sqrt{(n_A + 2)\,(n_B + 2) / n_A n_B} \propto T_C$ (arbitrary units) (see text).

The surface should mirror the T_C values of MPB compounds made with A and B metals from the first transition series. Indeed, these calculated trends agree well with the experimental ones (see Table 2), both predicting that the maximum T_C value should be found for the $V^{II}Cr^{III}$ pair.

The ferromagnetic contribution J_F

Although the ferromagnetic contribution to J cannot be explicitly calculated, some information about it can be obtained even from simple extended Hückel calculations. The exchange integral k_{ab} is directly proportional to the squared overlap density defined in Eq. (9.11) $\rho_{ab} = |a\rangle\ |b\rangle$. This contribution to the exchange interaction is always present, and it becomes the only contribution when the overlap S_{ab} between the two orbitals is zero. This is the case for the t_{2g}-e_g interactions in MPB analogs, where the overlap is zero by symmetry. The T_C values of up to 90 K found for those compounds that solely possess ferromagnetic pathways indicate that the ferromagnetic interaction can be quite strong.

To verify the presence of high $\rho_{t2g\text{-}eg}$ overlap density zones, we began with the results of the extended Hückel calculations described above for the dinuclear model complexes $[(NC)_5A^{II}–N{\equiv}C–Cr^{III}(NC)_5]$, where A = Co, Ni, or Cu, and B = Cr. The product $\rho_{t2g\text{-}eg}$ could be visualised by plotting projections of the magnetic orbital compositions taken directly from the extended Hückel output. Owing to their influence on the density overlap, both the angular and radial normalisation constants for all the single atomic wavefunctions were carefully checked. Figure 9.14 shows

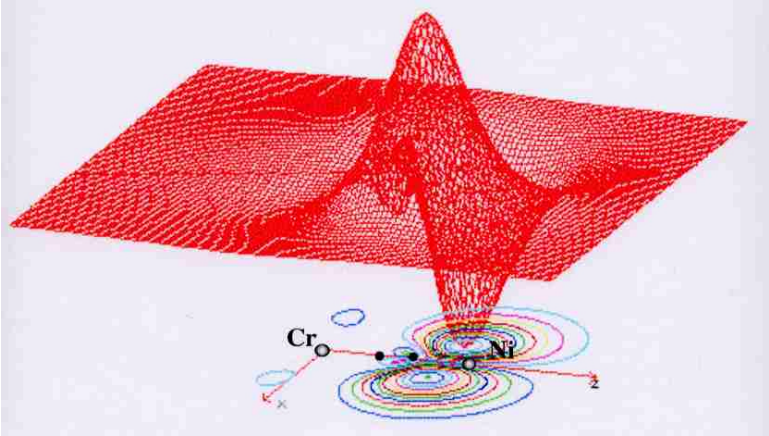

Fig. 9.14. Overlap density in the *xz* plane between the $\phi(t_{2g})$ *xz*-type magnetic orbital centered on Cr and the $\phi(e_g)$ z^2-type magnetic orbital centered on Ni.

the overlap density (in the *xz* plane) between the t_{2g} *xz*-type magnetic orbital centered on Cr and the e_g z^2-type magnetic orbital centred on Ni. The overlap density is symmetric with respect to the *z* axis.

A similar result was obtained for the monoatomic μ-oxo bridge in a Cu–VO complex [87]. Our result is counterintuitive for a diatomic bridge, where the spin density for the atom farthest from the metallic centre is expected to be low. Indeed, it is the strong delocalisation of the spin density on the nitrogen in the $[B(CN)_6]$ units that allows the strong overlap density and the strong ferromagnetic interaction. In contrast, for a μ-oxalato bridge, where the spin density is spread over the entire molecule, the overlap density is weak and so is the coupling [210].

9.3.3.2 Density Functional Theory Calculations

Progress in computer speed and memory and in density functional theory (DFT) techniques now make it possible to carry out calculations on very complex systems. Magnetic Prussian Blues are indeed complex systems to treat computationally. For example, the number of unpaired electrons per formula unit can be as high as 8 (as in a Cr^{III}–Mn^{II} system)

DFT computations on magnetic Prussian Blues were performed on two model systems, dinuclear complexes $[(CN)_5A–N{\equiv}C–B(CN)_5]$ and ideal face-centered-cubic extended solids. For a system with two identical centres A and B and one electron per centre, the method can be briefly summarized as follows.

For two orthogonal orbitals ϕ_a and ϕ_b, the spin eigenfunctions of the system are:

$$\Psi_{S,0} = (1/\sqrt{2})(|\phi_a\alpha\phi_b\beta - \phi_a\beta\phi_b\alpha|) \quad (9.12a)$$

$$\Psi_{T,0} = (1/\sqrt{2})(|\phi_a\alpha\phi_b\beta + \phi_a\beta\phi_b\alpha|)\ ;\ \Psi_{T,+1} = (1/\sqrt{2})(|\phi_a\alpha\phi_b\alpha|)\ ;$$
$$\Psi_{T,-1} = (1/\sqrt{2})(|\phi_a\beta\phi_b\beta|) \quad (9.12b)$$

Because the singlet state cannot be described by one single configuration, the J value ($J = E_S - E_T$) cannot be computed directly. Noodleman suggested a broken-symmetry (BS) solution [96, 211–213]:

$$\Phi_{BS} = |\phi_a \alpha \phi_b \beta| \quad \text{or} \quad \Phi'_{BS} = |\phi_a \beta \phi_b \alpha| \tag{9.13}$$

which is a mixed state, a combination of $\Psi_{S,0}$ and $\Psi_{T,0}$:

$$\Phi_{BS} = (1/\sqrt{2})[\Psi_{S,0} + \Psi_{T,0}] \tag{9.14}$$

The corresponding energy is $E_{BS} = (1/\sqrt{2})(E_S + E_T)$ and the coupling is given by:

$$J = 2\,(E_{BS} - E_T) \tag{9.15}$$

In the context of DFT calculations, therefore, it is possible to compute J from the energy of the broken symmetry state and the high spin state. Depending on the kind of calculations (HF, UHF, DFT, …) and the existence of some "spin-projection" process [96], other expressions of J have been used, such as:

$$J = 2\,(E_{BS} - E_{HS}) / S^2_{HS} \tag{9.16}$$

The main conclusion is that J can be obtained in a reasonable computing time from the difference of two energies. The calculation can be extended to systems with more than one electron per metal centre.

Dinuclear models

The first DFT papers on dinuclear models of Prussian Blues were published by Nishino, Yamaguchi et al. [101–103]. Their work continues a longstanding theoretical tradition of studying open-shell spin systems [81, 82, 84, 104, 105]. The first two papers deal with very simple A–N≡C–B systems in which there is only one bridge and no other ligands are attached to A and B [101, 102]. The third paper deals with $[(CN)_5A–N≡C–B(CN)_5]$ units [103]. In all three papers, the symmetry rules that we applied before are used to analyze the d-d orbital interactions. The correct sign of the effective exchange integrals J is found. The authors carried out ab initio unrestricted Hartree Fock (UHF) and DFT calculations to elucidate the nature of the magnetic orbitals.

For the unligated V^{II}–N≡C–Cr^{III} and Ni^{II}–N≡C–Cr^{III} units, the magnitudes of the calculated exchange integrals were much larger than the experimental values found for real dinuclear systems. We focus therefore on the last paper, which deals with more realistic situation in which the A and B centres have octahedra lcoordination environments. Figure 15a shows the orbital interaction in the A–N≡C–B entity. Figure 15b displays the molecular orbitals ϕ_A (HOMO) and ϕ_S (LUMO) built from the t_{2g} orbitals of the A and B metals and the π and π^* MOs of the cyanide ligand; these molecular orbitals are, respectively, (pseudo)antisymmetric and (pseudo)symmetric relative to a plane bisecting the A–B

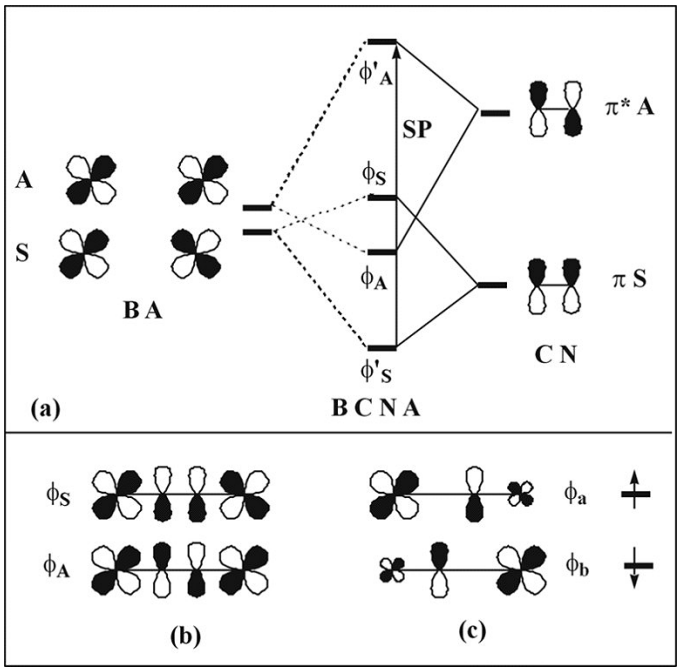

Fig. 9.15. (a) Orbital interaction schemes in the B–CN–A entity; (b) symmetric (S) and antisymmetric (A) natural MOs; (c) magnetic orbitals obtained by mixing the S and A MOs (adapted from Ref. [103]) (see text).

axis. Figure 9.15c represents the magnetic orbitals ϕ_a and ϕ_b built from ϕ_A and ϕ_S according to the relations within the UHF and DFT approximations:

$$\phi_a \text{ (spin up } \alpha) = \cos\theta\ \phi_A + \sin\theta\ \phi_S \quad (9.17a)$$

$$\phi_b \text{ (spin down } \beta) = \cos\theta\ \phi_A - \sin\theta\ \phi_S \quad (9.17b)$$

Then the authors apply the Heisenberg model to describe the energy gaps between the ferromagnetic (HS) and antiferromagnetic (LS) states and, using the approximate spin projection procedure (AP), find the following expression for the effective exchange integrals J_{AB} with various methods (X = UHF, DFT); the authors use the Hamiltonian $H = -2\ J_{AB}\ S_A\ S_B$:

$$J_{AP-X} = ({}^{LS}E_X - {}^{HS}E_X) / [{}^{HS}\langle S^2\rangle_X - {}^{LS}\langle S^2\rangle_X] \quad (9.18)$$

In addition to calculating J values, they also obtained an orbital picture of the exchange phenomenon and values for the atomic spin densities. Using the molecular field approach (Langevin–Weiss–Néel), they also computed Curie temperatures for the solid from the expression:

$$T_C = \sqrt{Z_A\, Z_B}\ |J_{AB}|\ \sqrt{S_A\,(S_A+1)\,S_B\,(S_B+1)}\ /\ 3k_B \quad (9.19)$$

where k_B is Boltzmann's constant, Z_A and Z_B are the numbers of magnetic neighbors of A and B, respectively, and S_A and S_B the spins of A and B. Some of their results are collected in Table 9.3.

Table 9.3.[a] Comparison of the computed J[b] and T_C[c] values with experiment.

System A–B	S_B	S_A	J_{AB}/cm^{-1}	T_C/K (calc)	T_C/K (exp)
Ni^{II}–Cr^{III}	3/2	1	+ 15.92	125	90
Ni^{II}–$Cr^{III}_{2/3}$				102	53
Mn^{II}–Cr^{III}	3/2	5/2	–7.01	116	90
Mn^{II}–$Cr^{III}_{2/3}$				95	60
V^{II}–$Cr^{III}_{2/3}$	3/2	3/2	–75.56	815	(315)[d]
V^{III}–Cr^{III}	3/2	1	–31.24	246	(315)[d]
Mn^{II}–V^{II}	3/2	5/2	–14.49	239	125

[a] Adapted from Ref. [103] and Table 9.2. [b] J is computed in a $[(NC)_5A–C{\equiv}N–B(NC)_5]$ model. [c] From Eq. (9.19). [d] The sample contains both V^{II} and V^{III}.

The agreement between computation and experiment is not exact, but to obtain a better fit the authors suggest the empirical law:

$$T_C\,(\text{exp}) = 1.2\ T_C\ (\text{calc}) - 49.9\ \text{K} \tag{9.20}$$

This expression gives very good agreements between experimental and theoretical values. The very large value for $|J|$ in the V^{II}–$Cr^{III}_{2/3}$ system (which is ten times larger than the value found for the Mn^{II}–Cr^{III} system) can be related to the strong participation of V^{II} in the ϕ_b orbital (Figure 9.15) compared to the Mn^{II}, whose orbitals are well localized (Figure 3 in [103], not shown here). Important new information provided by these calculations are the atomic spin densities. Some significant results are collected in Table 9.4.

Table 9.4 [a] Atomic spin densities in $[(NC)_5A–C{\equiv}N–B(NC)_5]$from UB2LYP methods

System A–B	$2S+1$[b]	A[c]	C[c]	N[c]	B[c]
Ni^{II}–Cr^{III} AF	2	–1.73	–0.12	0.07	3.06
Ni^{II}–Cr^{III} F	***6***	***+1.73***[d]	***–0.16***	***0.19***	***3.06***
Mn^{II}–Cr^{III}AF	***3***	***–4.75***[d]	***–0.17***	***0.12***	***3.05***
Mn^{II}–Cr^{III} F	9	+4.76	–0.09	0.11	3.06
V^{III}–Cr^{III} AF	***2***	***–2.02***[d]	***–0.17***	***0.15***	***3.06***
V^{III}–Cr^{III} F	6	+2.02	–0.05	0.04	3.06
V^{II}–Cr^{III} AF	***1***	***–2.82***[d]	***–0.23***	***0.19***	***3.03***
V^{II}–Cr^{III} F	7	+2.85	–0.04	0.05	3.06
Mn^{II}–V^{II} AF	***3***	***–4.74***[d]	***–0.14***	***0.14***	***2.63***
Mn^{II}–V^{II} F	9	+4.76	–0.07	0.15	2.66

[a] Adapted from Ref. [103]. [b] Spin multiplicity for the computed states (AF = antiferromagnetic coupling; F = ferromagnetic coupling). [c] Spin densities of A, C, N, and B; a positive sign means that the magnetic moments are aligned along the field and a negative sign the reverse. [d] Spin multiplicities shown in bold italics correspond to the coupling observed experimentally.

From Table 9.4, it can be concluded that (i) the chromium(III) centers bear the spin density foreseen from its +3 valence; in contrast, the spin density of vanadium(II) is significantly decreased by delocalisation; (ii) the carbon atom always bears a negative spin density, an observation that is consistent with Figgis's spin polarized neutron diffraction study of $[Cr^{III}(CN)_6]$ salts [78]; this effect is due to spin polarisation (SP) and is represented by the authors by the spin-flip excitation from the ϕ_S' to ϕ_A' orbitals shown in Figure 9.15; when the spin densities are decomposed into σ and π components, the SP effect is more significant for the π than for the σ network; (iii) there is a significant positive spin density on nitrogen atoms of the bridge; (iv) the spin density on the A ion is always less than expected from the valence, thus suggesting that there is significant spin delocalisation.

These calculations provide quantitative information about the mechanism of the exchange interaction through the cyanide bridge. One striking observation of the article is that, without cyanide bridging ligand, at the same A–B distance, the A–B interaction becomes negligibly small.

DFT calculations have also been carried out for the homodinuclear complexes L_nCu^{II}–N≡C–$Cu^{II}L_n$ and L_nNi^{II}–N≡C–$Ni^{II}L_n$ [106] based on the computational procedures described in Ref. [108]. The results are relevant to dinuclear complexes but not to Prussian blues, and thus this work is outside the scope of the present review.

At present, additional computations on various dinuclear models of Prussian blues are in progress, including a study of the effect of incorporating metals of different oxidation states or from the second row of the d-block, in order to determine whether larger J and T_C values than those found in the vanadium-chromium derivatives can be achieved. Indeed, larger $|J|$ values are foreseen [108].

Three-dimensional models

At approximately the same time as the computations on the molecular dinuclear models, three articles appeared on DFT calculations of three-dimensional networks, using computation packages adapted for solids [109–111]. These studies afforded important insights into the band structure and density of states (DOS, spin-polarized or not), the atomic spin density in the solid, and the crystal orbital overlap populations (COOP), a concept introduced by Hoffmann [112].

The first brief paper by Siberchicot was based on a local-spin-density approximation using the augmented spherical wave (ASW) method and including spin-orbit coupling [109]. Two species were studied: the ferromagnet $CsNi[Cr(CN)_6]$ [27] and the ferrimagnet $CsMn[Cr(CN)_6]$ [70]. The calculated magnetic moments (spin and total – spin+orbital) were in good agreement with the experimental values. The spin polarized partial densities of states on the chromium and nickel clearly showed semiconducting behaviour with a rather large gap at the Fermi level E_F, and localized d bands near E_F. The d band is split in energy by the octahedral ligand

field. For both solids, the empty $(e_g)^{0\downarrow}$ levels derived from the Cr^{III} orbitals are above the Fermi level.

In $CsNi[Cr(CN)_6]$, the filling of the d-bands is:

$[Ni^{II}]$: $[(t_{2g})^3(e_g)^2]^{\uparrow}$ $[(t_{2g})^3(e_g)^0]^{\downarrow}$,
$[Cr^{III}]$: $[(t_{2g})^3(e_g)^0]^{\uparrow}$ $[(t_{2g})^0(e_g)^0]^{\downarrow}$

The band structure is consistent with the observed ferromagnetic coupling between Ni^{II} and Cr^{III}. In comparison, for $CsMn[Cr(CN)_6]$ the filling is:

$[Mn^{II}]$: $[(t_{2g})^3(e_g)^2]^{\uparrow}$ $[(t_{2g})^0(e_g)^0]^{\downarrow}$,
$[Cr^{III}]$: $[(t_{2g})^3(e_g)^0]^{\downarrow}$ $[(t_{2g})^0(e_g)^0]^{\uparrow}$

which agrees with the experimental antiferromagnetic coupling between Mn^{II} and Cr^{III}.

The same two species were studied in more detail by Eyert and Siberchicot [110]. Again a local density approximation was employed, using augmented spherical waves (ASW) in scalar-relativistic implementations, taking particular care in the optimisation of empty spheres and to the Brillouin zone sampling. A new feature was the evaluation of the crystal orbital overlap populations, which permitted an assessment of the chemical bonding in the solid [112, 113]. The electronic structure was analysed by means of two sets of calculations, one non-magnetic and the other magnetic, the first serving as a reference for the discussion of the magnetic configurations.

The density of states and COOP analyses suggested the following: in the two compounds, the band structure reflects mainly the strong bonding within the cyanide and the ligand field splitting. In contrast, near the Fermi level (from –1.2 eV to 0.5 eV), the situation is completely changed: in the manganese derivative, the bands mix and split in a way reminiscent of the t_{2g}–t_{2g} overlaps in Figure 9.8, whereas in the nickel compound, they do not (as in Figure 9.9, t_{2g}–e_g). This difference has dramatic consequences for the magnetic properties.

The spin-polarized calculations demonstrate that the ground state is indeed ferrimagnetic in $CsMn[Cr(CN)_6]$ and ferromagnetic in $CsNi[Cr(CN)_6]$ (the ferrimagnetic state of $CsNi[Cr(CN)_6]$ is computed to be 9.8 mRyd higher in energy than the ferromagnetic state). The computed atomic moments are given in Table 9.5.

The spin-polarized densities of states for $CsMn[Cr(CN)_6]$ are given in Figure 9.17 and beautifully illustrate the opposite polarisations of the metallic bands $[Cr(t_{2g})^3]^{\uparrow}$ (at –1.5eV) and $[Mn(t_{2g})^3(e_g)^2]^{\downarrow}$ (at –2.0 and –0.5 eV). In addition, the polarisations of the bridging carbon and nitrogen atoms in the same energy range help to explain the mechanism of the polarisation. Indeed, a close examination of the spin polarized DOS in the Fermi level region level led the authors to "point out that the overlap of magnetic orbitals already present in the non-magnetic configuration completely fixes the antiferromagnetic coupling while disallowing a ferromagnetic correlation".

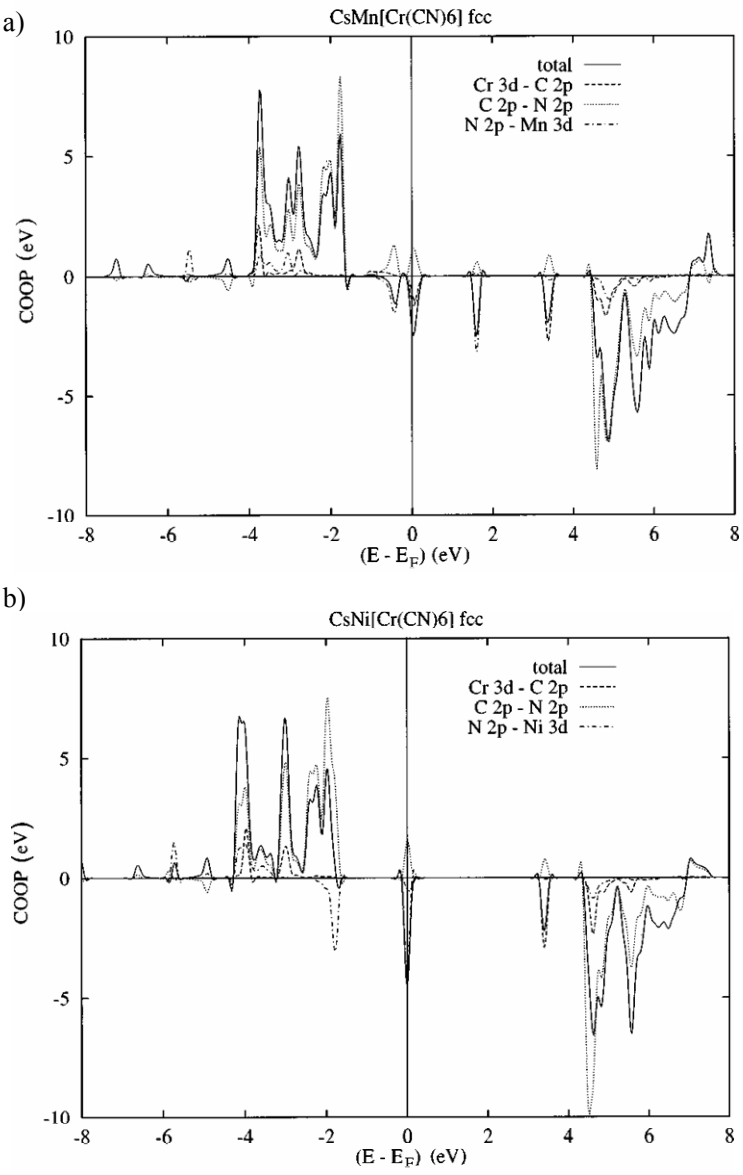

Fig. 9.16. Total and partial crystal orbital overlap populations (COOP): (a) in $CsMn[Cr(CN)_6]$; (b) in $CsNi[Cr(CN)_6]$ (from Ref. [110]).

An analogous demonstration results from the spin-polarized densities of states for $CsNi[Cr(CN)_6]$, given in Figure 9.18, where now the orthogonality of the $[Cr(t_{2g})^3]^{\uparrow}$ and the $[Ni(e_g)^2]^{\uparrow}$ orbitals leads to identical polarisations of these bands. The densities of states also show that the carbon and nitrogen atoms participate significantly in the exchange mechanism.

One important conclusion that can be drawn from this study is that the electronic interactions present three-dimensional Prussian Blue solids are very similar to those seen in discrete molecular analogs. Furthermore, exchange models such as that proposed by Kahn and Goodenough–Kanamori, involving t_{2g}–t_{2g} overlap and

Table 9.5. Local magnetic moments in $CsA[Cr(CN)_6]$ (A = Mn, Ni).[a]

Atom	μ/μ_B in $CsMn[Cr(CN)_6]$	μ/μ_B in $CsNi[Cr(CN)_6]$
Cs	0.001	0.001
A	–4.200	1.369
Cr	2.658	2.717
C	–0.061	–0.046
N	0.001	0.129
Cell	–2.000	5.000

[a] Adapted from Ref. [110].

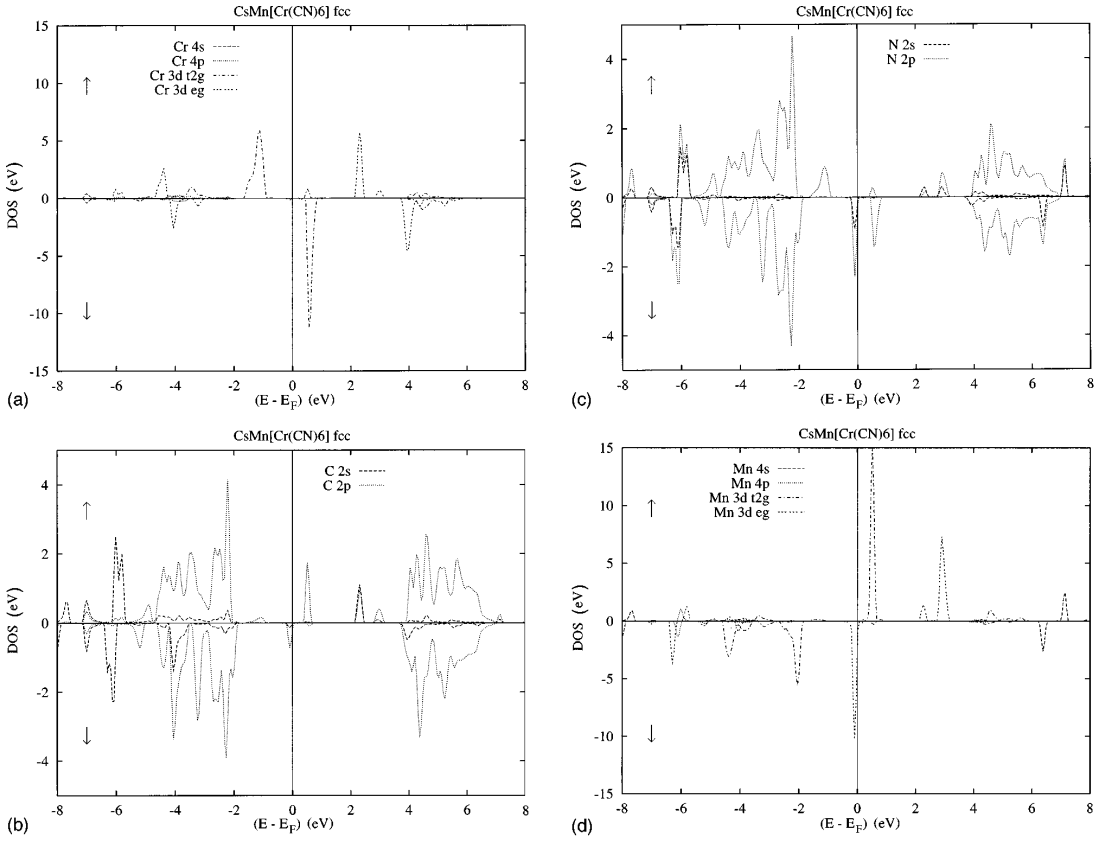

Fig. 9.17. Spin polarized partial densities of states of ferrimagnetic $CsMn[Cr(CN)_6]$ (from Ref. [110]).

orthogonality of the t_{2g} and e_g orbitals as described in Figures 9.8 and 9.9, do in fact constitute accurate descriptions of the electronic structures of Prussian Blues in the solid state, particularly near the Fermi level. The DFT calculations, however, afford much more quantitative information about the resulting magnetic properties.

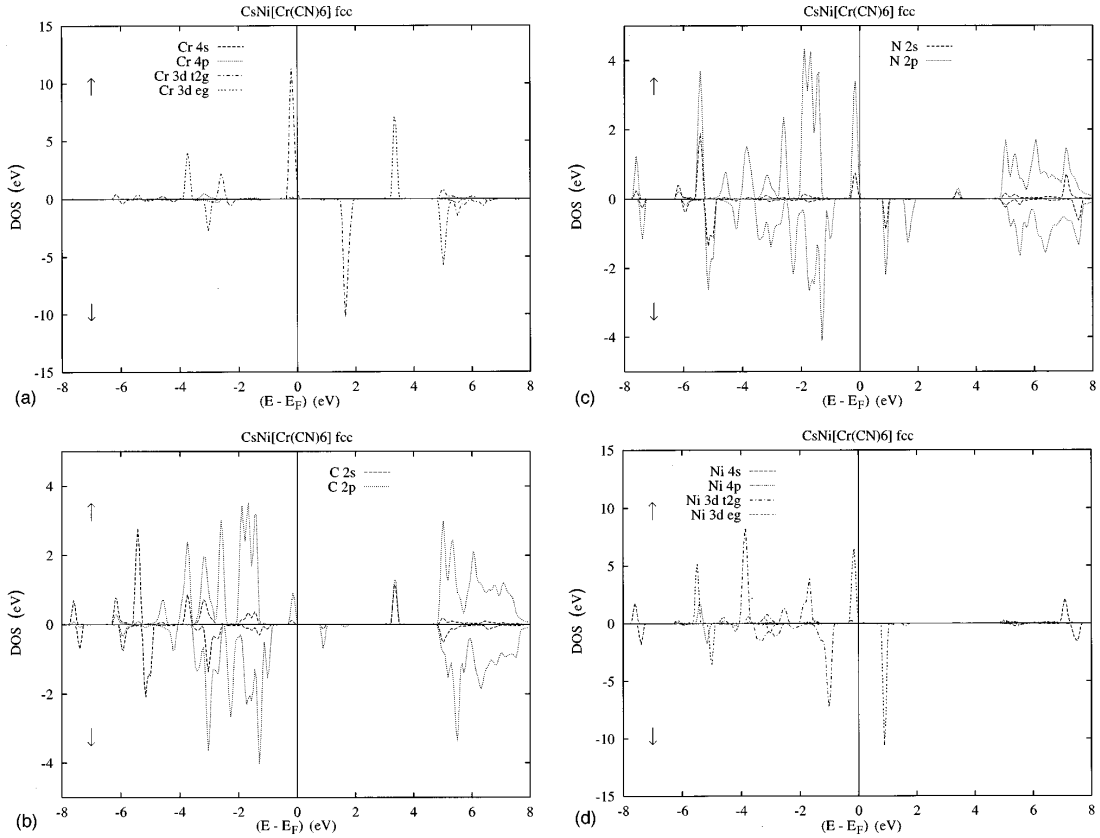

Fig. 9.18. Spin polarized partial densities of states of ferromagnetic $CsNi[Cr(CN)_6]$ (from Ref. [110]).

Periodic UHF – CRYSTAL calculations

Harrison et al. [111] carried out a study of several Prussian Blue compounds using the periodic Unrestricted Hartree-Fock approximation as implemented in the CRYSTAL package. The compounds studied were $KA[Cr(CN)_6]$ (A = V, Mn, Ni) and $Cr[Cr(CN)_6]$. Structural optimisation was performed, and the optimized structures closely resemble those determined experimentally. To compare the energies of the various magnetically ordered states, they obtained self-consistent field solutions, sometimes using a "spin-locking" procedure to constrain the initial total spin. The authors calculated the magnetic ordering energies and the relative contributions of exchange, kinetic and Coulomb interactions according to Anderson's model [114], as shown in Table 9.6.

The total energies clearly show the strong stabilisation of the ferrimagnetic state in the Cr^{III} and V^{II} compounds (corresponding to high T_Cs) and of the ferromagnetic state in the Ni^{II} derivative. From these results and an analysis of the Mulliken spin populations, the authors conclude that "an ionic picture of the metal-ligand interactions and a superexchange model of the magnetic coupling naturally emerges from first principles calculations of the ordering energetics of bi-metallic cyanides.

Table 9.6. Magnetic ordering energies in $Cr^{III}[Cr^{III}(CN)_6]$ and $KA^{II}[Cr^{III}(CN)_6]$ models.[a]

A	d configuration	Total [b,c]	Exchange [b]	Kinetic [b]	Coulomb [b]
Cr^{III}	$(t_{2g})^3$	4.33	14.70	–12.57	2.20
V^{II}	$(t_{2g})^3$	4.40	9.91	–2.78	–2.74
Mn^{II}	$(t_{2g})^3(e_g)^2$	0.79	14.70	0.29	–0.75
Ni^{II}	$(t_{2g})^6(e_g)^2$	–1.78	–7.49	5.60	0.11

[a] Adapted from Ref. [111]. [b] Values are in milliHartree. [c] positive values favor ferrimagnetic states; negative values favor the ferromagnetic states.

… Ferromagnetic coupling [is favoured] for the $A(e_g)^2$–$Cr(t_{2g})^3$ arrangement as the superexchange integral is dominant… Antiferromagnetic coupling is favoured for the $A(t_{2g})^3$–$Cr(t_{2g})^3$ arrangement where the effects of the orthogonality constraint on the metal d-orbitals is dominant. In the antiparallel configuration the orthogonality constraint is relaxed through delocalisation of the metal d-orbitals and concomitant polarisation of the orbitals of the CN group".

9.3.3.3 Valence Bond Configuration Interaction (VBCI) and Perturbation Theory

Güdel and Weihe have recently applied their valence bond/configuration interaction model to the A–N≡C–B units in materials related to Prussian Blues [115, 116]. They define the interactions between two d orbitals, a and b, and the π and π^* MOs of the cyanide as shown in Figure 9.19; the integrals are defined by the following one-electron Hamiltonian h:

$$V_a = \langle a|h|\pi\rangle;\ V_b = \langle b|h|\pi\rangle;\ V_a^* = \langle a|h|\pi^*\rangle;\ V_b^* = \langle b|h|\pi^*\rangle \tag{9.21}$$

As shown in Figure 9.20, the exchange splitting is obtained by mixing into the ground configuration selected one-electron excited configurations: ligand-to-metal charge transfer (LMCT) states, metal-to-metal charge transfer (MMCT) states, and metal-to-ligand charge transfer (MLCT) states. The wavefunction for each configuration is obtained and the interaction matrix elements with the ground state are calculated as described in the appendices of Refs. [115] and [116]. The energies

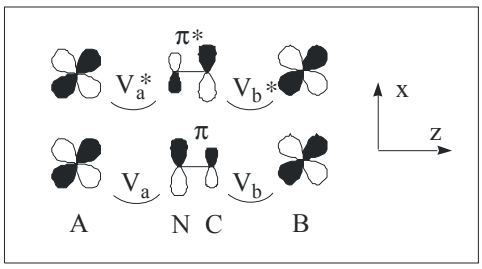

Fig. 9.19. Interactions between π symmetry orbitals in the A–NC–B entity (adapted from Ref. [115]).

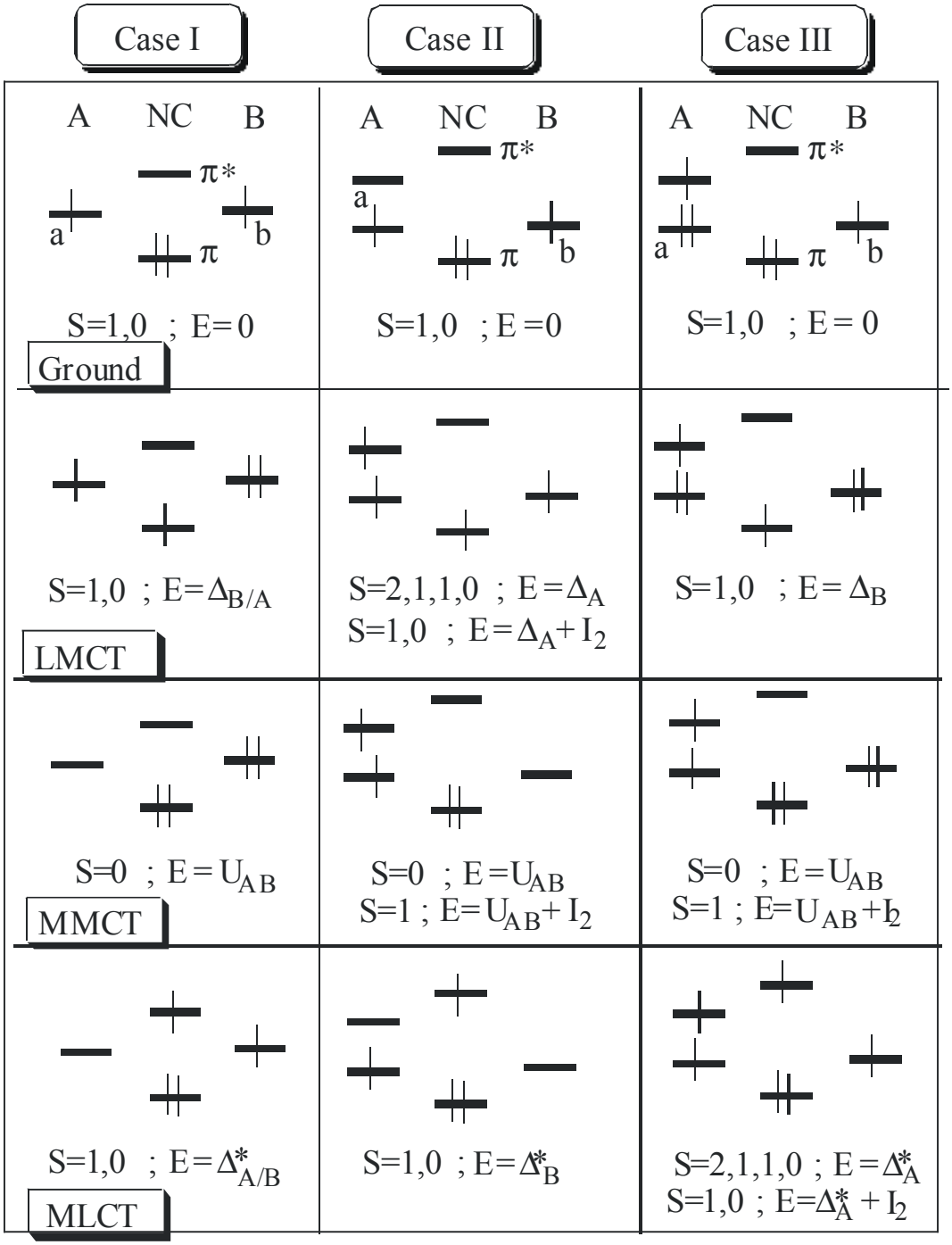

Fig. 9.20. Ground and excited configurations in the A–NC–B entity (adapted from Ref. [116]): Case I: interactions between singly occupied metallic a and b orbitals and π and π^*; Case II: interactions between singly occupied metallic a and b orbitals and π and π^*; Case III: interactions between singly occupied metallic a and b orbitals and π and π^*; from top to bottom: ground, LMCT, MMCT and MLCT configurations. For each configuration the possible spin states and the relative energies are shown (adapted from [115]).

Δ_A, Δ_B, Δ_A*, Δ_B*, and U_{AB} are defined in the Figure 9.20. I_2 is defined as a one-centre two electron exchange integral.

The authors suggest that one can choose a mean value Δ for all the LMCT and MLCT transition energies, a mean value V for all the interaction integrals and a mean value I for the one-centre two electron exchange integral. After making some other approximations, they arrive at simple expressions for J_{calc} that depend on the number of unpaired electrons residing on A and B, table 9.7:

Table 9.7. Calculated magnetic couplings for different A–N≡C–B linkages.[a]

A/B Elect. Config.	J_{calc}	Examples (A/B)
d^5 / d^3	$+ 32Q/15$ [b]	$Mn^{II}Cr^{III}$, $Mn^{II}V^{II}$, $Mn^{II}Mn^{IV}$
d^8 / d^3	$- 4Q + W/3$ [c]	$Ni^{II}Cr^{III}$
d^3 / d^3	$+ 32Q/9$	$Cr^{III}Cr^{III}$, $V^{II}Cr^{III}$
d^3 / d^1	$+ 16Q/3 - 2W/3$	$Cr^{III}VO^{IV}$
d^2 / d^3	$+ 8Q/3$	$Cr^{II}Cr^{III}$

[a] Adapted from Ref. [115]. [b] $Q = V^4 / \Delta^2 U$. [c] $W = [1 + \{(2U + \Delta) / U\} + 2 (U + \Delta)/\Delta] I/U$.

The authors made the debatable assumption that the parameters Q and W were constants (i.e., independent of the nature of A or B), and then carried out a least-squares optimization, with Q and W as adjustible parameters, to fit J_{calc} and J_{exp}. Using an expression similar to Eq. (9.19), the authors calculate the magnetic ordering temperature, obtaining a reasonably linear correlation with experiment. This approach, however, is intrinsically flawed: in the series of Prussian Blues in which the AB pairs are $Mn^{II}V^{II}$, $Mn^{II}Cr^{III}$, and $Mn^{II}Mn^{IV}$, the model predicts that J_{calc} should be invariant, and T_C should equal 280 K for all three compounds, because the electronic configuration of all three species is d^5 / d^3. In fact, the experimental Curie temperatures decrease monotonically across this series, from 125 to 90 to 49 K. The authors recognize that in this case the transferability of the parameters Q and W is not a good approximation, in line with the arguments presented earlier that J is strongly dependent on the energies (and diffuseness) of the orbitals on the metal centers, with early transition metals in low oxidation states giving rise to the largest J values. The authors conclude that "according to our calculations ordering temperatures much higher than those already achieved should not be expected for Prussian Blue analogs containing 3d metals," a conclusion similar to that obtained from semi-empirical calculations. This pessimistic but realistic conclusion leaves open the possibilities provided by the 4d and 5d transition metals. There is still hope for further improvements in T_C.

We would like to conclude this theoretical survey by mentioning some recent papers that use the Anderson model [114] and particularly the kinetic exchange contributions to explain the ferromagnetism experimentally observed in systems

where ferrimagnetism might be expected at first glance. Examples of such systems include certain Prussian Blues that contain the Cr^{III}–Fe^{II} pair [117], which is one of the exceptions we quoted before in discussing Table 9.1 and Figure 9.11, and certain non-Prussian Blue solids (constructed from octacyanometalate building blocks) that contain the Mo^{V}–Mn^{II} pair [119]. In this short review, we can only describe the highlights of the theoretical work on Prussian Blues and related cyanide-bridged model open-shell systems. The reader is referred to the articles cited for additional references to such studies.

9.4 High T_C Prussian Blues (the Experimental Race to High Curie Temperatures)

We are now in position to use the theoretical models to guide experiment and enhance the Curie temperature of Prussian Blue analogs. To set the stage, before we began our work, the highest ordering temperature seen for any Prussian Blue analog was $T_C = 90$ K.

Because we need interactions in the three spatial directions, for the B centre, a d^3, $(t_{2g})^3$ electronic configuration, $S = 3/2$, is better suited than an electronic configuration with $S < 3/2$: thus, V^{II}, Cr^{III}, Mn^{IV} are better suited for the B sites than are low-spin Mn^{III} and Fe^{III}. Because the ordering temperature is proportional to Z, the number of magnetic neighbors, a $MA_1[Cr(CN)_6]_1$ stoichiometry, in which each ion has six neighbors, should be preferred to a $A_1[Cr(CN)_6]_{2/3}$ stoichiometry, in which each ion has only four neighbors, everything else being equal. Furthermore, Prussian Blues with ferromagnetic interactions allow one to reach only $T_C = 90$ K [27], and thus a ferrimagnetic strategy must be looked for. For both energy and overlap reasons, the interaction between the metallic d orbitals and the cyanide π^* MOs increases with earlier transition elements, it should be better to work with chromium, vanadium or titanium, when the chemistry allows. In the $C_xMn_1[M(CN)_6]_1$ series (see Section 9.4.2), the T_Cs show a distinct dependence on the ion in the B site: 49 K for the $Mn_1[Mn^{IV}(CN)_6]_1$ derivative [69], 90 K for $Cs_1Mn_1[Cr^{III}(CN)_6]_1$ [70] and 125 K for $Cs_2Mn_1[V^{II}(CN)_6]_1$ [31]. From the Mn^{II} derivative of Klenze in 1980 to the V^{II} materials of Girolami in 1995 took 15 years. Because the ferromagnetic exchange pathways are non-negligible, if one wants to enhance the absolute value $|J|$ of a ferrimagnetic system, it is necessary to decrease the ferromagnetic contributions (see Eq. (9.2c)). This means choosing an A ion that has as few e_g electrons as possible. Figure 9.10 shows how this goal can be achieved: whereas Mn^{II} has two e_g electrons, Cr^{II} has only one (if high-spin), and V^{II} has none. Furthermore, the use of the early transition ions Cr^{II} and V^{II} will enhance the absolute value of the antiferromagnetic interaction by backbonding more effectively with the cyanide π^* orbital.

Indeed these approaches have worked pretty well [119]! Whereas $Mn^{II}[Cr^{III}(CN)_6]_{2/3}\bullet xH_2O$ has T_C = 60 K, $Cr^{II}[Cr^{III}(CN)_6]_{2/3}\bullet xH_2O$ has T_C = 240 K [28], and V^{II}/Cr^{III} Prussian blues have T_Cs that range from 315 K [29] to 376 K [40]. Nevertheless, from the Mn^{II} derivative of Babel in 1982 to the amorphous V^{II} analog of Ferlay in 1995 took 13 years. And four years more for Girolami's crystalline V^{II} compound. The situation deserves some comment.

9.4.1 Chromium(II)-Chromium(III) Derivatives

In 1993, we described the synthesis of two Prussian blue analogs prepared by adding $[Cr(H_2O)_6]^{2+}$ to $[Cr^{III}(CN)_6]^{3-}$ [28]. In the absence of a source of cesium cations, a light gray precipitate of stoichiometry $Cr^{II}[Cr^{III}(CN)_6]_{2/3}\bullet 10H_2O$ is isolated. The material has a single C–N stretching band in the IR spectrum at 2194 cm^{-1}, and this frequency suggests that all of the cyanide ligands are C-bound to Cr^{III}. Magnetisation measurements show that the compound orders ferrimagnetically at 240 K, although interestingly the saturation magnetisation suggests that some Cr^{II} centers are low-spin. Relative to the previous record for highest T_C for a Prussian blue, that of 90 K for Babel's or Gadet's compound, a T_C of 240 K represents a significant step towards room temperature.

In an attempt to increase the number of magnetic neighbors by preparing a 1:1 compound, the same reaction was carried out in the presence of Cs^+. Under these circumstances a green compound of stoichiometry $Cs_{0.67}Cr^{II}_1[Cr^{III}(CN)_6]_{0.9}\bullet 4.5H_2O$ is isolated [28]. The infrared spectrum of this compound, however, features two cyanide stretching bands due either to linkage isomerism or to a partial conversion of high-spin Cr^{II} centers (S = 2) to low-spin Cr^{II} centers (S = 1). The latter hypothesis is supported by the fact that the magnetisation at saturation is well below the expected value calculated assuming that all the Cr^{II} centers are high-spin [28]. As a result, the magnetic ordering temperature of 190 K, while still high for a Prussian blue analog, is lower than that of the 3:2 compound. Because the chemistry of the system did not allow further increase in T_C by increasing the A:B ratio to 1:1, we tried another approach: we hoped that compressing the solid under pressure would decrease the distances, enhance the orbital overlaps, increase the antiferromagnetic interaction, and thus increase the ordering temperature. Instead, a disaster happened. Compressing the sample under a pressure of 4 kbars causes all of the Cr^{II} centers to become low-spin, and the local antiferromagnetic coupling causes the solid to become diamagnetic below its ordering temperature because the spins of the low-spin Cr^{II} centers exactly cancel those of the Cr^{III} centers [120]:

$$M_T = M_{Cr}{}^{III} - M_{Cr}{}^{II} \tag{9.22a}$$

with Cr^{III}, d^3, $S = 3/2$ and high spin Cr^{II}, d^4, $S = 2$, one obtains:

$$M_T / \mu_B = |M_{Cr}{}^{III} - M_{Cr}{}^{II}{}_{HS}| = |(2/3) \times 3 - 1 \times 4| = 2 \tag{9.22b}$$

Instead, with Cr^{III}, d^3, $S = 3/2$ and low-spin Cr^{II}, d^4, $S = 1$, one obtains:

$$M_T / \mu_B = |M_{Cr^{III}} - M_{Cr^{II}_{LS}}| = (2/3) \times 3 - 1 \times 2 = 0 \; ! \qquad (9.22c)$$

This change was shown beautifully by the thermal variation of the magnetisation under pressure. In chemistry, as in Roman history, the Tarpeian rock is close to the Capitol. Three years later, with the same system, Sato, Hashimoto et al. used an electrochemical method and succeeded in obtaining a derivative with a T_C = 270 K, which was furthermore switchable from ferrimagnetic to paramagnetic electrochemically [121]. Two years later with the same electrochemically-synthesised chromium-chromium system, Miller et al. were able to prepare thin layers of materials, either amorphous or crystalline, with T_C ranging from 135 to 260 K depending on the oxidation states of the chromium. They observed a robust negative magnetisation in low field that they assigned to the single ion anisotropy of chromium(II) [122].

9.4.2 Manganese(II)-Vanadium(III) Derivatives

The hypothesis that earlier transition metals lead to stronger exchange interactions led us to replace the $[Cr^{III}(CN)_6]^{3-}$ precursor by $[V^{II}(CN)_6]^{4-}$ [32]. We have already commented on the higher T_C exhibited by the ferrimagnet $Cs_2Mn^{II}[V^{II}(CN)_6]$ (125 K) compared to its homologs $CsMn^{II}[Cr^{III}(CN)_6]$ (90 K) and $Mn^{II}[Mn^{IV}(CN)_6]$ (49 K) (see Section 3.2.4). Cs_2Mn^{II} $[V^{II}(CN)_6]$ is prepared in aqueous solution under argon from $K_4[V^{II}(CN)_6]$ and $Mn^{II}(OSO_2CF_3)_2(CH_3CN)_2$ in the presence of $Cs(OSO_2CF_3)$. It is an air-sensitive green solid. It crystallizes in a face-centered-cubic (fcc) lattice with a = 10.66 Å. Its magnetisation at saturation is in line with an antiferromagnetic coupling between vanadium and manganese. When $(NEt_4)_4[V^{II}(CN)_6]$ is treated with $Mn^{II}(OSO_2CF_3)_2(CH_3CN)_2$ in the absence of $Cs(OSO_2CF_3)$, the crystalline yellow solid obtained, formulated as $(NEt_4)_{0.5}Mn^{II}_{1.25}[V^{II}(CN)_5]\bullet 2H_2O$, is a strongly coupled ferrimagnet with T_C = 230 K. The colour of the two compounds, green and yellow, and the absence of intervalence band in the near-infrared spectrum indicates that there is no electron transfer between the metallic centres. X-ray powder diffracttion shows that the second compound is crystalline but does not adopt a fcc structure. The XRD pattern and the unusual CN^- to V ratio in the NEt_4 material suggest that the structure is more complex. Interestingly, Babel has shown that attempts to substitute cations larger ions than Cs^+ into the Prusian Blue lattice usually gives rise instead to lower dimensional structures with substantially decreased magnetic phase transition temperatures [74]. Even though the large NEt_4 cations prevent the adoption of the cubic structure, the high value of T_C suggests that the structure still consists of a 3D array of interacting spin centers, with a very strong antiferromagnetic coupling constant. The magnetisation data of the two compounds are revealing on this point. One of the characteristic features of ferrimagnetic materials is the presence of a minimum in the thermal $\chi_M T$ curve: the higher is the temperature of the min-

imum, the larger is the antiferromagnetic coupling constant J. $Cs^{I}_{2}Mn^{II}[V^{II}(CN)_6]$ exhibits such a minimum at about 210 K. However, there is no visible minimum in the $(NEt_4)_{0.5}Mn^{II}_{1.25}[V^{II}(CN)_5]\bullet 2H_2O$ data: because the saturation magnetisation allows one to rule out a ferromagnetic coupling, the minimum must be displaced above the observed temperature range and that $|J|$ must be strong. The hypothesis that the back-bonding with the cyanide π^* orbitals become more effective with V^{II} ions is fully confirmed. The conclusion of Ref. [31] was: "These two V-based molecular magnets represent an important step in the design of molecular magnets with high T_N. Through judicious choice of cations and metal centers, T_N values above 300 K should be possible." The stage was ready for another step.

9.4.3 The Vanadium(II)-Chromium(III) Derivatives

Our ultimate success in obtaining Prussian blues with ordering temperatures above room temperature resulted indeed from the idea to enhance J by maximizing the backbonding of the d orbitals of the metal A with the π^* orbitals of cyanide and returning to the idea that increases in T_C can be achieved by reducing the number of ferromagnetic pathways. The metal ion best able to accomplish both of these goals is V^{II}. Upon adding the Tutton salt $(NH_4)_2V(SO_4)_2\bullet 6H_2O$ to $K_3Cr(CN)_6$, a midnight-blue solid that has a stoichiometry of $V[Cr^{III}(CN)_6]_{0.86}\bullet 2.8H_2O$ precipitates from solution. The magnetic ordering temperature is 315 K.

Prepared in this manner, using Schlenk techniques, the expected $V^{II}[Cr^{III}(CN)_6]_{2/3}$ stoichiometry is in fact not obtained, and a non-stoichiometric, amorphous compound results instead, probably because it precipitates very

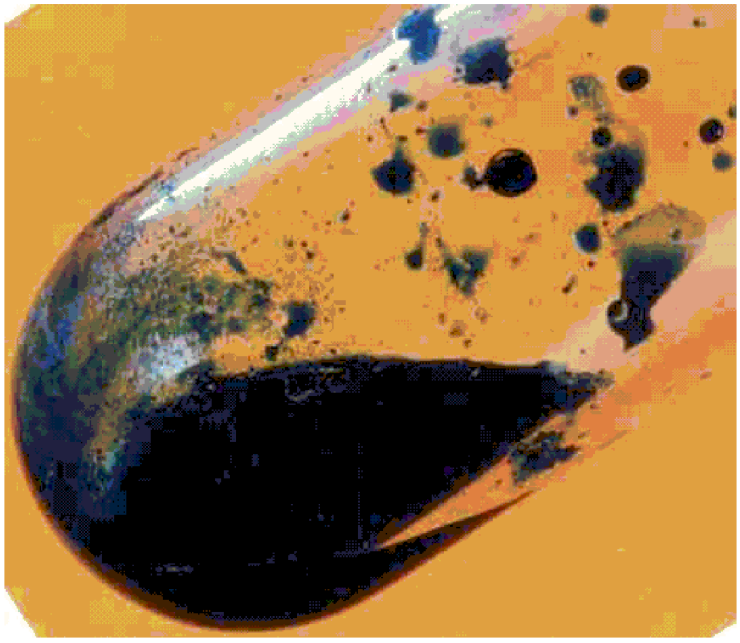

Fig. 9.21. "A midnight blue solid precipitates from solution…." Molecule-based magnets can be prepared under mild conditions. They are transparent and low density.

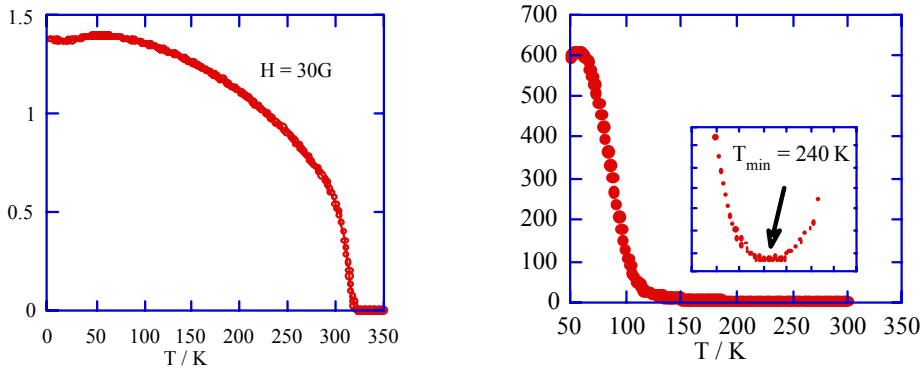

Fig. 9.22. Role of the oxidation state in VCr derivatives: thermal variation of (a) the magnetisation of $V^{II}_{\alpha}V^{III}_{1-\alpha}[Cr^{III}(CN)_6]_{0.86}\cdot 2.8H_2O$ ($\alpha = 0.42$); (b) product $\chi_M T$ of $V^{IV}O[Cr^{III}(CN)_6]_{2/3}$.

rapidly and the interstitial sites are occupied by a variety of species. The A sites contain a mixture of V^{II} and V^{III}, and the formula of the compound is best represented as $V^{II}_{\alpha}V^{III}_{(1-\alpha)}[Cr^{III}(CN)_6]_{0.86}\bullet 2.8H_2O$ with $\alpha = 0.42$. The magnetisation at saturation is very weak (0.15 μ_B) and fits perfectly with the above formulation. The coercive field corresponds to a very soft magnet (25 Oe at 10 K). The compound is very sensitive to dioxygen. In a comment accompanying the publication [119], Kahn underlined that on the one hand "*the synthesis of such a material can be considered as a cornerstone in the field of molecular magnetism*" … and that $V[Cr(CN)_6]_{0.86}\bullet 2.8H_2O$ was "*an excellent example on which to learn (or to teach) the basic concepts of molecular magnetism.*" On the other hand, Kahn pointed out that [VCr] "*is not a molecular compound, but rather an amorphous and non stoichiometric compound*", "*the saturation magnetisation is limited to 0.15* μ_B ...", "*the coercive field is only 10 Oe...*". This was the first Prussian blue system to exhibit a Curie temperature above room temperature, but it is far from perfect.

9.4.3.1 Improving the Magnetic Properties of VCr Room Temperature Molecule-based Magnets

Further improvements in the T_C for the V^{II}/Cr^{III} Prussian blue analogs have been achieved by varying the synthetic conditions so that the solids obtained are crystalline and more nearly stoichiometric. New syntheses were undertaken by our groups and some others, in particular Miller and Epstein, as recently reviewed [17, 18, 123, 124], and Hashimoto and Ohkoshi [25]. It would take too long to detail all the results. The reader is advised to consult the original papers. A set of non-

stoichiometric Prussian Blue analogs $M^I_yV[Cr^{III}(CN)_6]_z \cdot nH_2O$ (M = alkali metal cation) arose with T_Cs varying up to 376 K. We give hereunder some information on these new compounds. Many factors affect not only the successful synthesis of the compounds in the VCr series but also the magnetic properties of the resulting solids (Curie temperature, magnetisation at saturation, coercivity…). Particularly important is the crystallinity and/or the magnetic domain size of the particles. The structure of Prussian blues is rich in void spaces, channels, and (often) vacancies that can accommodate guest species (anions, cations, solvent…). These guest species can either improve or compromise the structural organisation of the material. To convince the reader that this chemistry is indeed not easy, we shall give only three examples in which the role of the solvent and of the starting materials ("innocent" counterions) was investigated: (i) The reaction carried out in H_2O with $[V(MeOH)_6]I_2$ as the starting material gives the compound $\{V^{II}_{0.58}V^{III}_{0.42}[Cr(CN)_6]_{0.77}\ (I^-)_{0.2}\ (NBu_4^+)_{0.1}\} \cdot 5H_2O$ (T_C = 330 K); (ii) The reaction in H_2O as solvent with the Tutton salt $K_2V^{II}(SO_4)_2.6H_2O$ as the starting material gives the compound $\{V^{II}_{0.78}V^{III}_{0.22}[Cr(CN)_6]_{0.56}\ (SO_4^{2-})_{0.28}\ (K^+)_{0.11}\} \cdot 4H_2O$ (T_C = 295 K); (iii) When the reaction is performed in methanol as solvent and $[V(MeOH)_6]I_2$ as the starting material, $\{V[Cr(CN)_6]_{0.69}\ (I^-)_{0.03}\} \cdot 1.5MeOH$ (T_C = 200 K) is obtained. The magnetisation curves can be found in Refs. [99, 125]. The counteranions and the solvents have large effects on the Curie temperatures and on the magnetisation at saturation. Large, weakly-coordinating anions such as I^- do not induce disorder in the structures and the magnetic properties are improved. As for the solvent, it can be expected that when the kinetics of solvent exchange in $[V(solvent)_6]^{2+}$ is faster, the substitution of the solvent molecules by cyanides around the V^{2+} ion is more effective, the structure is better organized, and the number of interactions between Cr and V increases. Among many synthetic attempts, four were successful in improving the situation: changing the V^{II}/V^{III} ratio to improve the magnetisation [126]; using large counterions and slow precipitation by the sol-gel technique to improve the regularity of the structure [40]; using alkali cations to change the stoichiometry [41]; and using V^{III} as a catalyst in the synthesis [127, 128].

Changing the V^{II}/V^{III} ratio to improve the magnetisation [126] relies on the observation that, in a VCr Prussian Blue ferrimagnet, the antiparallel alignment of the neighboring spins in the magnetically ordered phase leads to a resulting total magnetisation M_T which is the difference between the magnetisation arising from the of the chromium ions M_{Cr} and the magnetization from the vanadium ions, M_V:

$$M_T = | M_{Cr} - M_V | \tag{9.23}$$

Two situations may arise, one when the larger magnetic moments are borne by the chromium ions and are aligned parallel to an external applied field ($M_{Cr} > M_V$); the other when $M_V > M_{Cr}$. In the later case, the sign of the quantity ($M_{Cr} - M_V$) is reversed and the magnetic moments of the vanadium ions now lie parallel to

the field. In between, the magnetisation is zero. For example, in the analogs $(C^{I}_{y}V^{II}_{\alpha}V^{III}_{1-\alpha}[Cr^{III}(CN)_6]_z \bullet nH_2O$, it is easy to find that:

$$M_T = -(3z - \alpha - 2) \tag{9.24}$$

The spin values (magnetisation) of the compounds can be represented in a three-dimensional space, in which the value of α varies from 0 to 1 and z varies from 2/3 to 1. The spin values are described by the plane in Figure 9.23.

The compound $\{V^{II}_{0.45}V^{III}_{0.53}(V^{IV}O)_{0.02}[Cr(CN)_6]_{0.69}(SO_4)_{0.23}(K_2SO_4)_{0.02}\} \cdot 3H_2O$ synthesized in this context [126] has a saturation magnetisation $M_S = 0.36\ N_A\beta$. The calculated M_T value is positive ($M_T = +\ 0.36\ N_A\beta$). On the other hand, $\{Cs_{0.82}V^{II}_{0.66}(V^{IV}O)_{0.34}[Cr(CN)_6]_{0.92}(SO_4)_{0.20}\} \bullet 3.6H_2O$, prepared in the presence of Cs and containing vanadyl, presents $M_S = 0.42\ N_a\beta$. The calculated M_T value is negative ($M_T = -\ 0.36\ N_A\beta$). The absolute values are in good agreement with the experimental ones. The crucial difference between the two compounds is the sign of M_T, which is influenced by the balance between the values of z (Cr^{III}/V ratio) and the ratio V^{II}/V. Conventional magnetisation measurements give the absolute value of the macroscopic magnetisation but not the local magnetisation. Instead, X-ray magnetic circular dichroism (XMCD), a new X-ray spectroscopy developed with synchrotron radiation, is an element- and orbital-selective magnetic local probe. Direct information is obtained about the local magnetic properties of the photon absorber (direction and magnitude of the local magnetic moment). The signal appears whatever the shape of the sample (crystals, powders...). A chapter of Volume I of this series by Sainctavit, Cartier dit Moulin, and Arrio is

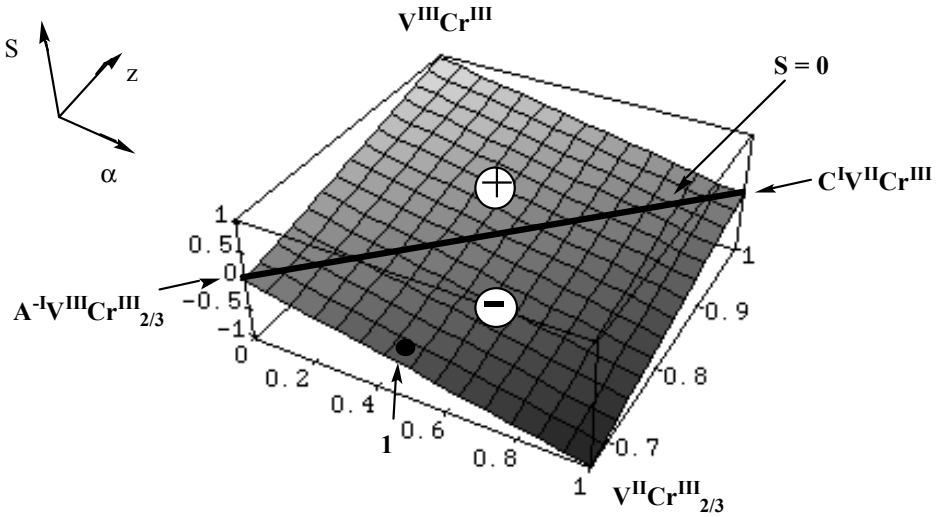

Fig. 9.23. Variation of the total spin (or magnetisation M_T) in the series $C^{I}_{y}V^{II}_{\alpha}V^{III}_{1-\alpha}[Cr^{III}(CN)_6]_z \cdot nH_2O$ as a function of the vanadium(II) fraction α and of the stoichiometry z ($M_T = -(3z - \alpha - 2)$. The sign of the magnetisation changes above and below the line $S = 0$ (see text).

devoted to this technique [129]: "Magnetic Measurements at the Atomic Scale in Molecular Magnetic and Paramagnetic Compounds". Figure 8, page 146 therein, gives the XMCD spectra at the chromium and vanadium edges and demonstrates: (i) The antiferromagnetic coupling between vanadium and chromium ions (inversion of the dichroic signal at the vanadium and the chromium K edges, for each compound); (ii) The opposite local magnetisation of both chromium and vanadium: for a given edge, the general shape of the dichroïc signal of the first compound is the opposite of that found in the second. Further useful applications of X-ray absorption (EXAFS, XANES at the K and $L_{2,3}$ edges and XMCD) in the study of Prussian Blues, in particular $CsNi[Cr(CN)_6]$ and $CsMn[Cr(CN)_6]$ can be found in Refs. [130–133]. For the present discussion, the conclusion is that it is absolutely necessary to control the stoichiometry and the vanadium oxidation states to avoid generating an antiferromagnet or, with complete oxidation of vanadium to vanadyl, the loss of the high T_C properties as in the $(V^{IV}O)[Cr(CN)_6]_{2/3}$ derivative (T_C = 115 K) [89] (Figure 9.22b).

Second, we found that precursors with large counterions afford a material that closely resembles the preceding VCr material but whose structure is more regular [40]. Combining aqueous solutions of the triflate salt $V(O_3SCF_3)_2$ with the tetraethylammonium salt $[NEt_4]_3[Cr(CN)_6]$ under anaerobic conditions affords a dark blue gel after about 10 min. The gel forms only if the reactant concentrations are above a certain threshold (in our experiments the concentrations were 0.02–0.06 mol l^{-1}). After 2h, the gel becomes less viscous and takes the appearance of a suspension. The suspended solids are collected by centrifugation and washed with water to afford a dark blue solid of stoichiometry $V^{II}_1[Cr^{III}(CN)_6]_{2/3}\bullet 3.5H_2O\bullet 0.1[NEt_4][O_3SCF_3]$. Unlike the material prepared in the presence of K^+, NH_4^+ and SO_4^{2-} counterions, this material is crystalline, with a fcc cell parameter of a = 10.54 Å. Presumably because it is more highly crystalline, it has a slightly higher magnetic ordering temperature of 330 K. When the sample is heated to 350 K, a change occurs and the ordering temperature is lowered slightly to 320 K. Although the nature of this change is still under investigation, one possibility is that the material simply dehydrates upon heating. Another possibility is that a slight rearrangement (rotation) of the $[Cr^{III}(CN)_6]$ octahedra leads to a smaller J value (see Scheme 9.2 below).

The next step was clear: change the stoichiometry to 1:1 by adding alkali metal cations [see Figure 9.24, derived from Eq. (9.19)]. If the synthesis is conducted in the presence of 4.5 equivalents of CsO_3SCF_3, the cesium salt $Cs_{0.82}V^{II}_1[Cr^{III}(CN)_6]_{0.92}\bullet 3.H_2O\bullet 0.1[NEt_4][O_3SCF_3]$ (or $Cs_{0.8}VCr_{0.9}$) is obtained. A similar reaction with the potassium salt $K_3[Cr(CN)_6]$ leads to $K_1V^{II}_1[Cr^{III}(CN)_6]_1\bullet 2H_2O,\bullet 0.1\ KO_3SCF_3$ (or KVCr). Table 9.8 gathers important characteristics of the three compounds. Figure 9.25 gives the X-ray powder diffractogram of KVCr, Figure 9.26 presents the thermal variation of the magnetisation and Figure 9.27 depicts the magnetisation vs. applied magnetic field at 5 K. The low value of the magnetisation of KVCr is perfectly understood by

Table 9.8. Properties of the three crystalline high-T_C VCr compounds of Ref. [40][a]

	$V^{II}_1Cr^{III}_{2/3}$	$Cs_{0.82}V^{II}Cr^{III}_{0.94}$	$K_1V^{II}_1Cr^{III}$
a/Å	10.54	10.65	10.55
T_C/K	330	337	***376***
T_C/K After treatment	320	337	365
$M_{saturation}$/kG cm^3 mol^{-1}	3.5	2.2	0.7
$M_{sat\ expected}$/kG cm^3 mol^{-1}	5.7	1.0	0.0
$H_{coercive}$/G	10	15	165
$M_{remnant}$/G cm^3 mol^{-1}	570	750	220
$T_{Closing\ hysteresis\ loop}$/K	350	350	380

[a] Adapted from Ref. [40].

looking at Figure 9.23: KVCr, with α and $z = 1$ should have a zero magnetisation (line $S = 0$). The observed low magnetisation at saturation is indeed the result of a very small departure of stoichiometry z from 1 or of the oxidation state of vanadium from +2. Further data, experimental details, and comments can be found in Ref. [40].

The fourth and last example we would like to address deals with the role of kinetics in the formation of such compounds. The sol-gel technique above was a first step in this direction. Furthermore, we discovered during our studies that: (i) in a perfect anaerobic atmosphere (glove box, 3 ppm O_2), the slowly precipitating

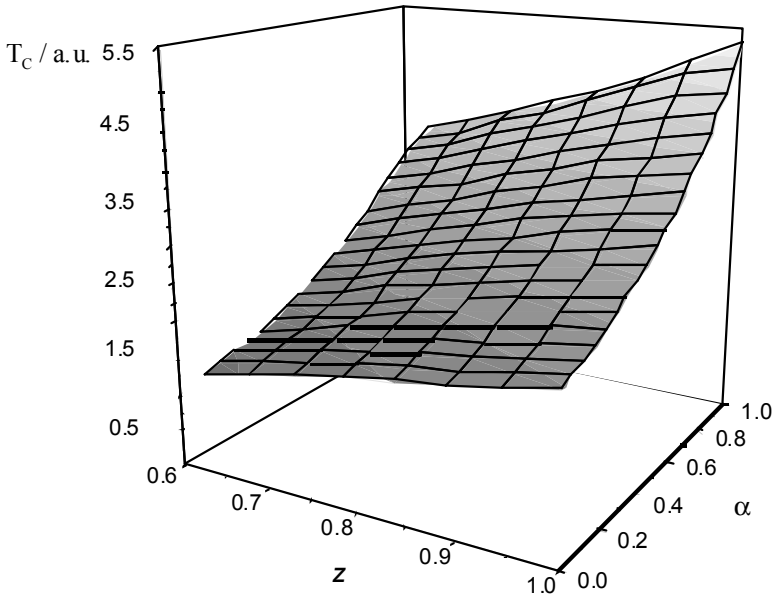

Fig. 9.24. Variation of the Curie temperature (arbitrary units) in the series $C_yV^{II}_{\alpha}V^{III}_{1-\alpha}[Cr^{III}(CN)_6]_z{\cdot}nH_2O$ as a function of the vanadium(II) fraction α and of the stoichiometry z.

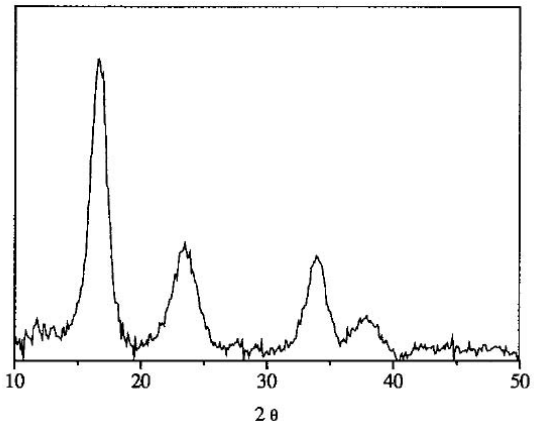

Fig. 9.25. X-ray powder diffraction of KVCr (from Ref. [40]).

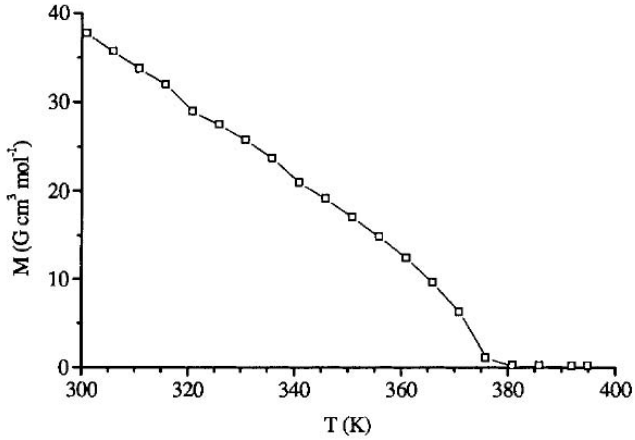

Fig. 9.26. Thermal variation of the magnetisation of KVCr (from Ref. [40]).

solid is no longer a room temperature magnet (compound 1 in Figure 9.28), in strong contrast with the results obtained by the Schlenck technique which lead to room-temperature magnets (with uncontrolled amount of oxidized vanadium in solution); (b) Some oxidation of the vanadium ion during the synthesis is necessary to reach a Curie temperature above ambient (compound 2 in Figure 9.28). Both observations prompted us to look more closely at the role of vanadium(III) in the synthetic process. The results are reported in Ref. [127].

We found that adding small amounts of V^{III} during the synthesis ($1\% < V^{III} < 4\%$) (Figure 9.29) led to derivatives with a stoichiometry close to the $V_1Cr_{2/3}$ ideal. The solids are free from V^{III}. Their structure, as judged from EXAFS data, comprises $[Cr^{III}CN)_6]$ units linked to octahedral V^{II} ions by bent C–N–V units (α = 168°) (Scheme 9.2). In contrast, when the samples are prepared in the absence of V^{III}, the

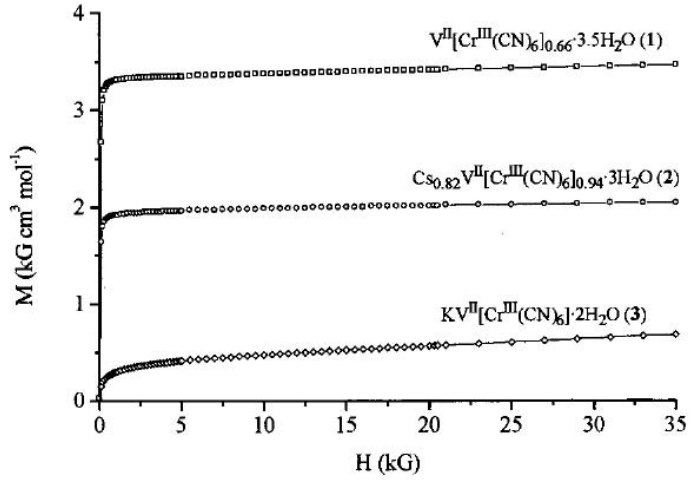

Fig. 9.27. Field dependence of the magnetisation of the VCr derivatives in Table 9.8 (from Ref. [40]).

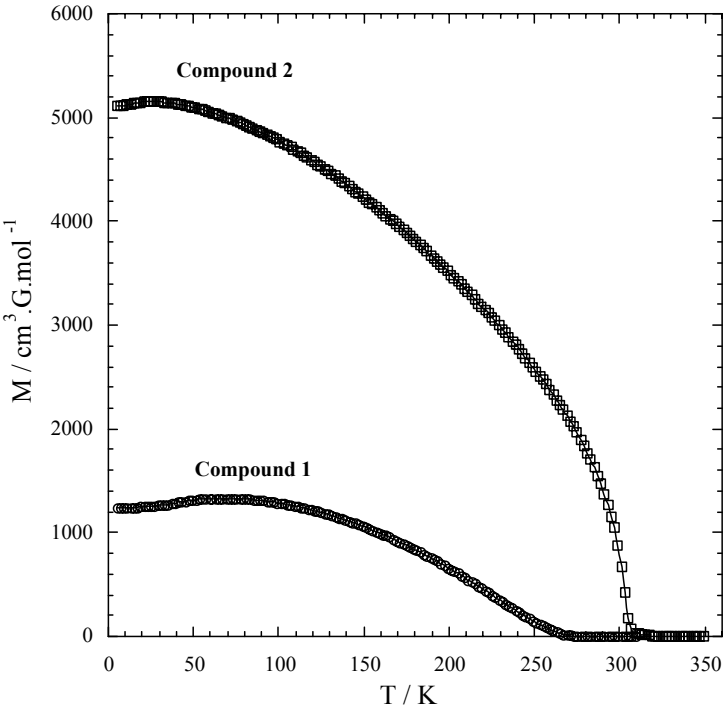

Fig. 9.28. Thermal dependence of the magnetisation of two compounds prepared with catalytic amounts of V^{III} (**2** , —□—) and without (**1** , —○—).

structures are disordered with a distribution of α angles and tilts of the $[Cr(CN)_6]$ octahedra.

The observed magnetisation fits well the $V_1Cr_{2/3}$ stoichiometry (Figure 9.30). The Curie temperatures obtained in this way are not the highest obtained so far but

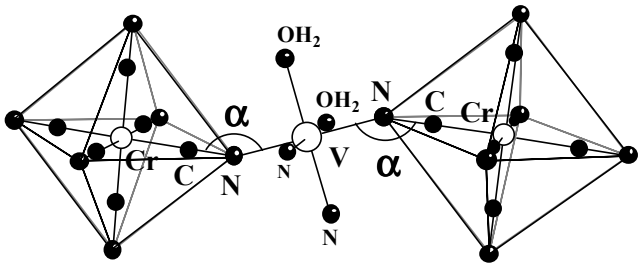

Scheme 9.2. Tilted configuration of $[Cr^{III}CN)_6]$ and $V(NC)_4(H_2O)_2$ octahedra.

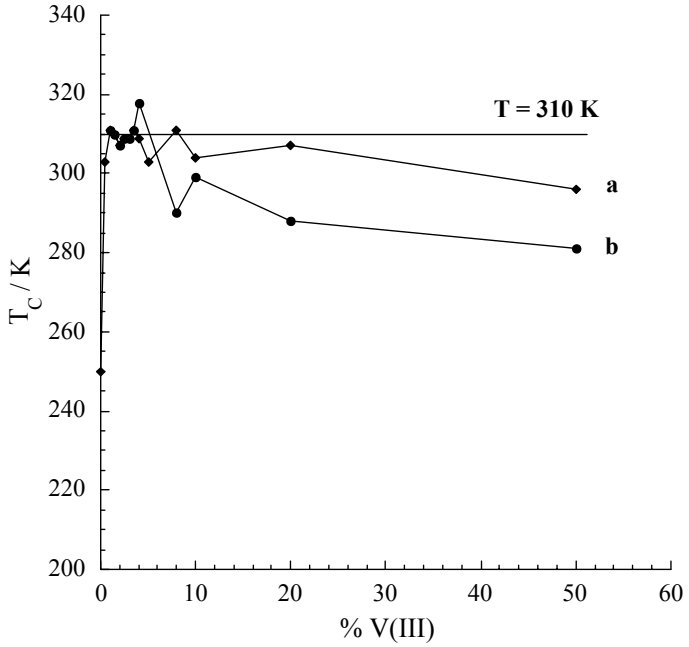

Fig. 9.29. Curie temperatures vs. percentage of V^{III} in solution during the synthesis under various conditions (see Ref. [127] for details).

they are reproducible and remain constant after heating the samples above T_C. The tilted configuration of the $[Cr^{III}(CN)_6]$ octahedra, reminiscent of the situation in distorted perovskites, is therefore a thermodynamically stable one. The structural model with α = 168° given in Scheme 9.2 allows a straightforward explanation of the higher T_Cs of the metastable samples: they adopt a (metastable) structure with α angles closer to 180° (corresponding to a smaller tilt of the $[Cr(CN)_6]$ octahedron) and therefore larger orbital overlaps, $|J|$ and T_Cs. Heating the sample and cycling the temperature brings the system to the stable structure with α angles closer to 168° and lower T_Cs. It is particularly significant that the stable T_C = 310 K value, reached here directly, is close to that of $V^{II}_1Cr^{III}_{2/3}$ in Table 9.8, synthesized by Girolami's sol-gel approach after cycling the temperature around T_C. The

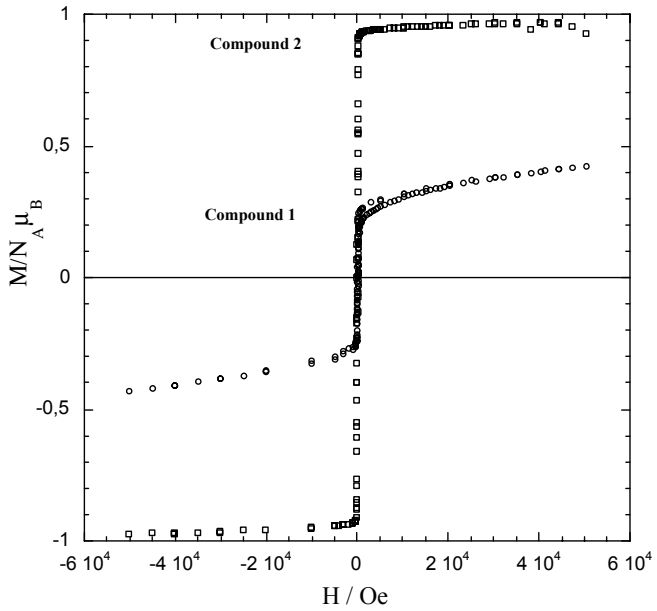

Fig. 9.30. Field dependence at 5 K of the magnetisation of two compounds prepared with catalytic amounts of V^{III} (**2** , —□—) and without (**1** , —○—).

key role of V^{III} can be demonstrated as well in the synthesis of VCr Prussian Blue analogs in which the stoichiometry is varied by inserting alkali metal cations (K, Rb, Cs); these materials have stable T_Cs between 340 and 360 K and magnetisations in agreement with the $V_1Cr_{5/6}$ stoichiometry [128].

9.4.4 Prospects in High-T_C Magnetic Prussian Blues

We list below some research directions which are currently explored by the magnetic Prussian Blue community. Among others: magnetic devices, thin layers and magneto-optical properties, dynamic magnetic properties, etc.

9.4.4.1 Devices Built from [VCr] Room-temperature Magnets

Once room temperature is reached, it becomes possible to think about applications and the design of demonstrators and devices. Molecule-based magnets such as the [VCr] systems are useful tools to illustrate easily, near room temperature, what a Curie temperature is. Figures 9.31 to 9.33 show several devices and demonstrators.

Figure 9.31 displays a very simple demonstration, in which a disk of [VCr], embedded in a polymer to protect it from air-oxidation, is attracted by a powerful perm

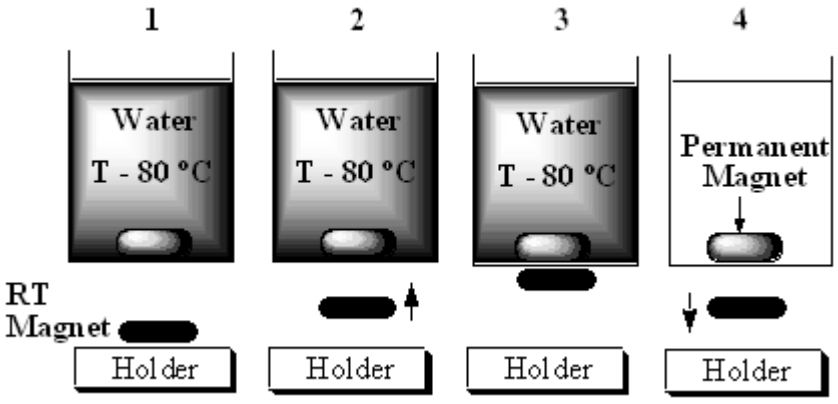

Fig. 9.31. Principle of a "flying" magnet.

anent magnet located just above (2). The permanent magnet is located at the bottom of a beaker filled with hot water: in contact with the hot bath, the temperature of the [VCr] disk increases (3). When it reaches T_C, the disk falls (4). Then, on cooling, it is ready to "fly" again when its temperature drops below T_C (1). One can dream of a machine built along the same lines, pumping water by means of solar energy (free) and an atmospheric temperature bath (free).

Figure 9.32 describes an oscillating magnet. The [VCr] compound is sealed in a glass vessel under argon and suspended at the bottom of a pendulum [equilibrium, position (2) in the absence of a permanent magnet]. It is then cycled between its two magnetic states: the 3D-ordered ferromagnetic state when $T < T_C$, and the paramagnetic state when $T > T_C$. The three steps are: (i) the room temperature

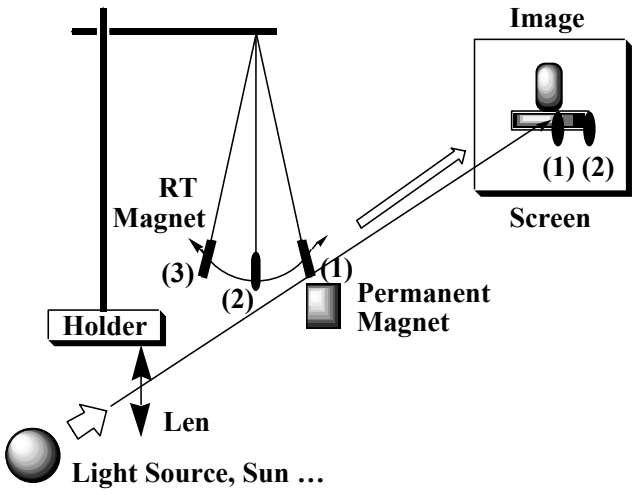

Fig. 9.32. Principle of an "oscillating" magnet.

magnet ([VCr]) is cold ($T < T_C$, ferrimagnetic state). It is attracted (→) by the permanent magnet and deviates from the vertical direction towards position (1). The light beam is focused at this position (1), just above the permanent magnet and heats the sample, the temperature of which increases; (ii) when $T > T_C$, the hot [VCr] magnet is in the paramagnetic state. It is no longer attracted and moves away from the magnet (←) under the influence of its own weight. It is then air-cooled and its temperature decreases; (iii) when $T < T_C$, the cold [VCr] magnet is attracted again by the permanent magnet (→) and returns to position (1). The system is ready for a new oscillation. The demonstrator works well, and millions of cycles have been accomplished without any fatigue. It is an example of a thermodynamical machine working between two energy baths with similar temperatures (sun and shadow) allowing the conversion of light into mechanical energy. Figure 9.33a shows a photograph of the demonstrator in use in our laboratory. Figure 9.33b shows another demonstrator that could be used as a magnetic switch or thermal probe: the [VCr] magnet located at the end of a diamagnetic bar,

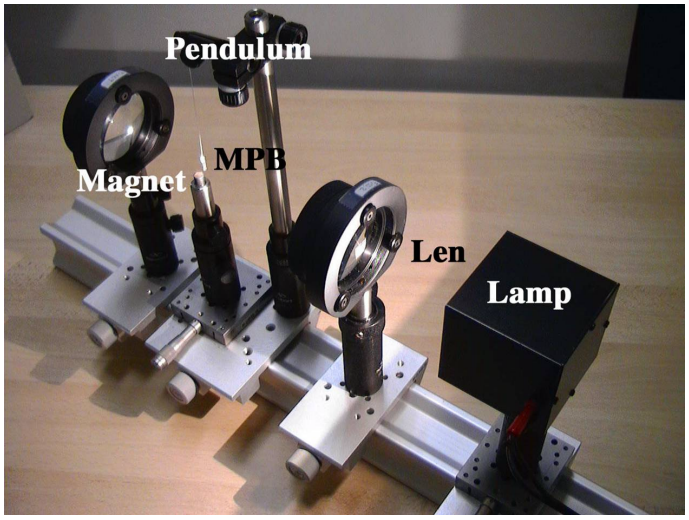

(a)

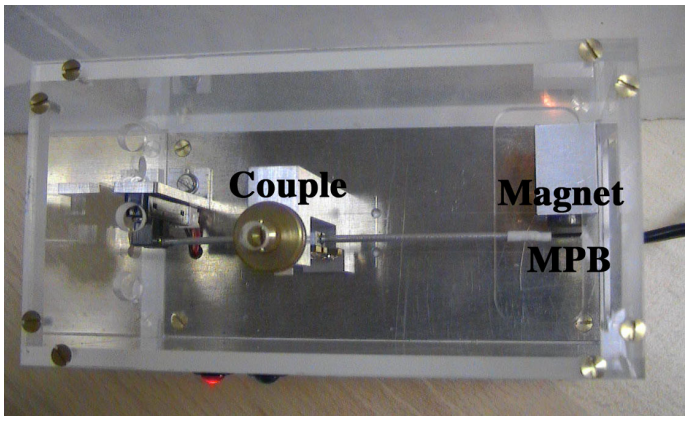

(b)

Fig. 9.33. Two demonstrators: (a) oscillating magnet transforming light in mechanical energy; (b) magnetic switch and thermal probe (see text).

can take two positions: when $T < T_C$, it is in contact with the permanent magnet, the temperature of which is tunable; when $T > T_C$ it is repelled by a mechanical couple installed on the rotation axis, hence opening or closing an electric circuit [134].

9.4.4.2 Thin layers, Electrochromism, Magneto-optical Effects

Magnetic Prussian Blue analogs display bright colors and transparency, among other interesting properties. To exploit these optical properties, it is useful to prepare thin films: a 1 μm thick film of vanadium-chromium magnet is indeed quite transparent. The best way to prepare thin films of these materials is by electrochemical synthesis or ion-exchange on Nafion membranes. Various films have been prepared from hexacyanoferrates or chromates [135]. To obtain [VCr] thin films, the experimental conditions must be adapted. One actually wants to produce and to stabilise the highly oxidisable V^{II} ion. Thus, strongly negative potentials are applied at the working transparent semiconducting electrode. The deposition of the [VCr] film is realised from aqueous solutions of $[Cr^{III}(CN)_6]^{3-}$, and aqueous V^{III} or $V^{IV}O$ solutions either at fixed potential or by cycling the potential. An interesting property of [VCr] thin films is the exhibition of electrochromism during cycling. The way is open for the preparation of *electrochromic room temperature magnets* (see Refs. [99, 136–138] for illustrations and details).

The magnetisation of a transparent magnetic film, protected by a transparent glass cover, can then be probed by measuring the Faraday effect. Spectroscopic measurements in the ultraviolet-visible range provide information about the magnetisation of the sample and about its electronic structure. Observing the Faraday effect at room temperature in these compounds is a first step towards demonstrating that the materials can be used in magneto-optical information storage. Hashimoto [136] and Desplanches [99, 137, 138] succeeded in obtaining from [VCr] room-temperature magnets a magneto-optical signal at room temperature through a transparent semi-conducting electrode. The thin films of VCr and CrCr materials presenting high T_Cs are protected by a patent [139]. Faraday effects are also observed in low-*T*c Prussian Blues [140]. Electrochemically prepared films of trimetallic Prussian Blue analogs exhibit second harmonic generation effects [142]. Even if further studies are needed to control the purity and the homogeneity of the air-sensitive layers and to correlate the magneto-optical effects with the local magnetisation of vanadium and chromium, a very promising area is open.

To conclude this section, we can state that, of all the Prussian Blue analogs prepared to date, the highest T_Cs are seen for solids isolated by adding V^{2+} to $[Cr^{III}(CN)_6]^{3-}$, and that the $K_1V^{II}{}_1Cr^{III}$ material is the current record-holder. Prussian Blues involving new precursors and new bimetallic pairs, some involving metal ions of the second and third period of the d block, may change the situation.

9.5 Prospects and New Trends

Space is lacking in this review to develop further aspects of the chemistry and physics of other magnetic Prussian Blues. Fortunately, many aspects have been reviewed recently and the interested reader will find valuable information in the references quoted below. We would like nevertheless to quote some promising areas of development. They show that besides the problem of high T_C much more can be learned from, and done with, magnetic Prussian Blues.

9.5.1 Photomagnetism: Light-Induced Magnetisation

A new field was opened in the magnetic Prussian Blues story and in molecular magnetism when Hashimoto and his team reported the existence of an exciting photomagnetic effect in a Prussian blue analog formulated $K_{0.4}Co_{1.3}[Fe(CN)_6]_1 \cdot 5H_2O$ (or $K_{0.3}Co_1[Fe(CN)_6]_{0.77} \cdot 3.8H_2O$, close to $Co_1Fe_{2/3}$), that has been known for a long time (Table 9.2) [142]. Starting from aqueous solutions of Co^{II} and hexacyanoferrate(III), Hashimoto obtained a powder, containing potassium ions, which exhibited a photo-induced enhancement of the magnetisation at low temperatures and an increase of the Curie temperature. Photoexcitation at the molecular level, in the Co–NC–Fe unit, gives rise to a modification of the macroscopic properties of the material, an important feature [143]. The authors suggested the presence of isolated diamagnetic Co^{III}–Fe^{II} pairs in a compound otherwise built from –Co^{II}–NC–Fe^{III}– units and a photo-induced electron transfer from Fe^{II} to Co^{III} through the cyanide bridge. The enhancement of the magnetisation and the increase in the Curie temperature simply follow from the increase of the number of magnetic pairs in the photo-induced state. The publication of this first result gave rise to an impressive series of findings by several groups. Theoretical studies were carried out by Yamaguchi [144] and Kawamoto [145] including a patent for an optical storage element [146], and experimental studies were carried out by Bleuzen [147, 148, 214], Gütlich [149], Hashimoto [25, 150–152], Miller [153], and Varret [154, 155], who defined the conditions of appearance of the phenomenon, pointing out the role of the ligand field around the cobalt, the role of the vacancies, the very specific role of the alkali metal cations, the presence of several phases, etc. There is not room here to give an exhaustive survey. Among many beautiful results, the first evidence of a photo-induced diamagnetic-ferrimagnetic transition [25, 147] and magnetic pole inversion [25, 150–152] can be underlined. Epstein and Miller studied the dynamics of the magnetisation and proposed a model of a glass cluster in the ground and photoexcited states, with an increase in spin concentration in the photo-induced phase [153]. Although the Co–Fe systems are still being actively studied [156–159], they are now joined by other systems constructed from octacyanometalates, developed by Hashimoto [25, 160], Mathonière [161, 162], Marvaud [163], etc. The field has been reviewed by several authors, emphasizing

the importance of optically switchable molecular solids. Varret, Nogues and Goujon in the Chapter entitled "Photomagnetic Properties of Some Inorganic Solids" in Volume I of this series [164], Hashimoto and Okhoshi [25] and more recently Sato [165,166], make many references to work in this illuminating field.

9.5.2 Fine Tuning of the Magnetisation

The flexibility of the Prussian Blues, especially the ability to adjust the composition at will, was used to modify the magnetisation of the systems, using the mean field model as a predictive tool (see Section 3.2.1). Okhoshi, Hashimoto and coworkers produced an impressive series of new results beginning with the coexistence of ferromagnetic and antiferromagnetic interactions in $Ni_xMn_{(1-x)}[Cr(CN)_6]_{2/3}$, a trimetallic Prussian Blue [167–169]. With the same theoretical model, they looked at the compensation temperature and other phenomena predicted by Néel [75]. They used competing ferromagnetic interactions to tune the compensation temperatures in the magnetisation of ferrimagnets and they were able to design systems with two compensation temperatures [170, 171]. They also described an inverted hysteresis loop combining a spin-flop transition and uniaxial magnetic anisotropy. Finally, they combined their efforts and experience in photomagnetism and magnetisation to characterize photo-induced magnetic pole inversion [172]. The results are reviewed in Refs. [25, 173]. The same authors review the very peculiar magnetic properties of $RbMn[Fe(CN)_6]$ in Ref. [174].

9.5.3 Dynamics in Magnetic and Photomagnetic Prussian Blues

The AC susceptibility was not systematically exploited in earlier studies of MPBs. Epstein and Miller opened this field. When measuring the AC susceptibility of different molecule-based magnets, they discovered unexpected new behavior, often assigned to spin-glass behavior, as described before in the photomagnetic CoFe PB analog [153, 175–178]. They found similar behavior in first-row transition metal hexacyanomanganates [179]. Other authors suggested similar conclusions in vanadium hexacyanochromates [180] and gadolinium hexacyanoferrates [181]. It appears that the synthetic conditions, the chemical stability, the crystallinity, the homogeneity, and the purity are important issues to control in order to understand the dynamics.

9.5.4 Nanomagnetism

The field is still in its infancy but several papers have recently appeared showing the interest and the potential of magnetic Prussian Blues for the preparation of

magnetic nanosized systems. In the trend to ever higher magnetic information storage densities, obtaining nanosize magnetized particles is an important issue, both for theory and applications. Prussian Blues allow top-down (breaking three-dimensional PB solids) or bottom-up (controlling crystalline growth from molecules in solution) approaches. The chemical flexibility of the PB analogs can be a great advantage in tuning the final properties. In 2000, Gao et al. announced that they were able to obtain VCr derivatives with T_C = 340 K, fcc lattice, a = 11.78 Å, stable in air for days, with an average particle size of 5 nm, presenting long range ferrimagnetic behavior and spin-glass behavior [182]. In 2001 Mann et al. prepared good quality inverse opals of $K_xCo_4[Fe(CN)_6]_z$ from polystyrene or silica colloïdal crystal templates [183]. Then, they adopted water-in-oil emulsions to synthesize crystalline cobalt hexacyanoferrate, cobalt pentacyanonitrosylferrate, chromium hexacyanochromate in the form of 12–22 nm particles organized in 100 particle superlattices [184]. They expected that the preparation method would be readily applicable toward the synthesis of other nano-sized molecule-based magnets. It was successful with nickel hexacyanochromate in the hands of Catala et al. who obtained 3 nm sized particles (with a wide distribution) [185]. Zhou adopted an electrodeposition technique in the nanocavities of aluminum oxide films to fabricate highly ordered Prussian Blue nanowire arrays 50 nm in diameter and 4 μm length [186]. Stiegman used the sol-gel technique competing with arrested precipitation to obtain superparamagnetic nanocomposites: transparent nickel hexacyanochromate and photomagnetic cobalt hexacyanoferrate [159]. Langmuir-Blodgett films, which are known to incorporate Prussian Blue itself [187, 188] are also able to trap MPB nanocubes in a thin film as shown by Delhaes et al. [189]. The field will most probably expand quickly if the difficult problem of characterisation of the new phases can be solved.

9.5.5 Blossoming of Cyanide Coordination Chemistry

The cyanide ligand has a long history in coordination chemistry and organometallic chemistry. It is known as a very dangerous, but also friendly, ligand. The reviews by Fritz and Fehlhammer [190] in 1993 and by Dunbar and Heintz in 1997 [60] pointed out the revival of cyanide chemistry. Molecular magnetism and MPBs have contributed to the blossoming of cyanide coordination and organometallic chemistry with new ideas, new concepts, new precursors (tetra-, penta-, hexa-, hepta-, octa-cyanometalates), new architectures, etc. Work by Ceulemans [191, 215], Decurtins [192, 193], Dunbar [194, 195], Hashimoto [196], Kahn [197], Julve [198], Long [199, 200], Mallah [201, 202], Marvaud [98], Murray [203], Okawa, Ohba and Inoue [204], Ouahab [205], Rey [206], Ribas [207], Sieklucka [208], and many others, show that there is considerable interest in this area.

9.6 Conclusion: a 300 Year Old "Inorganic Evergreen"

These new directions of development are clear indications that the field of magnetic Prussian Blues is very active, with various lines of development, in addition to the problem of reaching high critical temperatures, which was the main subject of the present chapter. The deep color of Prussian Blue was, and remains, a fascination for drapers, artists, and chemists. Magnetic and multifunctional Prussian Blues add a new facet to this attraction, from fundamental quantum mechanics to appealing applications, via solid state chemistry and physics. Ludi [209] was right when he pointed out that Prussian Blue is indeed an "inorganic evergreen." The statement is especially appropriate for its 300th anniversary, celebrated this year.

Acknowledgements

The authors dedicate this chapter to the memory of their colleague and friend O. Kahn, whose ideas inspired much of the work presented here. MV wishes to thank Drs. S. Alvarez, E. Ruiz, M. Julve, F. Lloret, B. Siberchicot and V. Eyert for illuminating discussions and suggestions about the theory of the systems. The authors are grateful to their coworkers, without whom these magnetic Prussian Blue studies could not have been done; their names appear in the cited articles. Funding from the Pierre et Marie Curie University at Paris, the Department of Energy through the Frederick Seitz Materials Research Laboratory at the University of Illinois at Urbana-Champaign, CNRS, the European Community (TMR and Marie Curie Programmes), I.C.R.E.A. Barcelona and the European Science Foundation (Molecular Magnets Programme) is sincerely acknowledged.

References

1. R. Wood, *Understanding Magnetism*, Tab Books Inc., Blue Ridge Summit, PA, 1988.
2. R.M. White, *Science* **1985**, *229*, 11–15.
3. P. Chaudhari, M. Flemings, *Materials Science and Engineering for the 1990s*; National Academy Press: Washington, 1989, pp. 94–96.
4. E. Köster, *J. Magn. Magn. Mater.* **1993**, *120*, 1–10.
5. L.B. Lueck, R.G. Gilson, *J. Magn. Magn. Mater.* **1990**, *88*, 227–235.
6. *Magnetic Molecular Materials,* Eds. D. Gatteschi, O. Kahn, J. S. Miller et al., Kluwer, Dordrecht 1991, NATO ASI Series E Vol. 198.
7. O. Kahn, *Molecular Magnetism*, VCH, Weinheim, 1993.
8. K. Itoh, M. Kinoshita, *Molecular Magnetism, New Magnetic Materials*, Kodansha, Tokyo, 2000

9. *Magnetism: Molecules to Materials I–IV*, Eds. J.S. Miller, M. Drillon, Vol. 1–4, Wiley–VCH, Weinheim, New York, 2001–2002.
10. *Molecular Magnets, Recent Highlights*, Eds. W. Linert, M. Verdaguer), Springer, Berlin, 2003.
11. J. S. Miller, A. J. Epstein *Angew. Chem. Int. Ed. Engl.* **1994**, *33*, 385–415.
12. D. Gatteschi, *Adv. Mater.* **1994**, *6*, 635–645.
13. J. S. Miller, *Chem. Eng. News* **1995**, October 2, 30–41.
14. D. Gatteschi, *Curr. Opin. Solid State Mater. Sci.* **1996**, *1*, 192–198.
15. P. Day, *Proc. Royal Inst. Great Brit.* **1998**, *69*, 85–106.
16. P. Day, *Phil. Trans. R. Soc. London, Ser. A* **1999**, *357*, 3163–3184.
17. J.S. Miller, A.J. Epstein, *MRS Bulletin* **2000**, November, 21–30.
18. J.S. Miller, *Inorg. Chem.* **2000**, *39*, 4392–4408.
19. M. Verdaguer, *Polyhedron* **2001**, *20*, 1115–1128; *Actualité Chim*. **2001**, Juin, 9–18.
20. P. Day, *Notes Rec. R. Soc. London* **2002**, *56*, 95–103.
21. C. P. Landee, D. Melville, J. S. Miller, Ref. 6, pp. 395–398.
22. M. Leuenberger, D. Loss, *Nature (London)* **2001**, *410*, 789–793.
23. R. Clément, P.G. Lacroix, D. O'Hare et al., *Adv. Mater.* **1994**, *6*, 794–797.
24. R.F. Ziolo, E. P. Giannelis, B. A. Weinstein et al., *Science* **1992**, *257*, 219–223.
25. S. Okhoshi, K. Hashimoto, *J. Photochem. Photobiol. C: Photochem. Rev.* **2001**, *2*, 71–88.
26. J.M. Manriquez, G.T. Yee, R.S. McLean et al., *Science*, **1991**, *252*, 1415–1417.
27. V. Gadet, T. Mallah, I. Castro et al., *J. Am. Chem. Soc.* **1992**, *114*, 9213–9214.
28. T. Mallah, S. Thiébaut, M. Verdaguer, et al., *Science* **1993**, *262*, 1554–1557.
29. S. Ferlay, T. Mallah, R. Ouahès et al., *Nature (London)* **1995**, *378*, 701–703.
30. W.R. Entley, G.S. Girolami, *Inorg. Chem*. **1994**, *33*, 5165–5166.
31. W.R. Entley, G.S. Girolami, *Science* **1995**, *268*, 397–402.
32. W.R. Entley, C.R. Treadway, G.S. Girolami, *Mol. Cryst. Liq. Cryst.* **1995**, 273, 153.
33. W.R. Entley, C.R. Treadway, S. R. Wilson et al., *J. Am. Chem. Soc.* **1997**, *119*, 6251–6258.
34. W.E. Buschmann, C. Vasquez, M.D. Ward et al., *J. Chem. Soc. Chem. Commun.* **1997**, 409–410.
35. V. Marvaud, T. Mallah, M. Verdaguer, *Inorg. Synth*. **2004**, *34*, 144–146.
36. V. Gadet, Ph.D. Thesis, Université Pierre et Marie Curie, Paris, **1992**.
37. W.R. Entley, Ph.D. Thesis, University of Illinois at Urbana–Champaign, **1995**.
38. C. Hélary, Ph.D. Thesis, Université Pierre et Marie Curie, Paris, **1996**.
39. S. Ferlay, Ph.D. Thesis, Université Pierre et Marie Curie, Paris, **1996**.
40. S.M. Holmes, G. S. Girolami, *J. Am. Chem. Soc.* **1999**, *121*, 5593–5594.
41. S.M. Holmes, Ph.D. Thesis, University of Illinois at Urbana–Champaign, **2000**.
42. Anonymous, *Miscellanea Berolinensia ad Incrementum Scientiarum* **1710**, *1*, 377–378.
43. J. Woodward, *Phil. Trans*., **1724**, *33*, 15–17.
44. J. Brown, *Phil. Trans.*, **1724**, *33*, 19–24.
45. B. Van Tiggelen in *Proceedings XXth International Congress on the History of Science*., Vol. II, Eds. G. Emptoz, P.E. Aceves-Pastrana, Brepols, 1998, 59–67.
46. A. Nieto-Galan, in *Lavoisier in European Context. Negotiating a New Language for Chemistry*, Eds. B. Bensaude-Vincent, F. Abbri, Canton, 1995, pp. 182–183.
47. B. Bensaude-Vincent, B. Van Tiggelen, A. Nieto-Galan, personal communications.
48. A.G. Sharpe, *The Chemistry of Cyano Complexes of the Transition Metals*, Academic Press, New York, 1976.
49. J.F. Keggin, F.D. Miles, *Nature (London)* **1936**, *137*, 577

50. A. Ludi, H.U. Güdel, *Struct. Bonding (Berlin)* **1973**, *14*, 1–21.
51. A. Ludi, H.U. Güdel, *Helv. Chim. Acta* **1968**, *51*, 2006.
52. A. Ludi, H.U. Güdel, *Inorg. Chem.* **1970**, *9*, 2224.
53. H.U. Güdel, *Acta Chem. Scand*. **1972**, *26*, 2169.
54. J.H. Buser, A. Ludi, H.U. Güdel, *J. Chem. Soc., Chem. Commun.* **1972**, 1299.
55. H.U. Güdel, H. Stucki, A. Ludi, *Inorg. Chim. Acta* **1973**, *7*, 121.
56. G. Ron, A. Ludi, *Chimia* **1973**, *27*, 77.
57. G.W. Beall, W.O. Mulligan, J. Korp et al., *Inorg. Chem.* **1977**, *11*, 2715.
58. M.B. Robin, *Inorg. Chem.* **1962**, *1*, 337.
59. M.B. Robin, P. Day, *Adv. Inorg. Chem. Radiochem*. **1967**, *10*, 249.
60. K. Dunbar, R.A. Heintz *Prog. Inorg. Chem.*, **1997**, *45*, 283–391 and the 466 references therein.
61. D. Davidson, L.A. Welo, *J. Phys. Chem.*, **1928**, *32*, 1191.
62. J. Richardson, N. Elliott, *J. Am. Chem. Soc.*, **1940**, *62*, 3182.
63. A. Ito, M. Suenaga, K. Ono, *J. Chem. Phys*. **1968**, *48*, 3597–3599.
64. H.J. Buser, P. Fischer, T. Studach et al., *J. Phys. Chem*. **1974**, *92*, 354.
65. P. Day, F. Herren, A. Ludi et al., *Helv. Chim. Acta* **1980**, *63*, 148.
66. B. Mayoh, P. Day, *J. Chem. Soc. Dalton Trans*. **1976**, 1483.
67. R.M. Bozorth, H.J. Williams, D.E. Walsh, *Phys. Rev*. **1956**, *103*, 572–578.
68. A.N. Holden, B.T. Matthias, P.W. Anderson et al., *Phys. Rev*. **1956**, *102*, 1463.
69. R. Klenze, B. Kanellakopulos, G. Trageser et al., *J. Chem. Phys.* **1980**, *72*, 5819–5828.
70. W.D. Griebler, D. Babel, *Z. Naturforsch*. **1982**, *37b*, 832–837.
71. D. Babel, W. Kurtz, W. in *Solid State Chemistry 1982*, Eds. R. Metselaar, H.J.M. Heijligers, J. Schoonman, Elsevier, Amsterdam, 1983, pp. 593–596.
72. H. Henkel and D. Babel, *Z. Naturforsch. B*, **1984**, *39*, 880.
73. M. Witzel and D. Babel, *Z. Naturforsch. B*, **1985**, *40*, 1344.
74. D. Babel, *Comments Inorg. Chem.* **1986**, *5*, 285–320.
75. L. Néel, *Ann. Phys. Paris* **1948**, *137*, 137–198.
76. A. Herpin, *Théorie du Magnétisme*, I.N.S.T.N.–PUF, Saclay, 1968.
77. J.B. Goodenough, *Magnetism and the Chemical Bond;* Interscience, New York, 1963.
78. B.N. Figgis, E.S. Kucharshi, M. Vrtis, *J. Am. Chem. Soc.* **1993**, *115*, 176–181.
79. F. Köhler, R. Lescouëzec, *Angew. Chem. Int. Ed. Engl*. **2004**, *43*, 2571–2573.
80. A.P. Ginsberg, *Inorg. Chim. Acta Rev*. **1971**, *5*, 45.
81. O. Kahn, B. Briat, *J. Chem. Soc., Faraday Trans*. **1976**, *72*, 268.
82. O. Kahn, B. Briat, *J. Chem. Soc., Faraday Trans*. **1976**, *72*, 1441.
83. J.J. Girerd, Y. Journaux, O. Kahn, *Chem. Phys. Lett.* **1981**, *82*, 534–537.
84. P.J. Hay, J.C. Thibeault, R. Hoffmann, *J. Am. Chem. Soc.* **1975**, *97*, 4884–4899.
85. O. Kahn, *Struct. Bonding (Berlin)* **1987**, *68*, 1063.
86. M.F. Charlot, O. Kahn, *Nouv. J. Chim*. **1980**, *4*, 567.
87. V. Gadet, M. Bujoli–Doeuff, L. Force et al., Ref. 6, pp. 281–295.
88. Ø. Hatlevik, W. E. Buschmann, J. Zhang et al., *Adv. Mater.* **1999**, *11*, 914–918.
89. S. Ferlay, T. Mallah, R. Ouahès et al., *Inorg. Chem.* **1999**, *38*, 229–234.
90. L.G. Beauvais, J.R. Long, *J. Am. Chem. Soc*. **2002**, *124*, 12096.
91. W.E. Buschmann, J.S. Miller *Inorg. Chem.* **2000**, *39*, 2411–2421.
92. S. Juszczyk, C. Johansson, M. Hanson et al., *J. Phys.: Condens. Matter* **1994**, *6*, 5697.
93. S. Juszczyk, C. Johansson, M. Hanson G. Malecki, *J. Magn. Magn. Mater*. **1994**, *136*, 45.
94. F. Herren, P. Fischer, A. Ludi, W. Hälg, *Inorg. Chem.* **1980**, *19*, 956.

95. V. Marvaud, C. Decroix, A. Scuiller et al., *Chem., Eur. J.* **2003**, *9*, 1677–1691 and 1692–1705.
96. E. Ruiz, S. Alvarez, A. Rodriguez–Fortea et al., Ref. [9], Vol, 2, p. 227–279.
97. R. Boca, *Theoretical Foundations of Molecular Magnetism*, Elsevier, Lausanne, 1999.
98. F. Fabrizzi de Biani, E. Ruiz et al., work in progress.
99. M. Verdaguer, A. Bleuzen, R. Garde et al., *Phil. Trans. Royal Soc. London, Ser. A* **1999**, *357*, 2959–2976.
100. M. Verdaguer, A. Bleuzen, V. Marvaud et al., *Coord. Chem. Rev*. **1999**, *192*, 1023–1047.
101. M. Nishino,S. Kubo, Y. Yoshioka et al., *Mol. Cryst. Liq. Cryst.* A **1997**, *305*, 109–128.
102. M. Nishino, S. Takeda, W. Mori et al., *Synth. Met.* **1997**, *85*, 1763–1764.
103. M. Nishino, Y. Yoshioka, K. Yamaguchi, *Chem. Phys. Lett*. **1998**, *297*, 51–59.
104. K. Yamaguchi, *Chem. Phys. Lett*. **1975**, *30*, 288–92.
105. L. Salem, *Electrons in Chemical Reactions: First Principles*, Wiley, New York, 1982.
106. A. Rodríguez–Fortea, P. Alemany, S. Alvarez et al., *Inorg. Chem.* **2001**, *40*, 5868–5877.
107. E. Ruiz, J. Cano, S. Alvarez et al., *J. Comp. Chem*. **1999**, *20*, 1391.
108. A. Rodríguez–Fortea, E. Ruiz, S. Alvarez et al., work in progress.
109. B. Siberchicot, T. Mallah, M. Verdaguer, *J. Magn. Magn. Mater.* **1996**, *157/158*, 417–418.
110. V. Eyert, B. Siberchicot, M. Verdaguer, *Phys. Rev. B*, **1997**, 56, 8959–8969.
111. N.M. Harrison, B.G. Searle, E.A. Seddon, *Chem. Phys. Lett.* **1997**, *266*, 507–511.
112. R. Hoffmann, *Solids and Surfaces: a Chemist's View of Bonding in Extended Structures*, VCH, New York, 1988.
113. V. Eyert, in *Density Functional Methods: Applications to Chemistry and Materials Science*, Ed. M. Springborg., Wiley, Chichester, 1997, pp. 233–304.
114. P.W. Anderson, *Phys. Rev*. **1959**, *115*, 2–13.
115. H. Weihe, H.U. Güdel, *Comments Inorg. Chem.* **2000**, *22*, 75–103.
116. H. Weihe, H.U. Güdel, H. Toftlund, *Inorg. Chem.* **2000**, *39*, 1351–1362.
117. A.V.Palii, B.S. Tsukerblat, M.Verdaguer, *J. Chem. Phys*. **2002**, *117*, 7896–7905.
118. L.F. Chibotaru, V.S. Mironov, A. Ceulemans, *Angew. Chem. Int. Ed. Engl.* **2001**, *40*, 4429–4433.
119. O. Kahn, *Nature (London)* **1995**, *378*, 677.
120. J. Bonjour, M. Verdaguer, unpublished observations.
121. O. Sato, T. Iyoda, A. Fujishima et al., *Science* **1996**, *271*, 49–51.
122. W.E. Buschmann, S.C. Paulson, C.M. Wynn et al., *Chem. Mater.* **1998**, *10*, 1386–1390.
123. J.S. Miller, J.L. Manson, *Acc. Chem. Res*. **2001**, *34*, 563–570.
124. A.J. Epstein, *MRS Bulletin*, November 2000, 33–40.
125. R. Garde, C. Desplanches, A. Bleuzen et al., *Mol. Cryst. Liq. Cryst. A* **1999**, *333*, 587–596.
126. E. Dujardin, S. Ferlay, X. Phan et al., *J. Am. Chem. Soc.* **1998**, *120*, 11347–11352.
127. R. Garde, F. Villain, M. Verdaguer, *J. Am. Chem. Soc.* **2002**, *124*, 10531–10538.
128. R. Garde, F. Villain, M. Verdaguer, unpublished results, to be submitted in *Inorg. Chem.*
129. P. Sainctavit, C.Cartier dit Moulin and M.-A. Arrio, Ref. [9], Vol. I, pp. 130–153.
130. M.A. Arrio, P. Sainctavit, C. Cartier dit Moulin et al., *J. Phys. Chem*. **1996**, *100*, 4679–4684.
131. M.A. Arrio, P. Sainctavit, C. Cartier dit Moulin et al., *J. Am. Chem. Soc.* **1996**, *118*, 6422–6427.
132. M.A. Arrio, A. Scuiller, P. Sainctavit et al., *J. Am. Chem. Soc.* **1999**, *121*, 6414–6420.

133. G. Champion, C. Cartier dit Moulin, F. Villain et al., *J. Am. Chem. Soc.* **2001**, *123*, 12544–12546.
134. M. Verdaguer, T. Mallah, S. Ferlay et al. in *Current Trends in Coordination Chemistry*, Eds. G. Ondrejovic, A. Sirota, Slovak Technical University Press, Bratislava, 1995, pp. 291–296; G. Keller, N. Galvez, F. Villain, unpublished work.
135. S. Ohkoshi, A. Fujishima, K. Hashimoto, *J. Am. Chem. Soc.* **1998**, *120*, 5349–5350.
136. M. Mizuno, S. Ohkoshi, K. Hashimoto, *Adv. Mater.* **2000**, *12*, 1955–1958.
137. M. Verdaguer, N. Galvez, R. Garde, et al., *Electrochem. Soc. Interface* **2002**, *11*, 28–32.
138. C. Desplanches, PhD Thesis, Université Pierre et Marie Curie, Paris, 2001.
139. S. Ohkoshi, K. Hashimoto, A. Fujishima, *Jpn. Patent* No. JP 1999–67593, 19990312, 1999.
140. M. Tozawa, S. Ohkoshi, N. Kojima et al., *Chem. Commun*. **2003**, 1204–1205.
141. K. Ikeda, S. Ohkoshi, K. Hashimoto, *Chem. Phys. Lett*. **2001**, *349*, 371–375.
142. O. Sato, T. Iyoda, A. Fujishima et al., *Science* **1996**, *272*, 704–706.
143. M. Verdaguer, *Science* **1996**, *272*, 698–699.
144. M. Nishino, Y. Kitagawa, T. Onishi et al., *Mol. Cryst. Liq. Cryst. A* **2000**, *343*, 151–156.
145. T. Kawamoto, Y. Asai, S. Abe, *Phys. Rev. Lett*. **2001**, *86*, 348–351.
146. T. Kawamoto, S. Abe, *Jpn Patent* No. JP 2000–282327, 20000918, 2000.
147. A. Bleuzen, C. Lomenech, V. Escax et al., *J. Am. Chem. Soc.* **2000**, 122, 6648–6652; 6653–6658.
148. V. Escax, A. Bleuzen, M. Verdaguer et al., *J. Am. Chem. Soc.* **2001**, *123*, 12536–12543; 12544–12546.
149. V. Ksenofontov, G. Levchenko, S. Reiman et al., *Phys. Rev. B* **2003,** 68, 0244151–0244156.
150. S. Ohkoshi, S. Yorozu, O. Sato et al., *Appl. Phys. Lett*. **1997**, *70*, 1040.
151. S. Ohkoshi, K. Hashimoto, *J. Am. Chem. Soc.* **1999**, *121*, 10591–10597.
152. S. Ohkoshi, N. Machida, Z.J. Zhong et al., *Synth. Met.*, **2001**, *122*, 523.
153. D.A. Pejakovic, J.L. Manson, J.S. Miller et al., *Phys. Rev. Lett.* **2000**, *85*, 1994–1997.
154. F. Varret, A. Bleuzen, K. Boukheddaden et al., *Pure Appl. Chem*. **2002**, *74*, 2159–2168.
155. V. Escax, A. Bleuzen, J. P. Itié et al., *J. Phys. Chem. B* **2003**, *107*, 4763–4767.
156. N. Shimamoto, S. Ohkoshi, O. Sato et al., *Chem. Lett*. **2002**, 486–487.
157. N. Shimamoto, S. Ohkoshi, O. Sato et al., *Inorg. Chem.* **2002**, *41*, 678–684.
158. V. Escax, A. Bleuzen, J. P. Itié et al., *C.R. Chimie* **2003**, 343–352; 1165–1173.
159. J.G. Moore, E.J. Lochner, C. Ramsey et al., *Angew. Chem. Int. Ed. Engl*. **2003**, *42*, 2741–2743.
160. Y. Arimoto, S. Okhoshi, Z.J. Zhong et al. *J. Am. Chem. Soc.* **2003**, *125*, 9240–9241.
161. G. Rombaut, C. Mathonière, P. Guionneau et al., *Inorg. Chim. Acta* **2001**, *326*, 27.
162. G. Rombaut, Thèse Université de Bordeaux, 2001.
163. J.M. Herrera,V. Marvaud, C. Mathonière, *Angew. Chem. Int. Ed. Engl.*, in press.
164. F. Varret, M. Nogues, A. Goujon, Ref. [9], Vol. I, 2001, pp. 257–295.
165. O. Sato, *Acc. Chem. Res*. **2003**, *36*, 692–700.
166. O. Sato, S. Hayami, Y. Einaga et al., *Bull. Chem. Soc. Jpn.* **2003**, *76*, 443–470.
167. S. Ohkoshi, O.Sato, T. Iyoda et al., *Inorg. Chem.* **1997**, *36*, 268.
168. S. Ohkoshi, T. Iyoda, A. Fujishima et al., *Phys. Rev. B* **1997**, *56*, 11642–11652.
169. S. Ohkoshi, K. Hashimoto, *Phys. Rev. B* **1999**, *60*, 12820–12825.
170. S. Ohkoshi, Y. Abe, A. Fujishima et al., *Phys. Rev. Lett.* **1999**, *82*, 1285.
171. S. Ohkoshi, T. Hozumi, M. Utsunomiya et al., *Physica B* **2003**, *329–333*, 691–692.
172. S. Ohkoshi, Y. Einaga, A. Fujishima et al., *J. Electroanal. Chem.* **1999**, *473*, 245.
173. S. Ohkoshi, K. Hashimoto, *Electrochem. Soc. Interface* **2002**, *11*, 34–38.

174. S. Ohkoshi, H. Hashimoto, *Kagaku Kogyo* **2003**, 56, 242–245.
175. D.A. Pejakovic, J.L. Manson, J.S. Miller et al., *J. Appl. Phys.* **2000**, *87*, 6028–6030.
176. D.A. Pejakovic, J.L. Manson, J. S. Miller et al., *Synth. Met*. **2001**, *122*, 529–533.
177. D.A. Pejakovic, J.L. Manson, C. Kitamura et al., *Polyhedron* **2001**, *20*, 1435–1439.
178. D.A. Pejakovic, J.L. Manson, C. Kitamura et al., *Mol. Cryst. Liq. Cryst. A* **2002**, *374*, 289–302
179. W.E. Buschmann, J.S. Miller, *Inorg. Chem*. **2000**, *39*, 2411–2421.
180. M. Sendek, K. Csach, V. Kavecansky et al., *Phys. Status Solidi A* **2003**, *196*, 225–228; 240–243.
181. M. Broschova, M. Mihalik, V. Kavecansky et al., *Czech. J. Phys*. **2002**, *52*, 325–328.
182. S. Gao, O. Bai, T. Yi, et al., *Huaxue Xuebao* **2000**, *58*, 1666–1669.
183. S. Vaucher, E. Dujardin, B. Lebeau et al., *Chem. Mater*. **2001**, *13*, 4408–4410.
184. S. Vaucher, J. Fielden, M. Li et al., *Nano Lett.* **2002**, *2*, 225–229.
185. L. Catala, T. Gacoin, J.P. Boilot et al., *Adv. Mater.* **2003**, *15*, 826–829.
186. P. Zhou, D. Xue, H. Luo et al., *Nano Lett.* **2002**, *2*, 845–847.
187. J.T. Culp, J.H. Park, I.O. Benitez et al., *Chem. Mater*. **2003**, *15*, 3431–3436.
188. G. Romualdo-Torres, B. Agricole, C. Mingotaud et al., *Langmuir* **2003**, *19*, 4688–4693.
189. G.R. Torres, B. Agricole, P. Delhaes et al., *Chem. Mater*. **2002**, *14*, 4012–4014.
190. W.P. Fehlhammer, M. Fritz, *Chem Rev*. **1993**, *93*, 1243 and references therein.
191. V. Mironov, L. Chibotaru, A. Ceulemans *J. Am. Chem. Soc.* **2003**, *125*, 9750–9760.
192. J. Larionova, M. Gross, M. Pilkington et al., *Angew. Chem. Int. Ed. Engl.* **2000**, *39*, 1605–1609.
193. M. Pilkington, S. Decurtins, *Chimia* **2001**, *55*, 1014–1016.
194. C.P. Berlinguette, D. Vaughn, C. Canada-Vilalta et al., *Angew. Chem., Int. Ed. Engl.* **2003**, *42*, 1523–1526.
195. C.P. Berlinguette, J.R. Galan–Mascaros, K.R. Dunbar, *Inorg. Chem*. **2003**, 42, 3416–3422.
196. Z. J. Zhong, H. Seino, Y. Mizobe et al., *J. Am. Chem. Soc.* **2000**, *122*, 2952–2953.
197. J. Larionova, R. Clérac, J. Sanchiz et al., *J. Am. Chem. Soc.* **1998**, *120*, 13088.
198. R. Lescouëzec, J. Vaissermann, C. Ruiz–Pérez et al., *Angew. Chem Int. Ed. Engl*. **2003**, *42*, 1483–1486.
199. L.G. Beauvais, J.R. Long *J. Am. Chem. Soc.* **2002**, *124*, 2110–2111; 12096–12097.
200. E.G. Tulsky, N.R. Crawford, S. Baudron et al., *J. Am. Chem. Soc.* **2003**, *125*, 15543–15553.
201. T. Mallah, A. Marvilliers, Ref. [9], Vol. II, 2001, pp. 189–226.
202. G. Rogez, S. Parsons, C. Paulsen, V. Villar, T. Mallah, *Inorg. Chem*. **2001**, *40*, 3836–3837.
203. K. Van Langenberg, S.R. Batten, K.J. Berry et al., *Inorg. Chem.* **1997**, *36*, 5006.
205. K. Inoue, K. Kikuchi, M. Ohba et al., *Angew. Chem*. **2003**, *42*, 4810–4813
205. J. Larionova, O. Kahn, S. Golhen et al., *Inorg. Chem.* **1999**, *38*, 3621.
206. K. E. Vostrikova, D. Luneau, W. Wernsdorfer et al., *J. Am. Chem. Soc.* **2000**, *122*, 718–719.
207. M.S. El Fallah, J. Ribas, X. Solans et al., *J. Chem. Soc., Dalton Trans.* **2001**, 247–250.
208. R. Podgajny, C. Desplanches, B. Sieklucka et al., *Inorg. Chem.* **2002**, *41*, 1323–1327.
209. A. Ludi, *J. Chem. Educ.* **1981**, *58*, 1013.
210. R. Cortes, M.K. Urtiaga, L. Lezama et al., *Inorg. Chem*. **1994**, *33*, 829–832.
211. R. Caballol, O. Castell, F. Illas et al., *J. Phys. Chem. A* **1997**, *101*, 7860–7866.
212. E. Ruiz, J. Cano, S. Alvarez et al., *J. Comput. Chem*. **1999**, *20*, 1391–1400.
213. J.M. Mouesca, C. Blanchet-Boiteux et al., *J. Am. Chem. Soc*. **2000**, *122*, 861–869; *J. Phys. Chem. A*. **2000**, *104*, 2091–2097.
214. A. Bleuzen, V. Escax, A. Ferrier et al., *Angew. Chem. Int. Ed. Engl*. **2004**, *43*, in press.
215. V.S. Hendrickx, V.S. Mironov, L.F. Chibotaru et al., *J. Am. Chem. Soc*. **2003**, *125*, 9750–9760.